

2014-05-30

Regulation of Cell Behavior at the Cell-Surface Interface

Morgan M. Stanton
Worcester Polytechnic Institute

Follow this and additional works at: <https://digitalcommons.wpi.edu/etd-dissertations>

Repository Citation

Stanton, M. M. (2014). *Regulation of Cell Behavior at the Cell-Surface Interface*. Retrieved from <https://digitalcommons.wpi.edu/etd-dissertations/296>

This dissertation is brought to you for free and open access by [Digital WPI](#). It has been accepted for inclusion in Doctoral Dissertations (All Dissertations, All Years) by an authorized administrator of Digital WPI. For more information, please contact wpi-etd@wpi.edu.

Regulation of Cell Behavior at the Cell-Surface Interface

Morgan M. Stanton

Department of Chemistry and Biochemistry

Worcester Polytechnic Institute



A Thesis Submitted to Worcester Polytechnic Institute

for the Degree of Doctor in Philosophy

May 2014

REGULATION OF CELL BEHAVIOR AT THE CELL-SURFACE INTERFACE

By

Morgan M. Stanton

A Dissertation


Submitted to the Faculty of the

WORCESTER POLYTECHNIC INSTITUTE

In partial fulfillment of the requirements for the

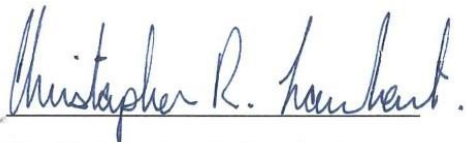
Degree of Doctor of Philosophy

in Chemistry



May 2014

APPROVED:



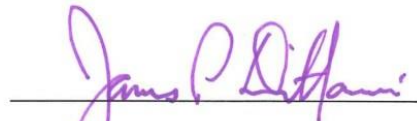
Dr. Christopher R. Lambert,
Major Advisor



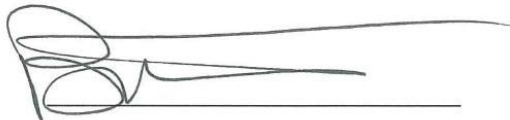
Dr. Arne Gericke,
Head of Department, Committee Member



Dr. John C. MacDonald,
Committee Member



Dr. James P. Dittami,
Committee Member



Dr. Bulent Mutus,
External Examiner, Committee Member

Acknowledgements

I would sincerely like to thank Dr. W. Grant McGimpsey for beginning my graduate education in his laboratory and Dr. Christopher R. Lambert for my continuing education and graduate experience. Dr. Lambert and Dr. McGimpsey have offered me guidance and encouragement throughout my research here at WPI and it was a privilege to have the opportunity to have worked with both of them. I would also like to thank my previous and current lab members including Dr. Peter F. Driscoll, Dr. Eftim Milkani, Dr. Robert E. Ducker, and Dr. Byung-Wook Park who worked with me as a graduate student and were willing to share their experience and knowledge. I would like to thank Aung Khaing and Ross Lagoy and our research assistants, Ann Plona, John Bladon, and Aung Lynn for all their help and support.

Outside of our laboratory group, I also received help and advice from Dr. Stephen Lambert, Dr. Christopher Malcuit, Dr. Robert Bellin, Allegra Parrillo, and Lucy Vilner. Their assistance was essential in developing the biological areas of my research and I appreciate the time they spent talking with me. I want to thank Dr. Nancy Burnham for devoting time towards educating me in AFM and her assistance in my research. I would also like to thank our collaborators Dr. John MacDonald, Dr. James Dittami, Dr. Chi Wen, and Dr. Arne Gericke for their input and work on our projects. I would also like to thank the WPI Department of Chemistry and Biochemistry for their support and encouragement throughout my time at WPI.

Finally, I would like to thank my family, my parents Marcy and Robert, and my brother Patrick. I would not have been able to accomplish this without their love and support.

Table of Contents

Acknowledgements	3
List of Abbreviations	8
List of Variables	9
Abstract	10
1.0 Introduction	13
1.0 General Introduction	13
1.1 Cell-Surface Relationship	17
1.1.1 Extracellular Matrix (ECM)	16
1.1.2 Integrins and Actin Cytoskeleton	18
1.1.3 Cell Adhesion	20
1.2 Surface Topography	22
1.2.1 Surface Roughness	23
1.2.2 Regular Surface Topographies	25
1.3 Surface Chemistry	26
1.3.1 Self-Assembled Monolayers (SAMs).....	27
1.3.1.1 Alkanethiols	29
1.3.1.2 Silanes	30
1.3.1.3 Phosphonic Acids.....	32
1.3.2 Biologically Active Surfaces	33
1.3.3 Microcontact Printing.....	36
1.3.4 Surface Wettability.....	37
1.4 Material Properties	39
1.4.1 Material Stiffness	39
1.4.2 Polydimethylsiloxane (PDMS)	42
1.4.3 Polystyrene (PS).....	43
1.5 Goals and Objectives	44
2.0 Experimental Techniques and Overview	46
2.1 Introduction	46

2.2 General Materials	46
2.2.1 Chemical Materials	46
2.2.2 Biological Materials	47
2.3 General Experimental.....	48
2.3.1 General Instrumentation.....	48
2.3.2 Rough and flat PDMS surface fabrication	49
2.4 Oxygen Plasma Treatment	50
2.5 ATR Infrared Spectroscopy	52
2.6 Contact Angle Goniometry	54
2.7 Atomic Force Microscopy.....	58
2.8 Fluorescence Microscopy.....	61
3.0 Super-hydrophobic, highly adhesive, PDMS surfaces	65
3.1 Introduction	65
3.2 Experimental Methods	67
3.2.1 Static, advancing, and receding contact angles.....	67
3.2.2 Drop volume measurements at 60°	67
3.2.3 Roughness measurements with AFM imaging	68
3.2.4 Grain threshold processing	68
3.3 Results and Discussion.....	69
3.3.1 AFM characterization of rough PDMS.....	69
3.3.2 Static contact angle and roughness	71
3.3.3 Solid-liquid contact.....	74
3.3.4 Surface free energy	76
3.3.5 Contact angle hysteresis and adhesion measurements.....	78
3.3.6 Impact of surface characterization	82
3.4 Conclusion.....	84
4.0 Fibroblast extracellular matrix and adhesion on micro-textured PDMS scaffolds.....	85
4.1 Introduction	85
4.2 Experimental Methods	86
4.2.1 AUTMS modification	86

4.2.2 Static contact angle	87
4.2.3 Cell seeding and growth on PDMS surfaces.....	88
4.2.4 AFM surface characterization and cell adhesion measurements	88
4.2.5 Morphology analysis.....	89
4.2.6 Immunofluorescence staining of fibroblasts on PDMS surfaces.....	90
4.2.7 Immunofluorescence staining of FN on PDMS after fibroblast extraction	91
4.3 Results	92
4.3.1 Surface characterization.....	92
4.3.2 Cell morphology and adhesion analysis	93
4.3.3 ECM arrangement.....	97
4.4 Discussion	98
4.5 Conclusion.....	104
5.0 Fibroblast behavior on chemically patterned and micro-roughened PDMS surfaces .106	
5.1 Introduction	106
5.2 Experimental Methods	108
5.2.1 Photoresist pattern on rough and flat PDMS surfaces	108
5.2.2 BSA and FN patterning on PDMS surfaces.....	108
5.2.3 PDMS and Petri dish surfaces for morphological and gene expression analysis ...	109
5.2.4 Cell seeding and imaging.....	110
5.2.5 Morphological analysis	111
5.2.6 AFM characterization of the surfaces	111
5.2.7 RNA isolation and cDNA synthesis	112
5.2.8 Relative / Real-time PCR.....	113
5.3 Results	115
5.3.1 BSA and FN patterning on PDMS.....	115
5.3.2 AFM characterization of surfaces	115
5.3.3 Fibroblast culture on surface pattern.....	118
5.3.4 Cell morphology analysis	120
5.3.5 Roughened substrate modulates ECM and adhesion molecule gene expression....	124
5.4 Discussion	127
5.5 Conclusion.....	133

6.0 Thermo-responsive, micro-rough cell scaffolds with controlled ECM and cytoskeleton	134
6.1 Introduction	134
6.2 Experimental Methods	137
6.2.1 Fabrication of PS surfaces	137
6.2.2 PIPAAm-PS	138
6.2.3 AFM characterization of the surfaces	140
6.2.4 ATR-IR spectroscopy	140
6.2.5 Cell seeding	140
6.2.6 Detachment of cell sheets and immunofluorescence staining	141
6.3 Results	142
6.3.1 Characterization of surface topography with AFM	142
6.3.2 Confirmation of PIPAAm surface grafting	144
6.3.3 Cell sheet formation of PIPAAm-PS	147
6.3.4 Cell sheet analysis with fluorescent microscopy	149
6.4 Discussion	152
6.5 Conclusion	157
7.0 Final Discussion	158
7.1 Introduction	158
7.2 PDMS vs. PS	158
7.3 Actin Cytoskeleton and Adhesion	161
7.4 ECM Assembly: Single Cell vs. Cell Sheet	164
7.5 MMP14 in Relation to Cell Sheet FN and Actin	166
8.0 Conclusions and Future Work	170
List of Figures	180
List of Tables	182
List of Equations	182
9.0 References	183

List of Abbreviations

2-D	Two-Dimensional	FWHM	Full Width at Half Maximum
2X	Twice	GA	Glutaraldehyde
3-D	Three-Dimensional	HTS	High Throughput Screening
AC	Alternating Contact	IR	Infrared
AFM	Atomic Force Microscopy	LCST	Lower Critical Solution Temperature
APTMS	3-aminopropyltrimethoxy silane	MMP	Matrix Metalloproteinase
ATR	Attenuated Total Reflectance	NHS	<i>N</i> -hydroxysuccinimide
AUTMS	<i>N</i> -(2-aminoethyl)-11-aminoundecyl trimethoxysilane	NIPAAm	<i>N</i> -isopropylacrylamide
BSA	Bovine Serum Albumin	PBS	Phosphate Buffered Saline
CAH	Contact Angle Hysteresis	PDMS	Polydimethylsiloxane
DMEM	Dulbecco's Modified Eagle Medium	PEG	Polyethylene glycol
ECM	Extracellular Matrix	PIPAAm	Poly(<i>N</i> -isopropylacrylamide)
EDC	<i>N</i> -(3-Dimethylaminopropyl)- <i>N</i> -ethylcarbodiimide hydrochloride	PIPAAm-PS	PIPAAm Grafted Polystyrene
FBS	Fetal Bovine Serum	PS	Polystyrene
FN	Fibronectin	P/S	Penicillin-streptomycin
FNFlat	FN coated flat PDMS	RGD	Arg-Gly-Asp
FN^{Rough}	FN coated rough PDMS	SAM	Self-assembled Monolayer
FN^{Petri Dish}	FN coated Petri Dish	SCFS	Single Cell Force Spectroscopy
		SiC	Silicon Carbide
		UN^{Petri Dish}	Unmodified Petri Dish

List of Variables

σ	Stress	$\Delta\theta$	Contact Angle Hysteresis
ε	Strain	θ_c	Critical Angle
η_c	Refractive Index of ATR Crystal	d_{\max}	Maximum Cantilever Deflection
η_s	Refractive Index of Sample	d_0	Baseline Cantilever Deflection
γ_{gs}	Interfacial energy, gas-solid	E	Young's Modulus
γ_{lg}	Interfacial energy, liquid-gas	f	Fraction of surface in contact with liquid
γ_{sl}	Interfacial energy, solid-liquid	f_{afm}	Masked Surface Area / Total surface area
γ_{total}	Surface Free Energy	F_{adh}	Adhesion of Cell
γ_l	Surface Tension	k	Cantilever Spring Constant
θ_a	Advancing Contact Angle	l	Roughness Sampling Length
θ_r	Receding Contact Angle	R_a	Roughness Average
θ^*	Static Contact angle on a rough surface	R_{rms}	Root Mean Squared Roughness
θ_0	Static Contact angle on a smooth surface		

Abstract

The growth and morphology of fibroblasts cultured on a physically and chemically modified surface was investigated. The need to understand cellular relationships with surface topography and chemistry is essential in the fields of biomedical engineering and biotechnology. It is well documented that mammalian cell behavior senses and responds to the surrounding micro- and nano- scale environment, but the research defining the chemistry, surface architecture, and material properties for control of this behavior is still in its infancy. The cell response to a substrate is complex, involving membrane proteins, extracellular matrix (ECM), cytoskeletal rearrangement, and changes in gene expression. Conventional cell culture is carried out on two-dimensional (2-D) cell culture platforms, such as polystyrene (PS) or glass, and forces cell behavior to adapt and adhere to an unnatural, planar environment. The biological behavior of these cells is used as a starting point for drug screening, implant design, and metabolic processes, but this is a misrepresentation of cells in their native environment. This discrepancy may be hampering biological research or initiating experimental efforts that are invalid. This body of work seeks to address these issues and contains established protocols for inexpensive, *pseudo* three-dimensional (3-D) culture scaffolds. The research described offers a multi-disciplinary approach for fabrication of biomaterials to achieve user defined or *in vivo* cell behavior using human fibroblasts.

To provide insight into the design of alternative cell culture templates we have analyzed cell-surface interactions and characterized the surface properties. The substrates fabricated utilized micro-roughened surface topography with 2 – 6 μm wide features and surface chemistry as a method for controlling cell behavior. Surface roughness was templated onto polydimethylsiloxane (PDMS) and PS. The fabricated polymer surfaces have been characterized

by atomic force microscopy (AFM), contact angle goniometry, fluorescence microscopy, and infrared (IR) spectroscopy. Initial studies of the textured surface yielded a super-hydrophobic surface with a 154° contact angle and high surface adhesion that was investigated using surface free energy calculations. This was followed by modification of the micro-roughness with self-assembled monolayers (SAMs), proteins, or thin films of polymer for use as a culture platform for cells. Cell behavior on the modified polymers was compared and analyzed against unmodified surfaces and tissue culture PS dishes. Cell morphology on rough PDMS surface was altered by the surface topography decreasing the average cell area to $1760 \mu\text{m}^2$ compared to an average cell area of $3410 \mu\text{m}^2$ on smooth PDMS. Gene expression changes were also noted with a 2.3 fold increase in the matrix metalloproteinase, MMP14, in cells on the rough surface compared to cells cultured on Petri dishes. Surface roughness was also combined with other surface modification methods for cell culture, including cell alignment and cell sheet engineering. $50 \mu\text{m}$ wide lines of fibronectin (FN) patterned on the rough PDMS induced cell directionality while still maintaining a *pseudo* 3-D culture system creating the first cell culture surface of its kind. The micro-roughness was also templated onto PS and chemically modified with a thermo-responsive polymer. This novel surface produced confluent cell sheets that detached from the surface when cooled below 32°C . Cell sheets cultured on the modified PS surfaces had an increase in FN fibril formation stimulated by the surface roughness when compared to cell sheets detached from a smooth, control surface.

The minor alterations to surface topology were proven to be effective in modifying cell biochemical response compared to cells cultured on flat substrates. Differences in surface topography and chemistry stimulated changes in cell adhesion, cytoskeletal arrangement, ECM composition, and gene expression. These cell properties were used as markers for comparison to

native cell systems and other reports of 3-D culture scaffolds. The mechanism of altering cell response is discussed in each chapter with respect to the specific type of surface used and compared to cell response and behavior on planar culture systems. New fabrication procedures are described that include the incorporation of other surface modification techniques such as SAMs, surface patterning, and thermo-responsive polymer grafting with surface roughness for original cell culture platforms to mimic an *in vivo* environment. The research presented here demonstrates that micro- and nano- changes to surface topography have large impacts on the cell-surface relationship which have important implications for research and medical applications involving adherent cells.

1.0 Introduction

1.1 General Introduction

The application of micro- and nanotechnology to surfaces delivers the tools necessary to stimulate cell behavior from the bottom-up, regulating control of the cell-surface interface. The idea and concept of nanotechnology was first hypothesized in 1959 by the physicist Richard Feynman in a lecture titled, “There’s Plenty of Room at the Bottom” in which he describes future technologies capable of manipulating single atoms and the miniaturization of data storage¹, but the field of nanotechnology wasn’t defined until 1986 by Eric Drexler². Drexler stated in his book *Engines of Creation*: “Molecules will be assembled like the components of an erector set. Just as ordinary tools can build ordinary machines from parts, so molecular tools will bond molecules together to make tiny gears, motors, levers, and casings, and assemble them to make complex machines.” The field was rapidly adopted by the engineering, physical, and medical sciences because of the versatility of nanotechnology. In the field of surface chemistry, nanotechnology allowed the fabrication of surfaces to be controlled at the molecular scale making them applicable for nano-patterning, biosensors, and microelectronics^{3, 4}. The ability for surface chemistry to manipulate biological interactions at the nano- and micro- scale could now be realized as well as observed with techniques such as atomic force microscopy (AFM). Since then, the field of surface chemistry has grown with increasing applications in biology, materials, and physics for a multi-disciplinary dynamic⁵. Surface chemistry has incorporated nanotechnology and micro-fabrication techniques for the design of surfaces that offer control over cell and tissue biochemical behavior.

In vitro cell studies are precursor models to understanding *in vivo* behavior. Thus, the impact of the *in vitro* environment on cell behavior must be fully understood to compare it to

behavior of cells in a native system. The development of substrates for cell culture requires three focal points to be addressed so the complex bio-surface relationship can be understood. These focal points are surface material, topography, and chemistry (Figure 1.1) and represent the main substrate influences for *in vitro* cell behavior. All of the focal points overlap with one another and changes to one point ultimately affects the other two. Alterations in this system leads to changes in cell signaling, adhesion, and gene expression. Understanding which substrate changes lead to the desired *in vivo* cell behavior will be fundamental for the future of cell culture *in vitro* experimentation.

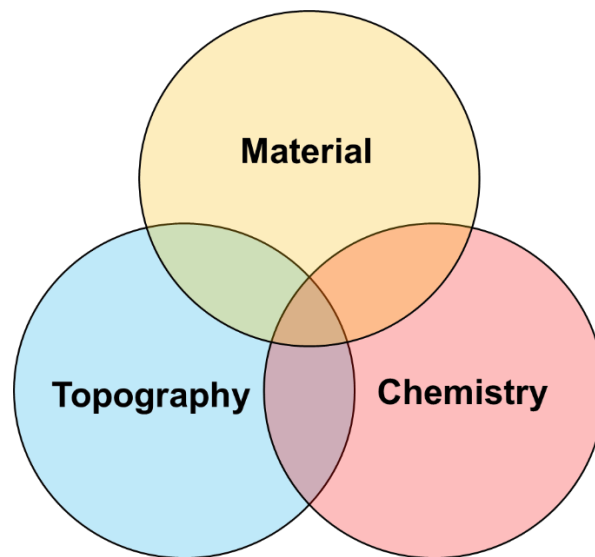


Figure 1.1. The three focal points of substrate influence on cell behavior.

The first focal point, material, is essential, as optical clarity, elastic modulus, and bulk material properties will be decided by the material chosen. Cells sense surface stiffness by the traction force needed for them to be motile and migrate. The second point, topography, describes the nano- and or micro- scale features of a surface. No surface is completely flat and all substrates have surface features. Cells sense these features during adhesion and migration and respond

accordingly by rearranging their cytoskeleton and extracellular matrix (ECM). The final point, chemistry, will define the molecular interactions cells and proteins will encounter on the surface. Surface chemistry can be controlled with deposition of self-assembled monolayers (SAMs) or thin films and is advantageous for defining cell adhesive or non-adhesive regions on the substrate. Together, these focal points are used for formation of biocompatible surfaces for cell culture. In this thesis, the term 'biocompatible' encompasses the traditional definition of a surface that causes no adverse effects in a biological system, but more importantly includes surfaces that encourage cell and tissue integration.

Overlap of the focal points are used for the design of substrates with specific surface properties to influence cell behavior. Colloidal micro-particles bound to a surface can be modified with a hydrophobic molecule to create super-hydrophobic wetting; a flexible polymer surface can be fabricated with nano-pillars to force localized cell adhesion; or a glass surface can be stamped with a protein pattern for directed cell growth. When compared to each other all of these samples would yield different cell behavior and the behavior would differ between different cell types. The ultimate goal of biomaterial and surface designs is to obtain *in vitro* data that gives insight into *in vivo* systems or to create a unique bio-environment for a singular, desired biological response. This is achieved with in-depth characterization of the surface and material properties and their effect on cell-surface interface. Although considerable advances have been made in understanding the impact of surface properties on biological functions, the field is still in its infancy and substantial work remains to grasp the complex interaction between biological mechanisms, cell performance, and various physical and chemical properties.

The remainder of the introduction will focus on: a summary of the cell-surface interface and a description of specific biological markers for monitoring cell response, current and past

research dedicated to the three focal points described, and how these focal points impact cell-surface relations. Although the work described is multi-disciplinary, the chemistry of each system is thoroughly discussed.

1.1 Cell-Surface Relationship

In a living tissue cells perform a variety of biochemical activities for tissue functionality. In this environment, cells are interacting with other cells and surrounding tissue in a 3-D system with extracellular chemical and biological signaling. This environment is complex and highly organized and mimicking that complexity *in vitro* is not currently possible, but a substitute for the system can be derived from simpler culture platforms and scaffolds with defined properties. Culture dishes and scaffolds have been utilized for studying cell behavior outside the body since 1839 when Theodor Schwann and Matthias Jakob Schleiden predicted humans were composed of cells^{6, 7}. In 1925, the American Type Culture Collection standardized mammalian cell culture protocols generating significant and reproducible biological research⁸. This led to reproducibility in cell culture systems, including glass or tissue culture polystyrene (PS) culture dishes, wells, or plates. PS culture dishes are inexpensive, optically transparent and a universally accepted cell culture system for *in vitro* studies. Cell behaviors on this environment are used as predictive assays for *in vivo* cell behavior. However, there is growing concern that the planar, 2-D environment of glass or PS alters cell biology and raises questions of the physiological relevance of cells on culture dishes^{9, 10}. The benefits of using PS or glass alternatives, such as 3-D culture systems, have been noted since 1972 when Tom Elsdale and Johnathan Bard cultured lung fibroblasts on fibrous collagen gels and compared them to cells on glass¹¹. Cells on the gel looked and exhibited behavior similar to human lung cells *in vivo*, while fibroblasts on the glass did not. The large differences in behavior between the two culture systems led Elsdale and Bard to ask, “Housed in more traditional

residences constructed of water and collagen instead of plastic or glass, do cells lead primitive, less cultured lives?” The question represents the doubt of 2-D plastic or glass culture as a representative model for a living organism. Since then, significant differences have been recorded when comparing cells on tissue culture PS and cells in 3-D or modified culture systems¹².

In vitro, the cell and cell ECM are in contact with the culture surface. The cell's interaction with this environment will determine its growth, migration, differentiation, ECM modeling, and survival¹³. The cell culture topography, chemistry, and bulk material properties can decide a cell's biochemical reaction, thus understanding of the cell-surface relationship is fundamental in applied biomedical science. A large volume of work has been completed in designing scaffolds and surfaces to influence the cell-surface interaction¹⁴, but because of the large number of variables (cell type, surface morphology, surface chemistry, bulk material) understanding the relationship between the cell and surface still remains a daunting task. By identifying the factors that control cell behavior *in vivo*, it is possible to design topographical surface features and chemistry *in vitro* to mimic the cell's native environment. Observing *in vivo* characteristics such as tissue stiffness, protein composition, and tissue porosity help model biomaterial surfaces.

1.1.1 Extracellular Matrix (ECM)

In a native environment, mammalian cells are anchored by highly organized, multifunctional proteins and polysaccharides, collectively known as the ECM. Through the ECM cells are capable of gathering information from their immediate physical and chemical environment¹⁵ as shown in Figure 1.2. ECM composition varies from tissue to tissue, but is typically composed of collagens, proteoglycans, fibronectin (FN), laminin, and other

glycoproteins. On a surface, cells will develop their ECM based on their surrounding micro- and nano environment. The ECM can directly or indirectly influence cell behavior and altering the ECM *in vitro* can control specific cell biochemistry^{16, 17} or ECM can be utilized for bio-interfaces to control cell adhesion. One of most widely studied and employed ECM proteins for surface modification is FN¹⁸. FN is a large glycoprotein dimer that is found circulating in the blood in a soluble, non-functional closed form or in an insoluble fibril form in the ECM¹⁹. Including FN or other ECM proteins on a surface encourages cell directionality, tissue integration, and wound healing^{20, 21}. The ECM is constantly being remolded as cells build up, reassemble, or degrade it and the processes are based on integrin assembly at the cell membrane²². The hierarchy of the ECM assembly is not well understood, but it is known that cellular integrins mediate the process and are essential for its formation.

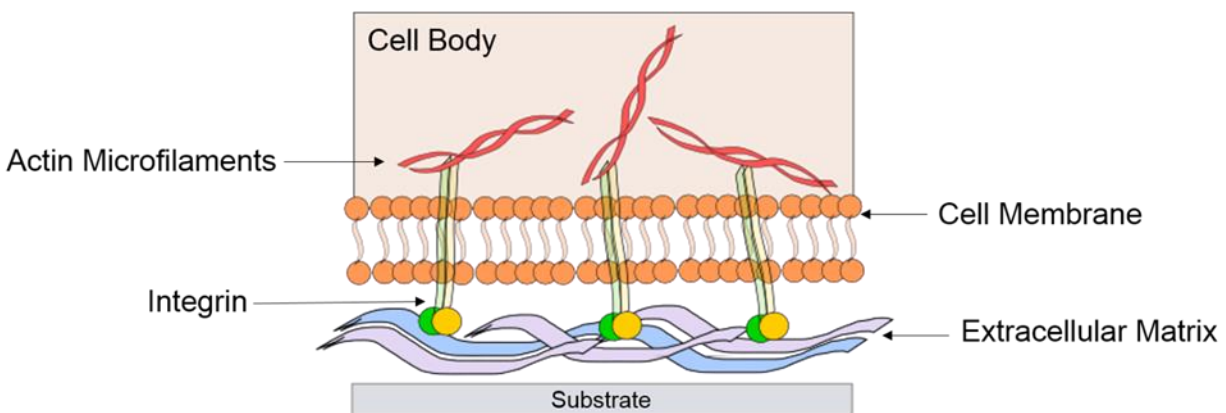


Figure 1.2. Schematic representation of cell-ECM interactions at the cell membrane.

1.1.2 Integrins and Actin Cytoskeleton

Changes in the a cell's environmental surrounding invoke changes in the cytoskeletal organization as well as the organization of the adhesive molecules in the cell such as integrins²³.

Integrins are transmembrane protein receptors between the ECM and the actin cytoskeleton (Figure 1.2). They are composed of two subunits, α and β . There are 18 known α subunits and 8 known β subunits with 24 combinations recorded²⁴. Each α - β combination has its own binding specificity and is capable of signaling through the cell membrane in either direction. The cell can signal through integrins to bind to the ECM (inside-out signaling) or changes in the ECM or surrounding environment can be chemically signaled to the cell (outside-in signaling). Outside the membrane, integrins are capable of recognizing certain amino acid sequences of individual ECM proteins and binding to them. One of the most commonly bound sequences by integrins is Arg-Gly-Asp (RGD) and is found in FN and collagen²⁵. The RGD sequence is recognized by most of the integrin α - β combinations. Binding of the integrins to the ECM elicits a cascade of cell signaling and response including cytoplasmic kinase activity, growth factors, ion channels, and cytoskeletal rearrangement²⁶.

As integrins bind to the ECM, they become clustered in the cellular membrane and stimulate the assembly of actin filaments. Once integrins contact the ECM, cells will extend filopodia projections from the leading edge of cell, the lamellopodia, for sensing the surrounding environment and continued spreading. Integrins at the tip of the filopodia will cluster and initiate the formation of focal adhesion points and actin stress fibers. The focal adhesion points are found at the ends of prominent actin filament (stress fibers). The actin filaments of the cytoskeleton are made up of two-stranded helical polymers of the actin protein that link to integrins. The actin cytoskeleton determines the shape of the cell (Figure 1.3) and is necessary for cell motion. As the cell creates more focal adhesion points, a signal is directed for the recruitment of cytoskeletal components at the lamellopodia. This generates a pulse to propel the cell forward using traction force on the surface²⁷, advancing the cell. The link between integrins and the actin cytoskeleton

is strong and alterations to the system can trigger a large variety of signal transduction events including morphology, motility, gene expression, and differentiation²⁸. Inside-out signaling to the integrins also occurs with cytoskeleton changes. Rearrangement of the actin cytoskeleton can signal integrin rearrangement and increase or decrease their ability to bind to the ECM¹³.

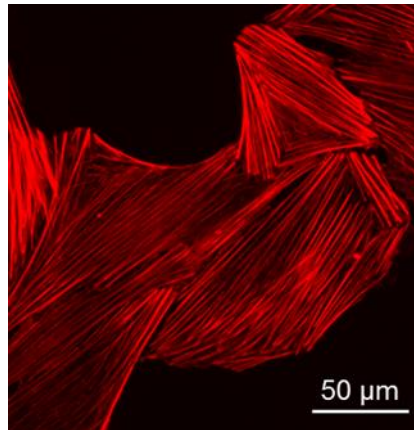


Figure 1.3. Fluorescent microscopy image of actin filaments (stress fibers) of the cytoskeleton in human fibroblasts.

1.1.3 Cell Adhesion

As described in the previous sections, cell adhesion is closely related to cellular ECM, integrins, and cytoskeletal organization. It is the first response that a cell achieves when coming into contact with a surface. For active cellular adhesion, the cell makes contact to the ECM through focal adhesion points that are a few square microns in area and located at the periphery of the cell. These points strongly bind the cell to the substrate by anchoring actin filaments with a plaque composed of proteins such as vinculin. Fluorescent labelling of vinculin is often used to visualize focal adhesions on a cell. The formation of actin stress fibers, as shown in Figure 1.3, are indicative of a cell cultured on a planar environment. Here, the cell is capable of large amounts of spreading and growth, putting tension on the cell membrane. The tension initiates focal adhesions to keep

the large cells adhered to the surface and actin fibers help anchor the cell to the 2-D environment²⁹. As the focal adhesions mature, the cell begins to also exhibit fibrillar adhesions. Here, soluble FN is converted into insoluble FN fibrils for the ECM in a process known as fibrillogenesis and present new adhesion points for integrins^{19,30}. Images of focal adhesion points and fibrillar adhesions can be seen in Figure 1.4. Creation of FN fibrils in the ECM is highly regulated by cell signaling and occurs only after the cell has been adhered for some time and has applied tension to the culture surface³¹. However, in 3-D cell culture matrices, this delay is not observed and instead co-organization of focal adhesions and fibrillar adhesions are noticed immediately. This is a significant difference of cell culture on a planar substrate compared to growth of cells within a 3-D matrix and it is possible to influence both focal adhesion and fibrillar adhesions by design of the cell culture platform.

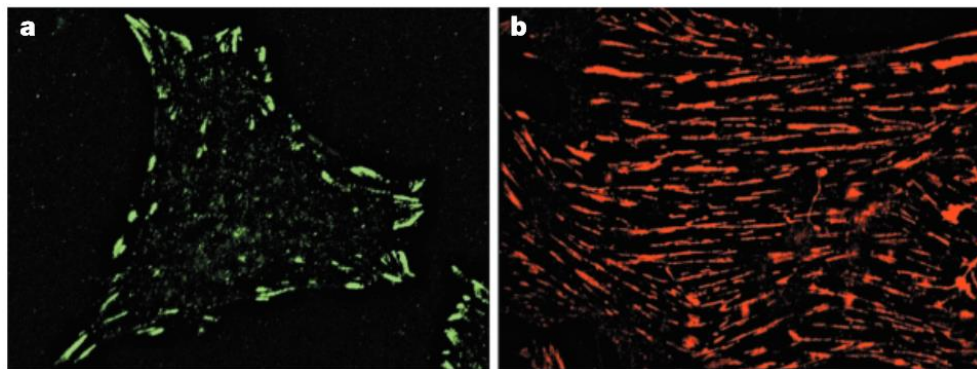


Figure 1.4. Human fibroblast with (a) focal adhesion points (b) and fibrillar adhesion sites fluorescently labelled³¹.

Nonspecific interactions of the cell with the substrate can also alter cell behavior. The nonspecific interactions can be classified as passive cellular adhesion. These include electrodynamic, steric, hydrophobic, and van der Waals forces between the cell membrane and the material surface³². These interactions do not require recognition of cellular membrane proteins³³.

Once cells have contacted a surface through passive adhesion they are constantly altering their cell membrane to stabilize the cell-material interface using active adhesion.

1.2 Surface Topography

Design of surface features to mimic a natural biological environment has been used by researchers over the past century. Micro- and nano- surfaces are found on many plants and animal species as seen in Figure 1.5, but the first recorded 3-D cell culture study was performed by Ross Harrison in 1907 while he was investigating the growth of nerve fibers². Harrison implanted frog embryos on a clotted frog lymph and inverted the system to create a hanging drop culture creating one of the first 3-D systems for cell culture. Unlike the work by Elsdale and Bard (Section 1.1), Harrison did not compare his 3-D drop culture to a 2-D platform and the novelty of his culture method wasn't recognized until much later on. Today, a large variety of techniques are used to alter the surface architecture to control or alter cell behavior, such as electron beam lithography¹³ and photolithography³⁴ to generate non-planar environments for cell culture. These techniques can be used to fabricate randomly oriented structures similar to Figure 1.5a and 1.5b or more ordered topographies similar to Figure 1.5c.

As mentioned in Section 1.1, a large portion of cell fate is decided by integrin-cytoskeleton arrangements and ECM organization of the cell. Alternations in ECM or integrin-cytoskeleton links can trigger a large variety of signal transduction events including morphology, motility, gene expression, and differentiation²⁸. Minor topographical features can be used to control these signaling events and even create cell culture conditions similar to a native cellular environment³⁵. Surface structure is imperative to biological function as observed in the variety of shapes and sizes

witnessed in the tissues of living organisms. An understanding of the wide range of surface textures in living organisms will lead to the development of artificial surface features for biomaterials to mimic native materials.

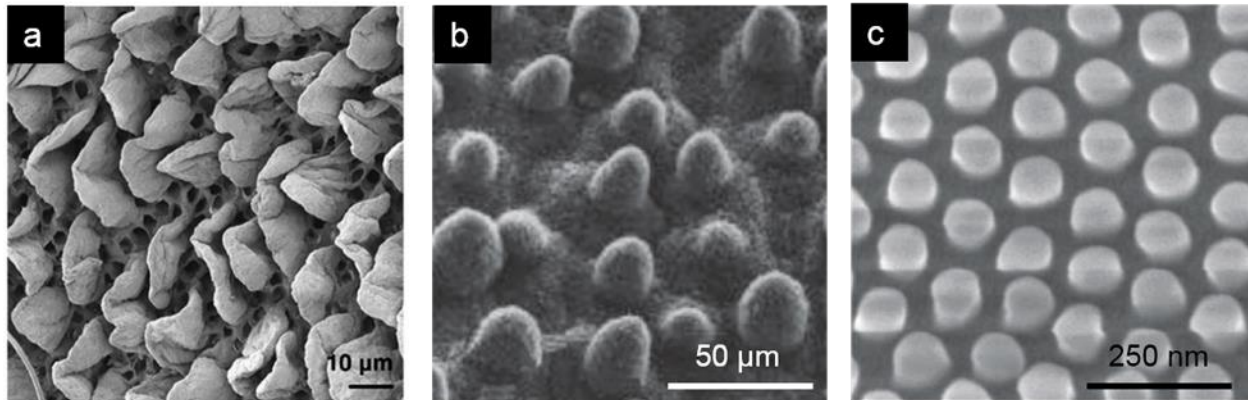


Figure 1.5. SEM images of (a) villi of rat intestine³⁶, (b) surface of lotus leaf³⁷, (c) and nanostructure of mosquito eye³⁷.

1.2.1 Surface Roughness

Surface roughness has been used as a simple method for altering a tissue scaffold surface. From a biomaterials perspective, roughening can offer an opportunity for integrating and binding living tissue to an inorganic prosthetic³⁸. Surface roughness relates to the degree of protrusions or depressions on a material surface. Random topographies that incorporate surface roughness are more easily fabricated and less expensive to generate than organized topographies. The average roughness value (R_a) or root mean squared roughness (R_{rms}) is used to quantify the degree of roughness of a surface by analyzing surface deviations from planar form³⁹. These values can be calculated on a 2-D line or a 3-D section of area. In 2-D, roughness parameters are evaluated over a single line or cross section. In 3-D, the surface area is divided into sections and the 2-D roughness parameters are calculated for each linear section and then averaged together for the final roughness

value. The R_a is defined as the average absolute deviation of the roughness irregularities from the mean line over sampling length (l) as described in Equation 1.1 and shown in Figure 1.6.

$$R_a = \frac{1}{l} \int_0^1 |y(x)| dx$$

Equation 1.1.

This parameter is well defined and easy to compare to other material R_a 's, but it is not ideal for quantifying small changes in the surface roughness.

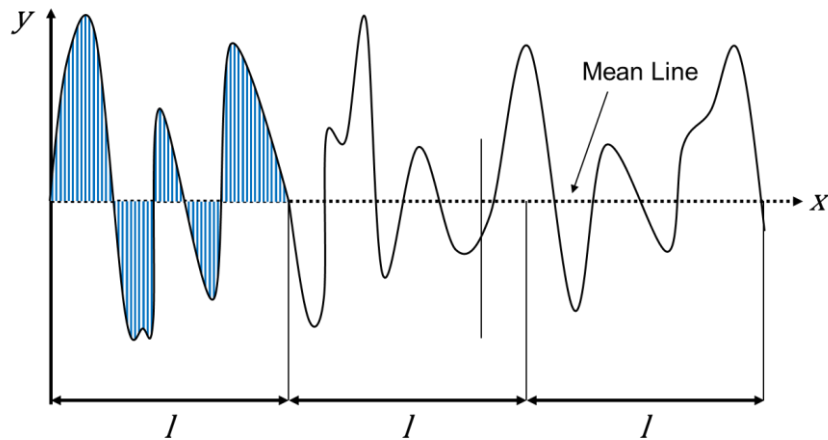


Figure 1.6. Graphical representation of roughness average (R_a) analysis on a horizontal cross-section of a surface. The shaded area represents the deviation of roughness from the mean line.

The R_{rms} parameter is defined as the standard deviation of the distribution of surface heights as seen in Equation 1.2 and is more sensitive to deviations in the mean line than the R_a . The R_{rms} is valuable for a statistical description of the surface's roughness⁴⁰.

$$R_{rms} = \sqrt{\frac{1}{l} \int_0^1 \{y(x)\}^2 dx}$$

Equation 1.2.

Roughness values can be calculated from surface analysis techniques such as atomic force microscopy (AFM). However, R_a or R_{rms} alone is not enough to define a surface's characteristics as some surfaces have similar R_a values but very different geometry or porosity. Visual images of the surface topography acquired using AFM, optical microscopy, or scanning electron microscopy are used in conjunction with roughness analysis for a complete understanding of the surface topography. Well controlled roughness has been achieved in a variety of procedures including surface blasting, oxide formation, and electron beam lithography^{30, 41}. The ease of fabricating these surfaces has been exploited on the surface of implants. For example, titanium implants into bone tissue often exhibit a degree of roughening for increasing integration of osteoblasts into the implant⁴². Subtle differences in roughness are detected by cells and have proved efficient in proliferation, metabolism, and differentiation^{31, 43}. Cells cultured on micro-rough surfaces form focal attachments that allow the cells to span between peaks on the surface forcing altered cytoskeletons and gene profiles⁴⁴. Nano-scale roughness has also been investigated and proven to be desirable for most cell types. The theory behind cell affinity for nano-roughness is the ability of the surface to resemble the nano-features of the ECM and act synergistically with cellular ECM modeling⁴⁵.

1.2.2 Regular Surface Topographies

More organized and well-defined topographies include surfaces with geometrical domains such as posts and grooves. Ordered textures are capable of aligning cells as they migrate. This phenomenon was demonstrated in 1964 when A. S. G. Curtis and Malini Varde noticed cells following the curvature of a glass coverslip⁴⁶. Grooves and ridges have been shown to align almost

every adherent cell type with the direction of the pattern⁴⁷ (Figure 1.7). This event is known as contact guidance. The cells alter their morphology to become more elongated and arrange their actin bundles with the groove. The depth and width of groove is also essential in determining organized cell growth⁴⁸. Loesberg *et al.* determined that a minimal groove depth of 35 nm and 100 nm groove width is needed for triggering fibroblast alignment⁴⁹. Smaller physical dimensions did not affect the cell morphology. Micro-posts are another commonly used geometric surface feature. They induce minimal cell alignment, but can alter cellular adhesion and proliferation⁵⁰.⁵¹. Ordered surface geometries are easy to compare between each other because their topography is more defined and quantified than roughness values.

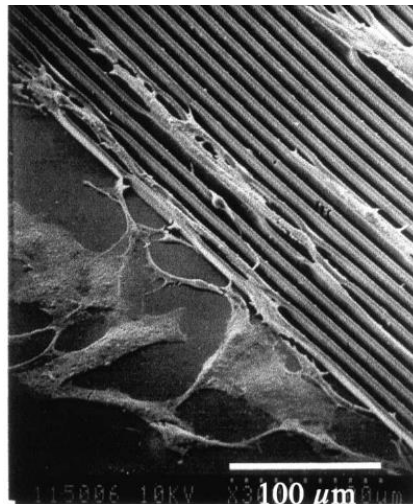


Figure 1.7. Example of epithelial cells aligning with 7 μm grooves, 3 μm deep⁴⁷.

1.3 Surface Chemistry

Chemistry at an interface has played a fundamental role in the development of nanotechnology over the past three decades. Molecular engineering and chemistry constrains the dimensions of a system for formation of nanocrystals, nanowires, and nanotubes⁵². Surface bound

molecules are a form of nanotechnology as they form 1 – 10 nm films or layers on a surface with the capability of being organized and patterned. Atoms and molecules at the surface experience a different environment from those in the bulk and exhibit different free energy, mobility, and structure³. Although material properties, such as hardness and plasticity, are not altered by surface chemistry, bulk properties have played a significant role in the design of biological substrates and materials^{53, 54}. Surface chemistry can define cell adhesive⁵⁵ and non-adhesive areas⁵⁶, cell morphology⁵⁷, and induce cell alignment and patterning⁵⁸. A cell is composed of many sophisticated, organized nanosystems (proteins, enzymes, DNA) and cell interactions with surface chemistry impacts the functionality of these systems. Surface modification is possible for metals, polymers, and glass and offers multiple surface chemistries for cell culture. Once a surface is incubated in a cell culture medium, immediate protein and salt deposition occurs followed by cell attachment and ECM formation between the cell and the surface. Surface chemistry indirectly effects cell behavior by altering protein and ECM deposition and changes in these factors control cell signaling and cell fate. There are a wide variety of protocols for altering surface chemistry and they will be discussed further in the following sections along with how they can be utilized for controlling biological behavior.

1.3.1 Self-Assembled Monolayers (SAMs)

Self-assembly describes a process in which a disorganized system becomes organized through individual interactions between components without any external influence. Hydrogen bonding, π - π stacking, and van der Waals forces are types of interactions that drive self-assembly. Self-assembled monolayers (SAMs) are an established method of functionalizing a surface and

engineering surface chemistry with approximately 1 – 3 nm of organic material⁵⁹⁻⁶¹. Bare, clean surfaces of metals, glass, and polymers readily adsorb organic materials in solution or gas decreasing the surface free energy; as the organic units organize the macromolecular assembly is more stable than the unassembled components⁶². The first studies of organic films on surfaces were conducted in 1920 by Irving Langmuir⁶³ and in 1935 by Katharine Blodgett⁶⁴ by depositing layers of fatty acids formed at the air-liquid interface onto solid substrates by physisorption. This work was continued by Bigelow *et al*⁶⁵ in 1946 using solution deposition of molecules to form hydrophobic monolayers on platinum surfaces. In 1983, the term ‘self-assembled monolayers’ (SAMs) was coined by Lucy Netzer, Jacob Sagiv, and Radu Iscovici after they analyzed the deposition of chlorosilane monolayers and multilayers onto silicon^{12, 66, 67}. In the same year Ralph Nuzzo and David Allara discovered absorption of disulfide monolayers onto gold⁶⁸. Since then SAMs have become a useful tool in modifying surfaces for a variety of applications including; wettability, patterned cell culture, catalysis, corrosion resistance, and surface based sensors⁶⁹⁻⁷¹. Examples of SAMs on a variety of substrates can be seen in Figure 1.8. SAMs and thin films have the ability to alter surface chemistry while bulk properties of the material are maintained. They have become a popular tool for altering surface chemistry because of their ease of use in ambient conditions and ability to tailor the surface properties of a large variety of materials.

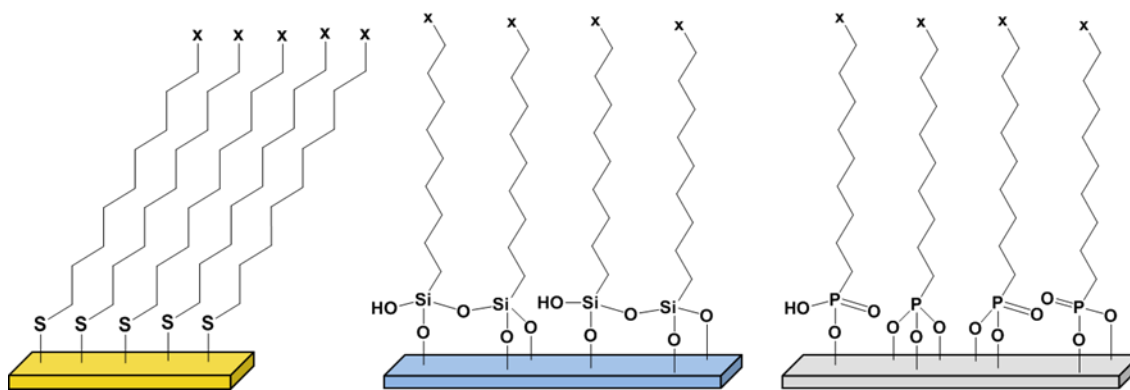


Figure 1.8. Schematic example of self-assembled monolayers (SAMs). (Left) Alkylthiol SAM on a gold substrate. (Middle) Alkoxysilane SAM on a glass substrate. (Right) Phosphonic acid SAM on a titanium oxide substrate. X can represent a variety of organic or inorganic head groups.

1.3.1.1 Alkanethiols

Alkanethiols on gold are the most studied of all the SAM systems. They are well characterized and the experimental conditions for their formation are now a standard in many different research laboratories¹⁵. Gold substrates are easily fabricated by evaporation of the metal onto silicon wafers, glass, or plastic surfaces and the metal is relatively inert making gold capable of being handled under normal atmospheric conditions. Thiols bind to gold with high affinity⁶⁸ and can remain stable on the surface for weeks after SAM deposition. Gold is also biocompatible and a widely used substrate for SAM-cell interaction studies¹³. The ease and convenience of the gold-thiol relationship has been exploited for the development of sensors, photovoltaics, and cell manipulation²⁸.

SAM preparation involves immersing a clean gold substrate in a low concentration of thiol solution in an organic solvent for 12 – 24 hours, removing the substrate, and rinsing away any physisorbed thiol. Once the gold is incubated in the thiol solution a two-step deposition process occurs; a thiol-gold bond is formed almost immediately followed by a slower reorganization of the

monolayer into a crystalline 2-D structure to stabilize the film⁵⁹. The organization of the monolayer is based on the terminal group (CH₃, OH, NH₂, PEG), the chain length of the molecule, and the interaction of the molecular components. Secondary modification of the layer can be used to covalently bind larger molecules or proteins.

1.3.1.2 Silanes

Silanes offer molecular surface modification for glass, silicon, quartz, and polymers. Organosilane SAMs typically have one organic moiety and three hydrolyzable moieties. Silane surface modification is commonly carried out with alkoxy groups as the hydrolysable components. Reactions with these molecules can be performed in the presence of water for hydrolytic deposition on a substrate with available hydroxyl groups. Only a small concentration of water for organosilane deposition is needed and is available on the substrate surface or atmosphere. An example of the hydrolytic deposition can be seen in Figure 1.9. The four-step reaction begins with hydrolysis of the three alkoxy groups. Condensation can occur producing oligomers of the silane. The oligomers and remaining monomers will hydrogen bond with hydroxyl groups on the substrate. The final step involves dehydration and the formation of a covalent bond with the substrate. The resulting monolayer is robust and can be stored for long periods of time. Silane deposition protocols are similar to thiol deposition protocols on gold. Substrates are incubated in a low concentration of alkoxy silane in an organic solvent at room temperature. Reaction times vary according to the silane chemistry and range between 1 and 6 hours. Solvent free, vapor deposition of silane may be carried out under vacuum at higher temperatures. Anhydrous deposition of organosilanes offers an alternative to hydrolytic silane deposition, but requires the presence of a catalyst and extended reaction times. Anhydrous deposition is executed with either

alkoxysilanes or chlorosilanes. Instead of three alkoxy groups, chlorosilanes have three chloro moieties making them highly reactive and requiring anhydrous environments. Chlorosilanes are more reactive with surface hydroxyl groups but they often produce disordered monolayers. Deposition parameters such as humidity, temperature, and silane concentration can alter the SAM dramatically^{59, 72}.

Unlike SAMs on gold, high quality ordered monolayers of silanes are difficult to produce⁷³. Changes in monolayer composition and uniformity can be altered by water concentration⁷⁴ where SAM pinholes and defects are formed. In the absence of water and with no catalyst, silane monolayers are inconsistent, but excess water can result in polymerization of the silane in solution that can form multi-layers of silane on the surface⁷⁵. Due to variability of these parameters, silanes on surfaces will be less ordered than thiols on gold, but the strength of the silane-surface bond makes silane SAMs more robust and stable than gold-thiol bonds. Like thiols, the organic groups of silanes are used for biocompatible surface or undergo secondary modification for formation of bioactive surfaces^{76, 77}.

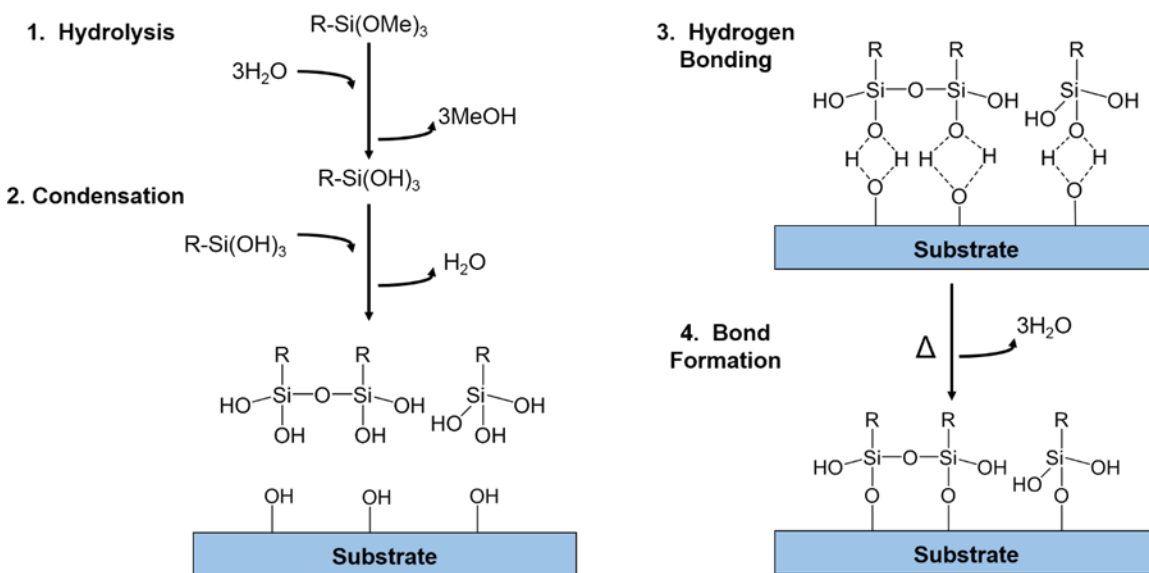


Figure 1.9. Hydrolytic deposition of an alkoxy silane onto a substrate.

1.3.1.3 Phosphonic Acids

Despite the large number of literature publications of thiols on gold and organosilanes on glass, research projects into SAMs for modifying metals used for engineering or industrial applications have been limited⁷⁸. This led to the development of phosphonic acids monolayers for metal and metal oxide surfaces, including aluminum oxide, titanium oxide, and indium tin oxide. Investigations into metal phosphonic acid chemistry have been rapidly growing since the early 1990s. Phosphonic acid films form protective, corrosion inhibiting layers on metals to prevent oxygen accessibility to the surface⁷⁹. Compared to silanes, phosphonic acids have a greater surface grafting density on titanium dioxide and zirconia⁸⁰. Binding of phosphonic acids to a metal results in various orientations of the molecule at the surface including mono, bi-, and or tridentate coordination to the surface. The acid binds by displacing hydroxide ions that are bound to the metal atoms at the surface⁸¹. A dilute solution of the required phosphonic acid is prepared in organic solvent or water and followed by metal or metal oxide surface incubation for at least 48

hours. For surfaces that can be damaged by phosphonic acid treatment, an alternative deposition method can be employed. Tethering by aggregation and growth (T-BAG) deposits a phosphonic acid SAM using multiple incubation and high temperature baking cycles to create a monolayer⁸². Monolayers of phosphonic acids are robust and stable and capable of undergoing secondary modification for new chemical moieties or biological molecules. The stability of phosphonic acids in physiological conditions and their high affinity for metals has led to investigations of SAMs on titanium for implants. Titanium substrates modified with phosphonic acids and RGD peptide sequences increased osteoblast proliferation when compared to osteoblasts on silane modified titanium or unmodified substrates⁸³. Although less studied than thiol and silane surface chemistry, phosphonic acid-metal chemistry has proven to be a useful tool for formation of stable, biocompatible surfaces on industrial metal substrates.

1.3.2 Biologically Active Surfaces

After deposition of a SAM, secondary chemical reactions are used to produce surfaces with functional biochemical moieties. The chemistry for attachment is limited only by known organic reaction mechanisms creating a large variety of attachment protocols. Secondary reactions on surfaces have been well documented^{71, 84} and provide pathways for attaching proteins, DNA, or other biologically active molecules⁸⁵. Binding of these molecules creates a surface that actively forces changes in cell membrane binding and cell signaling. A common secondary immobilization technique involves EDC/NHS (*N*-(3-Dimethylaminopropyl)-*N*-ethylcarbodiimide hydrochloride/*N*-hydroxy succinimide) chemistry for formation of an amide bond⁸⁶ to covalently bind proteins to a surface⁸⁷. The reaction mechanism can be completed in water and excess reagents of the reaction can be removed by rinsing the surface after incubation. A carboxylic acid terminated

SAM immersed in an aqueous solution of EDC/NHS will react with EDC to form an unstable ester intermediate, followed by a semi-stable intermediate with the NHS-ester, and a final reaction with a primary amine to form a stable amide bond (Figure 1.10).

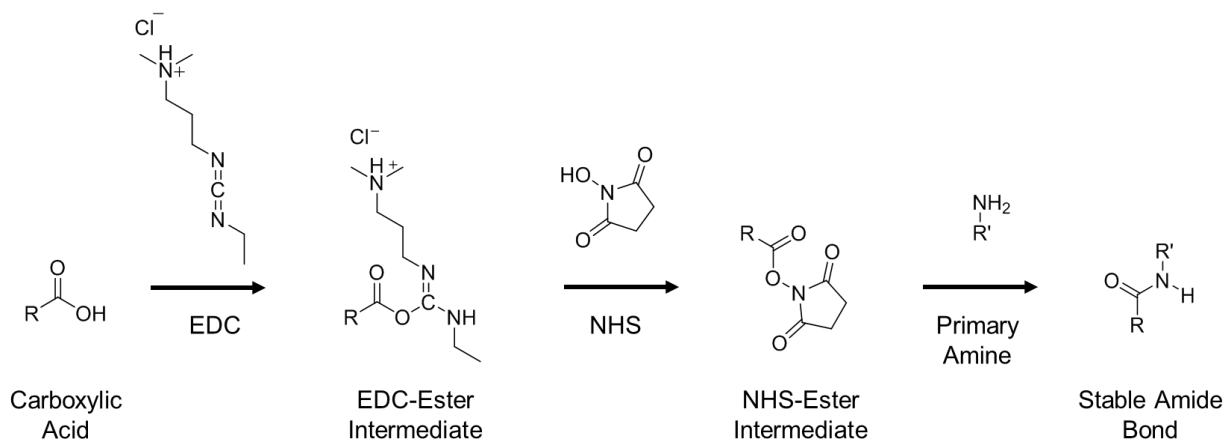


Figure 1.10. EDC/NHS amide bond formation

Other connection chemistries include pentafluorophenol and ‘click’ chemistry. Pentafluorophenol is another commonly used intermediate for forming an amide bond between a carboxylic acid SAM and amine functionalized biomolecule⁸⁸. More recently, click chemistry has been utilized as an organic route of attaching the desired biomolecule to a surface⁸⁹. Here, an azide terminated SAM is covalently linked to alkyne moiety using a copper catalyst for selective surface activation. For a catalyst free method of linking chemistry, an amine can be covalently attached to an aldehyde^{90,91}. Glutaraldehyde (GA) is one of the most commonly used aldehydes for this reaction as it will readily react with a primary amine to form an imine as a Schiff base (Figure 1.11). If the imine is tethered to a surface, the unreacted aldehyde moiety of the GA has the possibility for further modification with another amine in solution, making GA an ideal candidate for forming a linker between a surface and bioactive molecule.

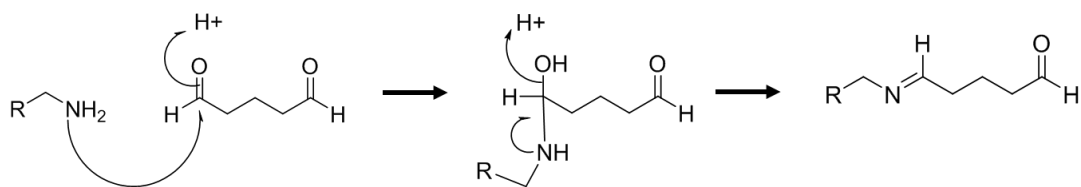


Figure 1.11. Schiff base formation between GA and a primary amine.

Physisorption of proteins onto surfaces is another simple technique to create a biologically active surface. Surfaces readily adsorb proteins onto the surface and create uniform layers almost immediately after incubation in a biological solution. For some biomedical research fields this has become a significant problem as protein adsorption disrupts the activity of bio-implants or attracts bacteria formation and increases the rate of infection. For more controlled protein deposition surface chemistry can influence adsorption. For bio-inert surfaces, surface bound molecules like polyethylene glycol (PEG), have shown to limit or eliminate protein binding altogether⁹². Other SAMs can promote protein adsorption and increase cell adhesion to those sites⁹³. Physisorption of a proteins represents a facile method for surface modification, but understanding why and how they adsorb to the surface is not fully understood. Parameters such as ionic strength, temperature, and buffer can alter the adsorption behavior⁹⁴, but it is agreed the major driving force behind protein adsorption is an entropy gain from the release of surface adsorbed water and salt ions and from structural rearrangements inside the protein⁹⁵. At low surface densities, proteins will orient themselves so oppositely charged regions contact the surface as seen in Figure 1.12a. Analogously, if the surface is hydrophilic, proteins will make surface contact with their hydrophilic residues. As the protein density of the surface increases, Figure 1.12b, protein-protein interactions become more dominant and proteins will re-orient themselves for less overall repulsive forces⁹⁶. Once the proteins are attached to the surface they can be difficult to remove creating a robust and stable bioactive surface if kept in a sterile, buffered salt solution. FN and bovine serum albumin

(BSA)⁹⁷ are common proteins to modify metals, polymers, and glass for cell adhesive and non-adhesive areas respectively.

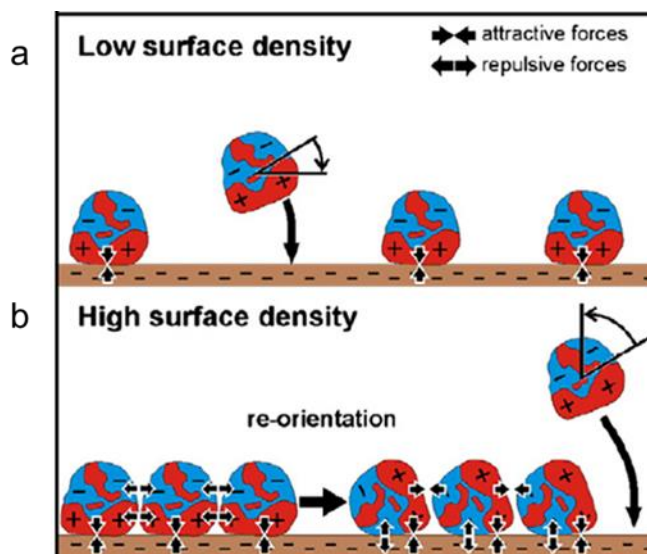


Figure 1.12. Example of protein deposition on a surface at (a) low (b) and high surface densities. The blue and red domains of individual proteins represent negatively and positively charged amino acids respectively⁹⁵.

1.3.3 Microcontact Printing

Microcontact printing was developed as a controlled method to “ink” a desired molecule or protein to a polymer stamp and print the pattern onto a substrate⁴. This technique is well defined and is commonly used with polydimethylsiloxane (PDMS) stamps. Features on the stamp’s pattern can be macroscopic down to 1.0 micron⁹⁸. Stamps are reusable so the pattern is consistent from one sample to the next. Patterns on the stamp are most commonly made using soft lithography⁹⁹. A silicon wafer is coated with a layer of photoresist (20 – 100 μm thick) and exposed to UV light through a patterned chromium/quartz mask. The areas exposed are rinsed

away with a base, leaving the patterned photoresist. Uncured PDMS prepolymer can be poured over the photoresist cast and allowed to cure with moderate heat. The final PDMS stamp is then peeled away from the photoresist-wafer to produce a stamp for microcontact printing. The stamp surface is modified or inked with a desired molecule and stamped onto a flat, clean substrate. The molecule is transferred from the stamp on the surface in the pattern of the stamp. A final optional step includes backfilling of the unmodified portion of the substrate with a different molecule by incubation of the stamped surface in a dilute solution of the 2nd molecule. A schematic example of the process is shown in Figure 1.13.

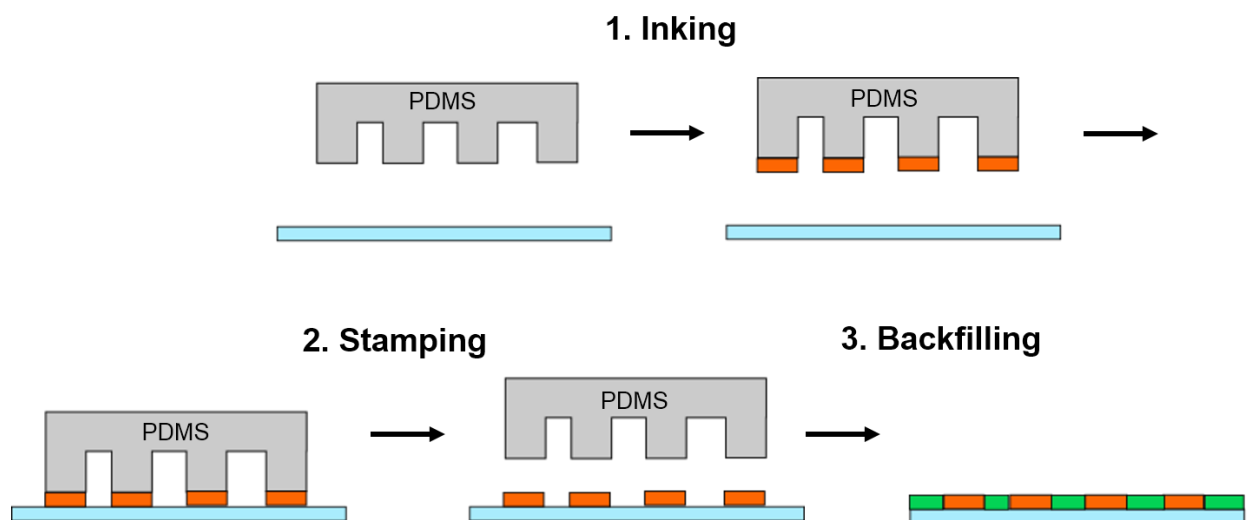


Figure 1.13. Example of microcontact printing. (1) A PDMS stamp is inked with a desired molecule and (2) stamped to transfer the molecule to the surface. (3) Backfilling with a 2nd molecule is used to cover the rest of the unmodified areas of the surface.

1.3.4 Surface Wettability

Surface wettability (hydrophobicity, hydrophilicity, surface free energy) is a prominent factor in many cell-substrate interactions as all biological systems are water based. Wettability is not dictated alone by surface chemistry; surface topography also plays a major role^{100, 101}, but wettability has been included in this introductory section because of the many reports that combine

chemistry and hydrophobicity¹⁰²⁻¹⁰⁴. Surface wettability is determined by measuring the contact angle of microliter drops of water at the surface as described in Section 2.4. It has been well documented that specific cell types prefer surfaces with specific hydrophobicity or hydrophilicity¹⁰⁵. As an example, Hela cells have a greater adherence on surfaces with a contact angle of 50°, but human umbilical vein endothelial cells prefer surfaces with a 40° contact angle¹⁰³. Chemical and topographical surface properties each contribute to wettability, so it is difficult to quantify cell behavior based on surface chemistry or topography alone. Both it should be assumed that both take some responsibility for cell behavior and protein adsorption¹⁰⁶. Altering wettability can be used in conjunction with techniques like microcontact printing to pattern hydrophobic or hydrophilic areas to encourage guided cell adhesion¹⁰⁷.

Surface wettability also establishes surface free energy. When a surface is formed there are disruptions of the intermolecular bonds and the surface becomes less energetically favorable than the bulk of the material. The surface free energy can then be defined as the excess energy of the surface when compared to the bulk. The amount of free energy at a surface depends on various factors such as material, chemistry, temperature, and interfacing material¹⁰⁸. As a quantitative measurement of surface properties, surface free energy determines if a surface is *high energy* or *low energy* by analyzing the ability of a liquid to spread or not spread on the surface. The easiest method for calculating the surface free energy is to examine the contact angles of different liquids (polar and non-polar) at the surface. Non-polar liquid molecules will interact with each other and the surface through weak van der Waals forces, but polar liquid molecules will interact with each other and the surface through dipole-dipole forces and hydrogen bonds. The sum of these interactions is used for analysis of surface energy²⁹. Surface free energy is limited in characterizing surface properties and cannot determine bulk mechanical properties, such as

strength or hardness¹⁰⁹, but is useful for the quantifying surface properties. Surface energy calculations and equations are presented in Chapter 3.

1.4 Material Properties

Bulk material properties and their effect on cell culture are studied in the field of mechanobiology¹¹⁰. The majority of materials chosen for cell culture systems are based on price, availability, and biocompatibility. Common materials include PS, glass, acrylamide, PDMS, and metal films. Deciding on the bulk material for experimentation is essential as it is a building block for altering the surface and chemistry of the scaffold¹¹¹. Optical transparency, electrical conductivity, biocompatibility, and flexibility are parameters that may be essential for successful alteration of cell behavior. When replicating or trying to mimic a region in a living organism the natural material properties of that system should be taken into account. Brain tissue and fat are much softer and more malleable when compared to muscle or bone. Even out of a native environment, cells can be cultured without difficulty. Cells are robust and are capable of growth and proliferation on a wide variety of materials, but their observed *in vitro* behavior may not represent cells *in vivo*.

1.4.1 Material Stiffness

The elasticity of a material is quantified by the material's elastic or Young's modulus (E) and is equal to the stress applied to a material divided by the strain as described in Equation 1.3. Deformation of a material (ΔL) can be divided by the material's resting length (L) to give strain

(ϵ) and the stress applied to the material (σ) is defined as the applied force (F) divided by the cross sectional area (A). The linear portion of a stress-strain curve defines the Young's modulus¹¹².

$$E = \frac{\text{Stress}}{\text{Strain}} = \frac{\sigma}{\epsilon} = \frac{F/A}{\Delta L/L} = \frac{F \times \Delta L}{A \times L} \quad \text{Equation 1.3}$$

Cells sense as substrates stiffness and Young's modulus¹¹³ just as they can sense chemistry and surface architecture. Certain cell types prefer stiffer or softer materials. Cells that naturally grow in a harder environment, such as osteoblasts, will more readily proliferate on a harder substrate *in vitro*¹¹⁴, but skeletal muscle cells, myoblasts prefer softer gels¹¹⁵. Vascular smooth muscle cells on stiffness gradients have demonstrated directed migration from a soft gel to a stiffer gel in less than 24 hours¹¹⁶. The stiffness of the material not only affects the cell, but how the cell affects the material. Cells are capable of deforming a softer material and can even produce enough force to bend certain objects^{117, 118} as seen in Figure 1.14.

Table 1.1. Table of Young's Modulus Values

Material	Young's Modulus, E
Steel ^a	212 GPa
Titanium ^a	115.7 GPa
Silica Glass ^a	72.4 GPa
Polylactic Acid ^b	3.5 – 10 GPa
Polystyrene ^a	~3.5 GPa
PDMS ^d	2.6 MPa
Collagen Gel ^c	1.5 KPa

References: a¹¹⁹, b¹¹¹, c¹²⁰, d¹²¹

Different biomaterials can provide unique Young's moduli (Table 1.1). In the case of polymers, there can be more control over the modulus. The mechanical properties of polymers are influenced by molecular weight, side groups, and the degree of crosslinking. Increasing the crosslinking density or decreasing the crosslinking density during polymer synthesis will result in a stiffer or softer polymer respectfully. These changes however impact the immediate surface chemistry interacting with the cell and noted alterations in cell behavior cannot be completely linked to changes in the substrate stiffness.

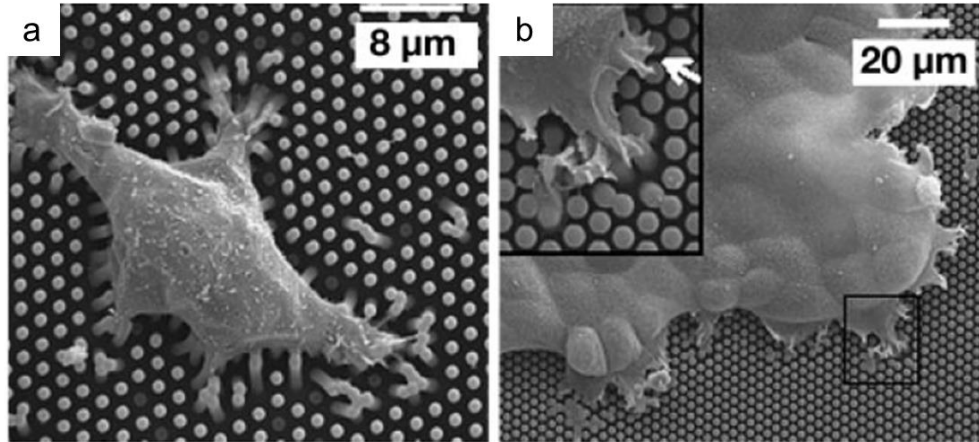


Figure 1.14. Example of (a) a single epithelial cell and (b) and a epithelial cell monolayer deforming PDMS micro-pillars due to the traction force needed for their migration¹¹⁷.

1.4.2. Polydimethylsiloxane (PDMS)

One of the most commonly used polymers for fabrication of biomaterials is PDMS (Figure 1.15). It has been utilized in microfluidics, cell culture scaffolds, microcontact printing, and implants^{122, 123}. PDMS is physiologically inert, biologically compatible, has low toxicity, and is thermally stable¹⁵. The polymer has a low elastic modulus making it flexible and easy to handle and PDMS is optically transparent making it suitable for optical microscopy studies. The surface of PDMS can be physically modified or chemically modified and is often used as a substrate for cell culture. PDMS is capable of casting micron sized features and details on a template. Although PDMS has been used successfully in a wide variety of applications, it does present some drawbacks. PDMS is a porous polymer which has been shown to absorb hydrophobic molecules from a solution¹²⁴. This porosity is also creates a swelling effect when PDMS is placed in common organic solvents^{125, 126}. Despite these shortcomings, PDMS continues to be utilized for bioresearch

because of its versatility as a biomaterial. PDMS has the ability to be cured with different elastic moduli¹²¹ and is can have the surface modified with thin films or SAMs¹²⁷.

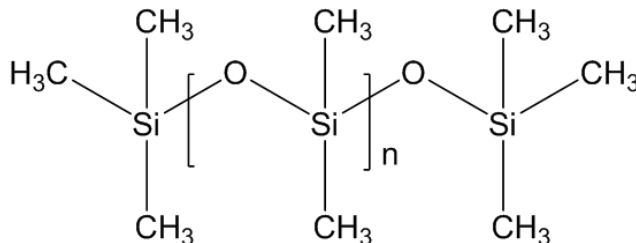


Figure 1.15. PDMS chemical structure.

1.4.2. Polystyrene (PS)

The first Petri dish was developed in 1887 by Julius Richard Petri to culture his bacteria. The dish was made of glass and was continued to be a standard in biology cultures until the mid-1960's when molding technology allowed the dishes to be mass produced from polystyrene (PS) (Figure 1.16a). The basic Petri dish design has remained the same and PS manufacturing has grown to incorporate culture flasks and well plates. This has made PS the most widely used substrates for cell culture studies. PS plates are optically transparent making them ideal for microscopy research and because they are so widely used, they are relatively inexpensive. PS on its own is not biocompatible, so dishes are exposed to corona discharge or plasma to generate oxygen ions that graft onto the PS chains (Figure 1.16b). The modification creates a more hydrophilic surface that is more apt for cell adhesion and spreading and is often referred to as tissue culture PS¹²⁸. The uniformity of the PS dish and flask fabrication provides a system for cell culture with reproducible results and a universally accepted substrate for comparative cell biology.

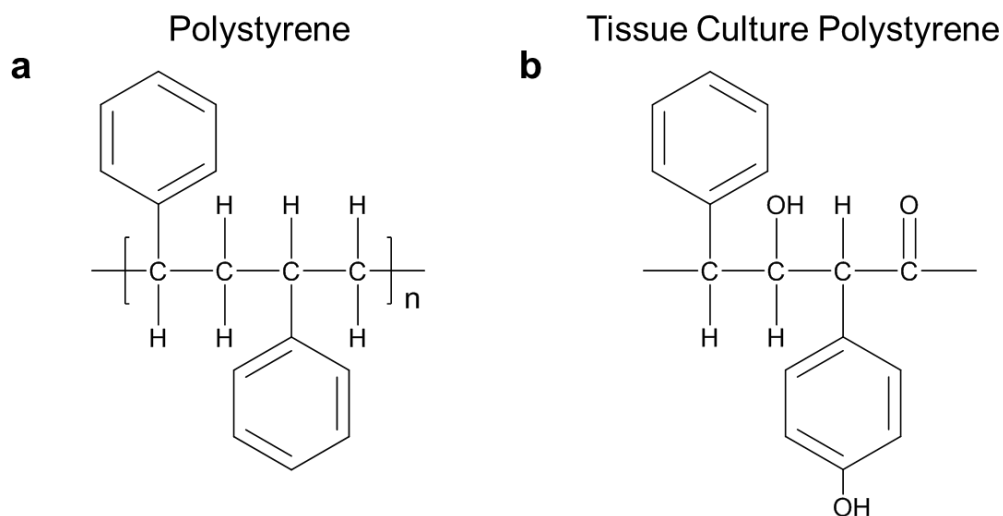


Figure 1.16. (a) PS chemical structure and (b) an example of tissue culture PS chemical structure.

1.5 Goals and Objectives

The main goal of this thesis was to design a cell culture surface to replicate and mimic an *in vivo* environment to generate physiologically relevant cells. This was carried out using a micro-roughened polymer substrate as the culture surface for human fibroblasts and comparing these cells to cells cultured on flat controls. Cell characteristics such as adhesion, cytoskeleton arrangement, gene expression, and ECM composition were examined for fibroblasts cultured on the different substrates. Changes in cell response are directly linked to the polymer chemistry, flexibility, and micro-roughness. The objectives to achieve this goal using surface topography and chemistry are as follows:

1.) Fabrication of a micro-structured surface that is easily reproducible in multiple laboratory settings

- Experimental methods require minimal equipment
- Characterization of physical features of the surface

2.) Application of surface chemistry onto topography for biocompatible cell culture surfaces

- Ensure surface encourages cell growth and tissue integration
- Characterization of chemical moieties present at surface

3.) Access cell behavior of cells cultured on modified surfaces

- Analyze cell behavior using bio-markers including extracellular matrix (ECM), cell adhesion, and cytoskeleton arrangement
- Compare cells on modified surfaces to cells cultured on unmodified substrates, cells in 3-D matrices, and cells *in vivo* systems

4.) Utilize surface design for specific cell behavior

- Cell organization and alignment
- Formation and detachment of cell sheets

2.0 Experimental Techniques and Overview

2.1 Introduction

All of the materials, instruments, and protocols described relate to research projects in the following chapters. Specific details of experimental procedures will not be given here, with the exception of general experimental protocols shared throughout the chapters. Protocols specific to each project will be given in the subsequent chapters. An overview of the theory of how the instrument operates in relation to surface chemistry, topography, and materials science is also provided.

2.2 General Materials

2.2.1 Chemical Materials

PDMS polymer casts were prepared using a Sylgard-184 kit from Dow Corning (Midland, MI). Wet/dry, 4000 grit, SiC paper (Part No. 40400014) was purchased from Struers, Inc. (Cleveland, OH). Polished silicon wafers were purchased from Virginia Semiconductors (Fredericksburg, VA). De-ionized water came from a Millipore (Billerica, MA) Synergy UV water purification system that produces water with a resistivity of 18M Ω . Ethanol, methanol, and acetone were purchased from Pharmco-AAPER (Brookfield, CT). Formamide, 99.5%, dimethyl sulfoxide (DMSO), 99.8% *N*-isopropylacrylamide (NIPAAm), benzyl alcohol, benzophenone, and glutaraldehyde (GA) were purchased from Alfa Aesar (Ward Hill, MA). *N*-(2-aminoethyl)-11-aminoundecyl trimethoxysilane (AUTMS) and 3-aminopropyltrimethoxysilane (APTMS) were purchased from Gelest, Inc. (Morrisville, PA). Microposit S1813 photoresist and Microposit Developer CD-30 were purchased from Dow (Marlborough, MA).

N,N'-methylenebis(acrylamide) (bis-acrylamide) was purchased from Amresco (Solon, OH). NaIO₄ was purchased from Sigma Aldrich (Saint Louis, MO).

2.2.2 Biological Materials

Human fibroblast cells derived from normal foreskin were purchased from the American Type Culture Collection (CRL-2097, Manassas, VA). Sterile Petri dishes for cell culture (Part No. 25384-302) were purchased from VWR (Radnor, PA). Phosphate buffered saline (PBS), Dulbecco's Modified Eagle Medium: Nutrient Mixture F-12 (DMEM/F12), penicillin-streptomycin (P/S), and trypsin-EDTA were purchased from Cellgro (Manassas, VA). Hyclone Fetal Clone III (FBS) was purchased from Fisher Scientific (Pittsburg, PA). Triton X-100 was purchased from Alfa Aesar (Ward Hill, MA), and rhodamine phalloidin was purchased from Biotium Inc. (Hayward, MA). Normal goat serum was purchased from Rockland Immunochemicals (Gilbertsville, PA). H-300 fibronectin primary antibody and goat anti-rabbit IgG-FITC secondary antibody were purchased from Santa Cruz Biotechnology (Dallas, TX). Alexa Fluor 555 Goat Anti-mouse IgG, Alexa Fluor 633 phalloidin, Hoechst 33342 trihydrochloride trihydrate, and MEM non-essential amino acids were purchased from Life Technologies (Grand Island, NY). Fibronectin (FN) from human plasma (Part No. F2006), concanavalin A, and hVIN-1 anti-vinculin were purchased from Sigma-Aldrich. Bovine serum albumin (BSA), fraction V was purchased from EMD Chemicals (Philadelphia, PA). RNase-free DNase I was purchased from New England Biolabs (Ipswich, MA). qScript cDNA Supermix and SYBR Green Supermix were purchased from Quanta Biosciences (Gaithersburg, MD). GoTaq Green Mastermix was purchased from Promega (Madison, WI). Human extracellular matrix and adhesion molecule PCR array and RT² SYBR Mastermix purchased from Qiagen (Germantown, MD).

2.3 General Experimental

2.3.1 General Instrumentation

- **Contact Angle Measurements:** Rame-Hart Automated Dispensing System (Netcong, NJ) Model No. 100-00 and a Net GmbH 1394 digital camera. Contact angle analysis was done with Rame-Hart Drop Image Standard v.2.0.10 software.
- **Oxygen Plasma Treatment:** SPI Supplies (West Chester, PA) Plasma Prep II.
- **AC AFM:** Asylum Research MFP3D microscope (Santa Barbara, CA) and WaveMetrics (Portland, OR) analysis software.
- **Roughness Calculations and Horizontal Cross Sections:** Gwyddion 2.28 (Brno, Czech Republic) analysis software.
- **Wide-Field Fluorescent Microscopy:** Nikon (Melville, NY) E600 fluorescent microscope with a Nikon DS-Qi1 Quantitative Monochrome digital camera. Images analyzed with Nikon NIS-Elements: Basic Research v4.0 software.
- **Confocal Microscopy:** Leica (Buffalo Grove, IL) SP5 Point Scanning Confocal with Leica DMI 6000 CS microscope base. Images analyzed with Leica LAS AF v2.0.2 software.
- **ATR FT-IR:** FT-IR spectroscopy was performed with a Bruker (Billerica, MA) Hyperion 3000 microscope equipped with a 20x attenuated total reflectance (ATR) objective with a germanium crystal and a liquid nitrogen cooled mercury-cadmium-telluride (MCT) detector. Data acquisition and analysis was performed with Bruker OPUS v.7.0 spectroscopy software.

2.3.2 Rough and Flat PDMS Surface Fabrication

The research projects of the thesis revolve around the micro-roughness of a polymer surface. The templating procedure for the PDMS substrate remains the same for each chapter and is described here. The SiC paper was sonicated in ethanol for 10 minutes, rinsed with fresh ethanol, dried in a stream of nitrogen, and baked for 15 minutes at 70°C to remove any residual ethanol that might be absorbed in the SiC paper. PDMS pre-polymer (10:1; elastomer: hardener) was poured over the clean SiC paper and placed under reduced pressure (~100 mm Hg) for 3 hours. The paper and PDMS were baked at 70°C for a minimum of 6 hours. After cooling, the paper was gently peeled away from the PDMS cast to give a micro-roughened polymer surface. A schematic of the process is seen in Figure 2.1. The cast surfaces were sonicated in ethanol for 5 minutes, dried in a stream of nitrogen, and baked at 70°C for 20 minutes before any measurements were made. Flat PDMS surfaces were cast on polished silicon wafers and were prepared the same way as the roughened PDMS surfaces.

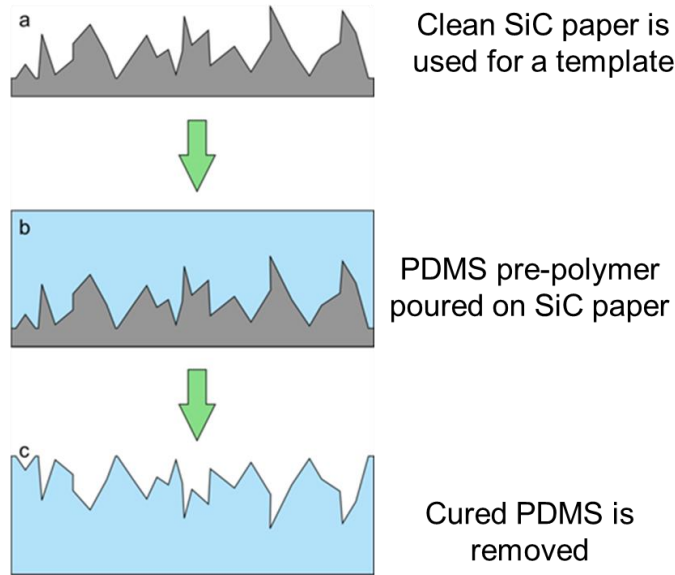


Figure 2.1. Schematic of PDMS casting process. (a) SiC paper is cleaned. (b) PDMS pre-polymer is poured on the SiC paper surface and allowed to cure. (c) SiC paper is removed leaving a PDMS replica of the rough surface.

2.4 Oxygen Plasma Treatment

Plasmas are used to create chemically reactive groups at the surface of a relatively inert material. As mentioned in Section 1.3.1.2, organosilane deposition requires hydroxyl groups at the surface of the substrate to be modified with a SAM. For a large majority of substrates, hydroxyl groups will only occur at the surface with chemical treatment¹²⁹ or exposure to oxygen plasma¹³⁰. Oxygen plasma contains highly excited atomic and radical species that are used for surface modification of materials for cell culture¹³¹. The plasma process is accomplished through the use of a low pressure, radio frequency induced gas discharge. The surface to be hydroxylated is loaded into the reaction chamber and evacuated under a vacuum pump. The carrier gas, O₂, is drawn over the surface and exposed to radio frequency power that is applied around the chamber and results

in ionization. Subsequent electrons collide with neutral gas molecules producing chemically active free radicals, ions, and free electrons. Plasma treatment is a useful tool for surface modification because it does not alter the bulk properties of the material as the active plasma depth is only few nanometers. The treatment modifies most surfaces uniformly, and there are no harmful byproducts of the reaction. The increased temperature of the chamber does limit polymer exposure time and polymers with lower melting points will begin to melt if treated too long.

During oxygen plasma treatment, two processes are occurring simultaneously: etching of the surface with atomic oxygen to give volatile reaction products and formation of oxygen containing functional groups at the surface¹³². Other than hydroxyl groups, oxygen plasma treatment will also generate C=O, C-O, and C-O-C bonds at the surface therefore increasing the surface free energy. Some polymers, such as PDMS, are naturally hydrophobic, but after plasma exposure, the increase in surface energy significantly increases the hydrophilicity of the system. Polymer surface modification with plasma is not energetically favorable and the increase in surface energy is not permanent for some polymers. Untreated, short polymer chains in the bulk of the polymer will migrate to the surface to bring the surface chemistry back to its original form in a process known as ‘aging’¹³³. The aging process can depend on the polymer, plasma exposure time, heat, and other environmental parameters making it essential for organosilane deposition to occur immediately after hydroxyl formation on the surface. Polymers that have a higher cross-linking density, such as PS, are stable after plasma treatment¹³⁴ and therefore less prone to aging.

Small amounts of physical deformation can occur on PDMS surfaces during plasma exposure. During oxygen plasma treatment the surface will become brittle due to the fast changes in surface chemistry. PDMS surfaces are known to buckle and break during this stage resulting in

nano- to micro- sized pits or cracks in the surface¹³⁵. This process must be acknowledged if surface roughness is being evaluated.

2.5 ATR Infrared Spectroscopy

Functional group analysis of monolayers on polymer substrates was carried out by attenuated total reflectance (ATR) infrared (IR) spectroscopy. Traditional IR instrumentation is capable of analyzing liquids and solids using IR transmission spectroscopy. Liquids are examined as thin films between two IR transparent plates and solids are ground into a powder to be pressed into a pellet or used as a paste causing issues with reproducibility in sample preparation. Thicker samples, not capable of physical alteration, are also difficult to image with transmission IR. If the effective path length of the sample is too large the IR energy will be mostly absorbed and the resulting signal cannot be detected. An IR equipped with ATR accessory can avoid these issues and is more useful for quantitative analysis of thicker samples. ATR-IR spectroscopy operates by measuring changes that occur in an internally reflected IR beam when the IR beam is in contact with sample (Figure 2.2).

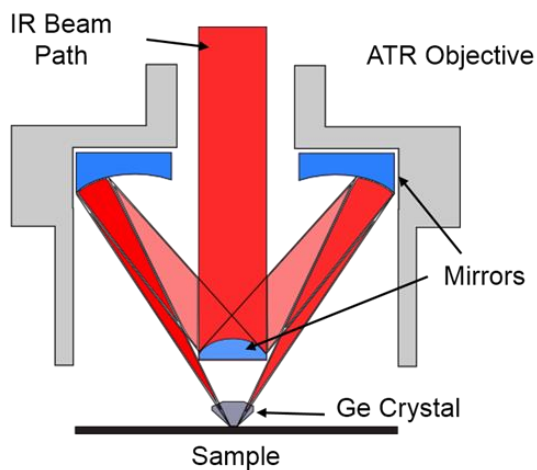


Figure 2.2. Example of ATR objective for obtaining IR spectra from a sample using a Ge crystal.

The IR beam is directed at a specific angle into a crystal with a high refractive index and the internal reflectance creates an evanescent wave that extends beyond the crystal into the surface of the sample¹³⁶. The evanescent wave projects only few microns beyond the crystal surface, so strong contact between the sample and crystal is essential. In regions of sample IR absorption, the evanescent wave will be attenuated and an IR spectrum can be produced. The formation of an evanescent wave and success of ATR-IR is based on Snell's law of refraction between two materials with two different refractive indices. In the case of ATR-IR, the refractive indices are from the sample (η_s) and ATR crystal (η_c) and for achievement of AT-IR, η_c must be greater than η_s . A beam of radiation travelling through the ATR crystal will experience total internal reflection if the angle of incidence (θ_i) is greater than the critical angle (θ_c). The critical angle is defined as the angle of incidence when the refracted angle is equal to 90° ¹³⁷. In terms of Snell's law the critical angle is given in Equation 2.1.

$$\theta_c = \sin^{-1} \frac{\eta_s}{\eta_c} \quad \text{Equation 2.1}$$

In total internal reflectance, an IR absorbing material at the interface of the crystal will absorb the energy transmitted from the evanescent wave and the reflected IR beam will be attenuated. An example of ATR-IR evanescent wave and its formation is seen in Figure 2.3.

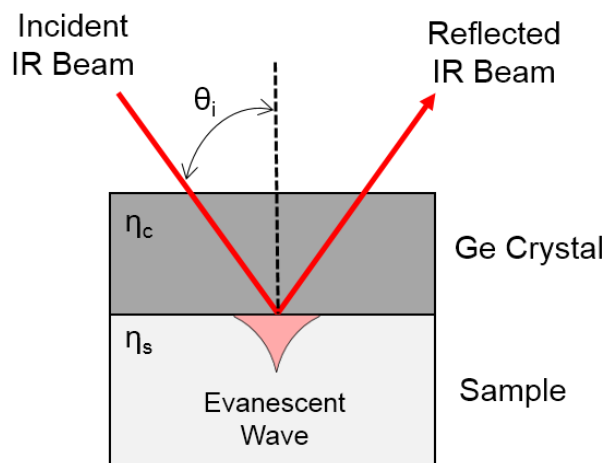


Figure 2.3. Example of evanescent wave formation when an IR beam undergoes total internal reflectance in a Ge crystal with a high refractive index (η_c) at the interface of a sample with a lower refractive index (η_s). For this to occur the angle of incidence (θ_i) must be greater than the critical angle.

If ATR-IR is being used for nanometer thick SAMs or thin films on a surface, the IR absorption signal will be significantly decreased compared to transmission IR for a liquid or solid form of the sample. Some frequency shifts in IR absorption bands between surface monolayers and the pure samples are also observed. The frequency shifts of surface bound molecules compared to a regular array is dependent on the degree of coupling between the vibrations of neighboring molecules and the surface. Specifically, the translational or rotational motions of molecules on a surface may be restricted as compared to the motions of a free molecule in solution shifting the frequency of absorption¹³⁸.

2.6 Contact Angle Goniometry

Contact angle goniometry is a non-destructive, macroscopic technique that measures the ability of water or solvents to spread on a surface. Measurement of static contact angles is important for accessing the functional groups present at the surface of a SAM or film^{139, 140}. A

surface is said to be wetting (hydrophilic in the case of water) if the contact angle is less than 90° and non-wetting (hydrophobic in the case of water) if the contact angle is greater than 90° , and super-hydrophobic if it is over 150° ¹⁴¹. Static measurements are obtained by depositing a $1 - 2 \mu\text{L}$ drop of de-ionized water on the substrate. The angle (θ) at which the drop of water (or other liquid) rests on the liquid-solid interface meets is measured (Figure 2.4.).

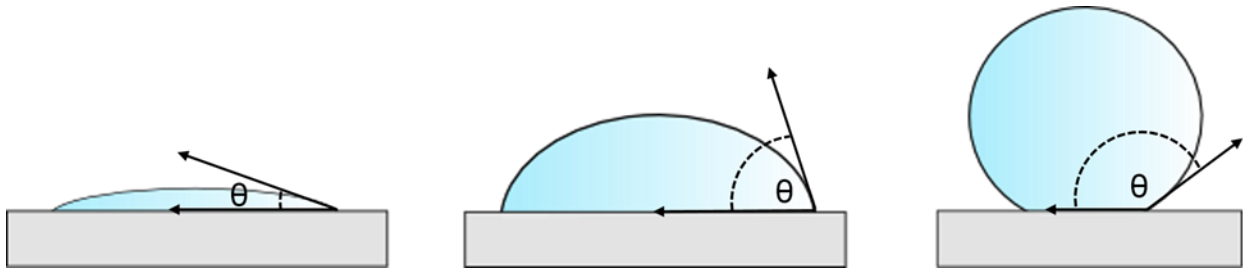


Figure 2.4. Static contact angle schematic. Examples of different contact angles (θ) taken by measuring the static contact angle between the substrate and liquid droplet.

A drop resting on a surface with a defined contact angle ($\theta > 0^\circ$) exists in a partially wetting equilibrium state. If, $\theta = 0^\circ$, that state is defined as complete wetting. Partial wetting can be described with Young's equation¹⁴² (Equation 2.2). The mechanical equilibrium of a contact angle is expressed in terms of force balance using a three phase system: liquid, gas, and solid as seen in Figure 2.5. Here, the interfacial energy of the solid-liquid (γ_{sl}), the interfacial energy of the liquid-gas (γ_{lg}), and the interfacial energy of the gas-solid (γ_{gs}) can describe the contact angle. Changes in the interfacial energy variables result in changes in the measured contact angle¹⁴³.

$$\gamma_{gs} - \gamma_{sl} = \gamma_{lg} \cos\theta \quad \text{Equation 2.2}$$

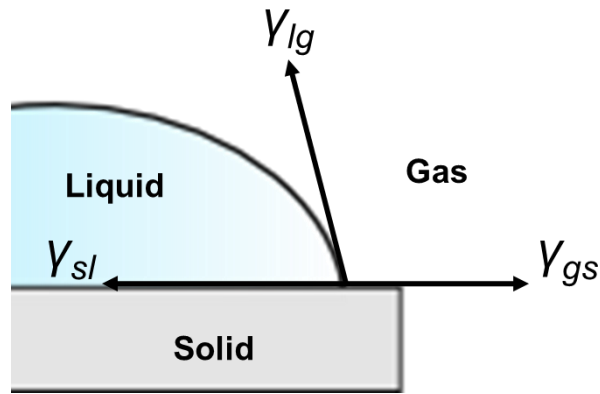


Figure 2.5. Force balance at the three phase contact line of a drop partially wetting a surface expressed in the variables of Young's equation.

In an ideal system, the shape of the liquid drop would be completely determined by the surface tension of the liquid. In a pure liquid, each molecule in the bulk system is pulled equally in every direction by its neighboring molecules resulting in a net zero force. This is not true for a liquid drop. Liquid molecules exposed to the surface are pulled inward, by the neighboring molecules creating an imbalance in the net force. This causes the liquid to contract its surface area to maintain its lowest surface free energy and is known as surface tension. Thus, a measured contact angle is the result of the liquids surface tension and external forces¹⁴⁴.

To further analyze the wetting properties of a surface, advancing and receding contact angles are obtained by first dispensing a drop on the surface, then increasing and decreasing the volume of the drop by a specific volume and taking the respective angles¹⁴⁵ as seen in Figure 2.6. When the drop is first placed on the surface and the volume is increased the contact angle measured is known as the advancing angle (θ_a), when the volume is decreased, the angle measured is known as the receding angle (θ_r). The difference between the advancing and receding angles ($\theta_a - \theta_r$) is the contact angle hysteresis ($\Delta\theta$). All surfaces that exhibit non-zero contact angles will also have

observable hysteresis¹⁰⁹. The hysteresis arises from various properties on the surface including surface roughness and chemistry. $\Delta\theta$ is a indicative of the energy and force required to move a drop bound to a substrate revealing certain surface properties¹⁴⁶. The $\Delta\theta$ has valuable information about the adhesive properties of a surface. A low hysteresis ($<10^\circ$) is indicative of a surface with low adhesion, while a high hysteresis ($>20^\circ$) indicates high adhesion¹⁴⁷. Combined with the static contact angle, θ_a , θ_r , and $\Delta\theta$ provide a comprehensive summary of the surface free energy, chemical composition, wettability, and adhesion.

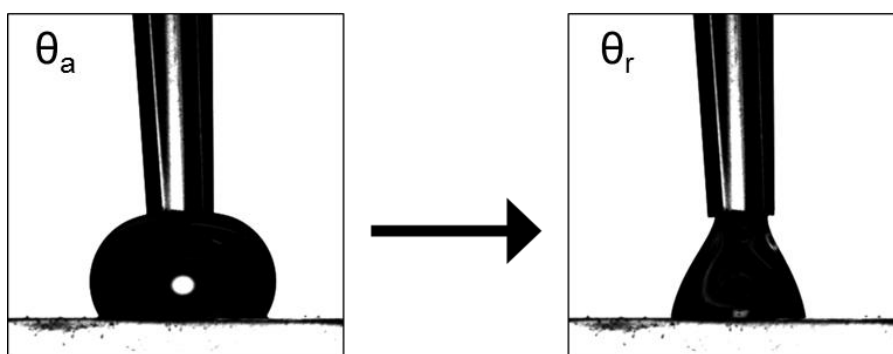


Figure 2.6. Example of water drops to be measured for advancing and receding contact angles. Advancing (θ_a) (left) and receding (θ_r) (right) contact angles.

To define the physical properties of the surfaces, surface wetting models can be used to predict how a liquid is interacting with the micro- and nano- scale features of a surface. The two most common models used are the Wenzel¹⁴⁸ and Cassie-Baxter¹⁴⁹ wetting models. Both models take into account surface roughness and observed contact angles, but the Wenzel model assumes there is no air underneath the droplet, while the Cassie-Baxter model assumes there are air pockets trapped beneath the droplet due to surface roughness. Both models can be successful in describing the liquid-solid interface depending of the wetting observed during experimentation. More details and figures about Wenzel and Cassie-Baxter wetting models are discussed in Chapter 3.

2.7 Atomic Force Microscopy (AFM)

Atomic force microscopy (AFM) is a high resolution imaging technique for studying and imaging surfaces with nano- or micro- scale physical or chemical features^{150, 151}. AFM uses a sharp tip (5 - 10 nm) typically made with silicon or silicon nitride to probe the surface (Figure 2.7). Operation of the AFM is based on the measurement of deflective or adhesive forces in contact with the tip.

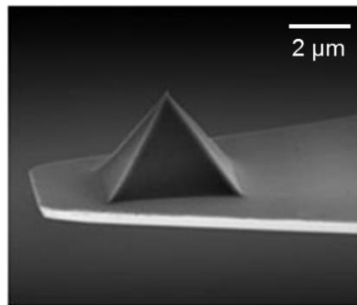


Figure 2.7. Example of a tip used for AFM imaging

The tip is rastered across the surface using piezoelectric scanners, building up an image a line at a time. The piezoelectric scanner allows for precise movements in the x , y and z axis. As the tip interacts with the surface it deflects and twists the cantilever. The movement is detected by a laser beam reflected from the backside of the cantilever into a photodiode as shown in Figure 2.8. The sum of the measured deflections generates a 3-D image of the topography of the surface.

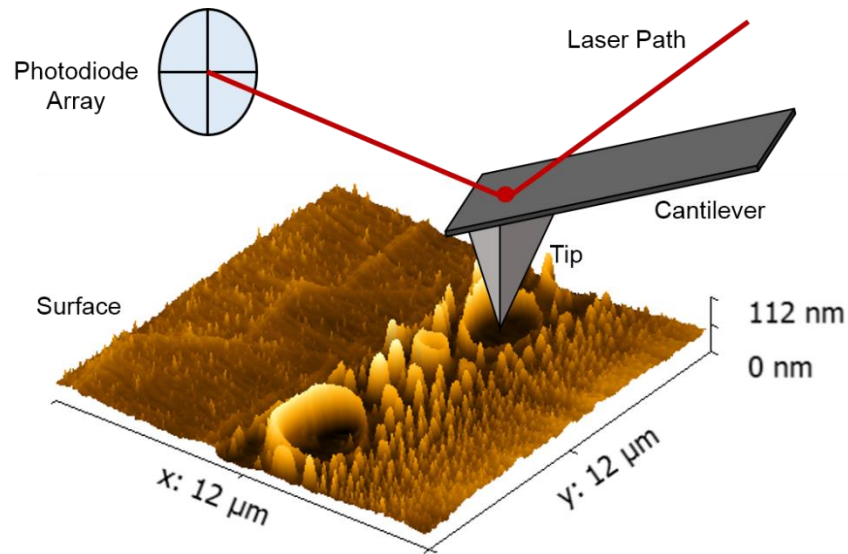


Figure 2.8. Schematic diagram of AFM tip and cantilever probing the surface with a split photodiode detector.

There are three principal modes of AFM imaging, contact mode, intermittent contact mode (also known as tapping mode) and non-contact mode. Contact mode holds the AFM tip in constant contact with the surface and the deflection of the cantilever is measured. In intermittent contact mode or alternating contact mode (AC mode) the cantilever is oscillated at high frequencies and the change in amplitude is measured. AC mode is a less destructive method for analysis of the surface if the substrate is soft or easily scratched. For non-contact mode the microscope is operated in AC mode, except it is kept a fixed distance from the surface (~10 – 100 nm) and is ideal for very delicate surfaces or biological samples. AFM imaging is performed under normal atmospheric conditions, in liquids, or in ultra-high vacuum, making AFM ideal for analysis of environmentally sensitive specimens, such as cells or bacteria¹⁵². Other imaging techniques like, scanning electron microscopy, require specific, high vacuum environments not suited for biological samples and typically samples must be conductive for imaging. AFM does not have

these problems and data collected is not only used for imaging, but other measurements such as surface roughness and surface chemical composition¹⁵³.

Non-imaging modes are used with the AFM to quantify mechanical properties of a sample. Force imaging or force curves are produced by measuring cantilever deflection in the z direction of a single point on a sample surface. The tip is driven into the surface at a specific deflection set-point and then retracted¹⁵⁴ as shown in Figure 2.9. The hysteresis in the deflection is proportional to the adhesion force. At the start of the measurement, (1) a large distance separates the tip and sample and there are no interactions. (2) As the tip approaches the sample attractive forces pull on the tip. Once the forces exceed the stiffness of the cantilever the tip jumps into contact with the sample. (3) After contact, deflections are dominated by electronic repulsion between the tip and sample and the tip may begin to deform the surface. (4) During retraction of the cantilever, the tip-sample distance increases, but adhesion bonds formed during contact pull the tip toward the sample. (5) After continued retraction the spring constant of the cantilever overcomes the adhesion force and cantilever pulls off sharply. (6) The tip-sample distance continues to decrease and returns to an equilibrium position. This data is used for material stiffness properties and surface adhesion measurements. The tip of the cantilever can be modified so specific biological interactions can be measured including DNA binding¹⁵⁵ and cell adhesion¹⁵⁶.

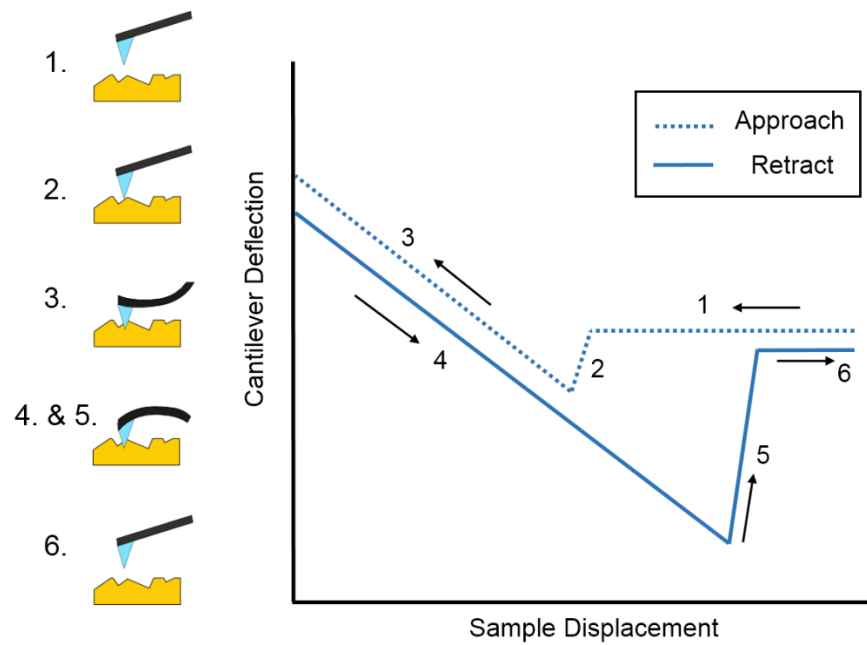


Figure 2.9. Graphical representation of an AFM force-distance curve. The AFM tip is brought into contact with the sample and then retracted. The effect the sample has on the tip is plotted as deflection of the cantilever against the displacement of the sample in the z direction.

2.8 Fluorescence Microscopy

Cell biology and viability can be examined with bright-field microscopy and fluorescent microscopy. Fluorescence microscopy is a vital tool in examining and quantifying molecular organization within a cell. The fluorescence observed can be described by a Jablonski diagram in Figure 2.10. A fluorophore resting at the singlet ground electronic state (S_0) can be excited, by absorbing light energy, to a higher vibrational energy level in the first excited singlet state (S_1). The fluorophore will relax to the lowest vibrational energy level in S_1 , known as internal conversion, and finally relax back to S_0 releasing the energy as fluorescence emission. The basic function of fluorescence microscopy is to irradiate a sample with specific wavelength, then separate the sample fluorescence from the excitation light. George Stokes first described

fluorescence in 1852 and noted that fluorescence emission always occurred at a longer wavelength (lower energy) than the excitation light. The most common losses of excitation energy are the rapid decay to the lowest vibrational level of S_1 and that a fluorophore will generally decay to a higher vibrational energy level in S_0 . The phenomenon is known as Stokes' shift and is also shown in Figure 2.10. Other factors, such as solvent effects, excited-state reactions, and energy transfer, can also contribute to the Stokes' shift¹⁵⁷.

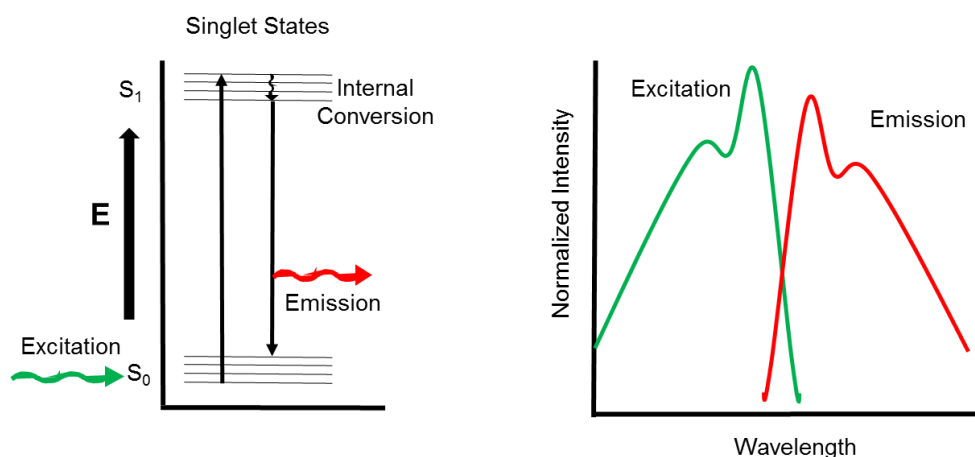


Figure 2.10. (Left) Jablonski diagram of molecular fluorescence. (Right) Example of molecular fluorescence spectrum and Stokes' shift between excitation and emission maximum.

For imaging fluorescently labelled samples wide-field fluorescence microscopy is a commonly used technique. In this system a light source, usually a mercury or xenon arc lamp, passes light through fluorescent filter cube as shown in Figure 2.11. This light is passed through the excitation filter where the desired wavelengths are allowed through and blockage of unwanted wavelengths occur. The light then encounters the beam splitting dichromatic mirror where shorter wavelengths of light are reflected and longer wavelengths can pass through. The fluorophores in the labelled sample are excited and their emission light passes through the dichromatic mirror into

the emission filter. The emission filter removes any residual excitation light that passed the mirror. The image of the sample is now transmitted to the observation tubes or electronic detector. Wide-field fluorescence microscopes can accommodate 4 – 6 different cubes so a variety of fluorophore wavelengths can be observed in a single sample.

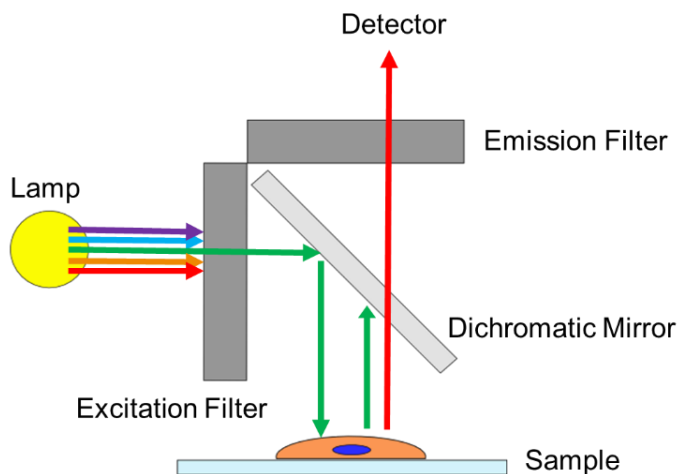


Figure 2.11. Illustration of a filter cube for wide-field fluorescence microscopy imaging.

Although wide-field fluorescence is a useful tool for imaging biological samples, secondary fluorescence emitted by the sample away from the region of interest can interfere with the focused image. This is most common in thicker samples where secondary fluorescence above and below the focal plane degrades resolution. Wide-field fluorescence is not capable of addressing this issue, but confocal microscopy can be used to regain resolution. Confocal microscopy offers several advantages to traditional wide-field fluorescence microscopy including: shallow depth of field, elimination of light out of the focal plane, and the ability to collect stacks of images (Z-stacks) from thicker specimens. Using a wide-field microscope, samples are saturated completely with light and the majority of the sample fluoresces. With confocal, the

sample is scanned with focused beams of light or lasers, termed “point scanning” allowing the acquisition of optical sections. The fluorescence emitted from these sections are passed through the dichromatic mirror to a detector pinhole aperture. Only light in the focal plane of the optical section is allowed to pass, efficiently removing any light from out-of-focus or background fluorescence¹⁵⁸, allowing high resolution images to be achieved inside a thick sample. Sequential collection of multiple optical sections, a Z-stack, in a single frame can build a 3-D image or movie of the sample making confocal a useful imaging tool for biological systems or tissue sections. Z-stacks can also be compressed into a single image for a maximum composite image of the entire specimen.

For thinner samples, such as SAMs and thin films on substrates, is not possible with the naked eye or even bright-field microscopy due to the nanometer thickness of the chemistry. Observations of surface chemistry using optical microscopy require physisorption or covalent attachment of a fluorescent molecule or dye. Commonly used organic chemistry can be used to link fluorescent molecules to the surface. Carboxylic acid terminated films can be covalently bound to an amine carrying fluorophore using carbodiimide and succinimide chemistry to form an amide bond¹⁵⁹ and aldehyde terminated monolayers will rapidly attach to an amine-containing molecules⁹⁰. Covalent attachment of fluorophores to SAMs or thin films is only limited to the available surface chemistry⁷¹. SAMs that are not capable of being labeled can be observed with AFM or if the surface is reflective, grazing incidence IR spectroscopy.

3.0 Super-hydrophobic, highly adhesive, polydimethylsiloxane (PDMS) surfaces

3.1 Introduction

Recent interest in super-hydrophobic surfaces has been inspired by the self-cleaning property of the lotus leaf and other natural, biological surfaces^{37, 101, 160-162}. The term “lotus effect” has been used to describe surfaces with this wetting phenomena. With a contact angle greater than 150°, these super-hydrophobic surfaces typically have a low surface energy, a low contact angle hysteresis (< 10°), and low adhesion, allowing water drops to roll off the surface at a small tilt angle. Replications of the lotus leaf and other biological surfaces that have lotus wetting properties are of interest because of their self-cleaning applications. As a drop of water rolls off the lotus surface, dirt and debris are collected and removed from the surface. However, this is not the only possible super-hydrophobic state. More recently there have been reports of the fabrication of super-hydrophobic surfaces that are also highly adhesive¹⁶³⁻¹⁶⁶. These surfaces are super-hydrophobic with a large hysteresis (> 20°), and upon 180° inversion of the surface, water drops will remain adhered in the same position. The term “petal effect” has been coined to describe such surfaces; named for the rose petals that exhibit these properties¹⁶⁷. Rose petal surfaces are composed of nanostructure ridges embedded on a microstructure. Water drops cannot penetrate the ridges making the petals super-hydrophobic, but can penetrate the microstructure for increased adhesion. Petal surfaces offer a unique platform for lab-on-a-chip applications. Micro, spherical drops pinned to a surface create the ability for rapid biological or chemical analysis¹⁶⁸ and the development of droplet transport mechanisms and microliter sampling^{169, 170}.

The properties of the surface that give rise to a super-hydrophobic wetting state include chemical composition and the geometry of the substrate. The most commonly cited wetting states for a rough surface are described by the Cassie-Baxter¹⁴⁹ and Wenzel¹⁴⁸ models. In the Cassie-Baxter model a water droplet will sit on top of the rough surface and air pockets are trapped underneath the droplet (Figure 3.1a). The Wenzel model predicts a complete wetting state where all the pores on the surface are in complete contact with the water droplet (Figure 3.1b). The Cassie-Baxter model can describe surfaces that replicate or are similar to the lotus leaf. Water drops cannot penetrate into the micro or nanostructure of the surface and therefore easily roll off. Water drops on a natural or fabricated “petal” surface can penetrate the microstructure, but not the nanostructure, allowing the drop to adhere to the surface while still staying super-hydrophobic¹⁶⁷. A cartoon representing a drop partially penetrating the surface can be seen in Figure 3.1c.

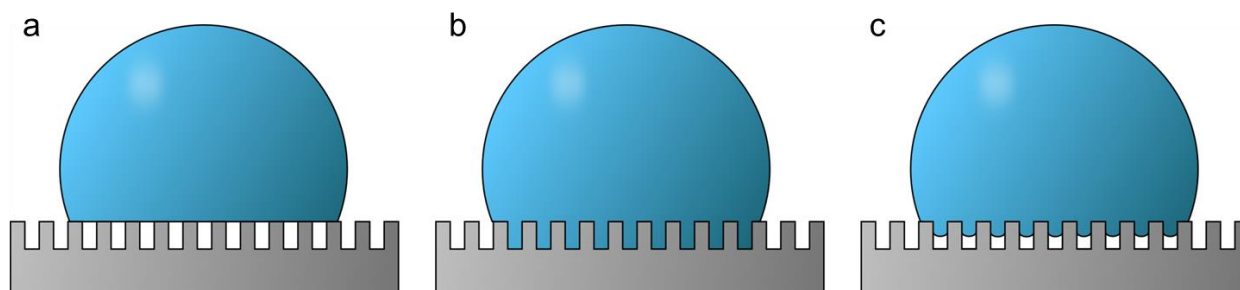


Figure 3.1. Cassie-Baxter and Wenzel wetting states on micrometer scale. (a) Cassie-Baxter wetting state. (b) Wenzel wetting state. (c) Hybrid wetting state where the liquid can partially penetrate air pockets in the surface.

Here, we present a fast and reliable method of fabricating a non-uniform, polymer surface with super-hydrophobic and high adhesive properties from a readily available template. Unlike previous reports of super-hydrophobic surfaces and natural examples (*i.e.* rose petal), no nano-scale roughness was included in our design protocol, simplifying the fabrication process¹⁷¹. PDMS

was templated from SiC paper, producing a surface with micron scale features. Using SiC paper simplifies the experimental procedure by eliminating fabrication of micro- or nano- scale surface features that require the use of photolithography techniques⁵⁰. PDMS is a non-toxic, optically transparent polymer used in soft lithography, microfluidics, and medical devices. Chemically, the polymer presents methyl moieties at its surface, rendering it hydrophobic and making it an ideal substrate for creating a super-hydrophobic surface and eliminates the need for further chemical derivation the surface. The templating method may also be used for other castable materials and possibly as a prototype for more complex surfaces. The simplicity of the procedure and the ample characterization of the surface make this method widely applicable and easy for large scale production.

3.2 Experimental Methods

3.2.1 Static, Advancing and Receding Contact Angles

Three, 3 x 2 cm sections were taken from each type of PDMS surface and six contact angle measurements were made on each section. Static contact angle measurements were made with water drops between 3 and 6 μL . Advancing (θ_a) and receding (θ_r) contact angles for water, formamide, and DMSO were made by lowering a 2.5 μL drop to the surface and increasing the volume (advancing) and then decreasing the volume (receding) by 1 μL . New surfaces were used for each test liquid.

3.2.2 Drop Volume Measurements at 60°

The adhesive properties of the surfaces were characterized using a modification of a method described by Bormashenko *et al*¹⁷². Briefly, three samples were taken from each rough

and flat PDMS surface and one measurement was made per surface. The PDMS surface was placed on a graduated, rotating, protractor modified with a platform. At 0° (parallel to the ground), a volume of water approximately 5 μL less than the estimated roll off volume was deposited on the surface. The platform was rotated to 60°; if the drop maintained its position without sliding for one minute, 1 μL of water was then added to the drop. Droplet additions and one minute time intervals were repeated until the drop slid off or down the surface. The previous volume was then recorded as the maximum, critical volume at a 60° angle.

3.2.3 Roughness measurements with AFM imaging

AFM imaging was completed with an Agilent 5500 and PicoView 1.8.2 (Santa Clara, CA) imaging system using NT MDT (Santa Clara, CA) CSG01 cantilevers with a resonant frequency of 10 Hz and a nominal force constant of 0.06 N/m. Three topography images (45 x 45 μm) were taken in contact mode for each rough PDMS surface, each SiC paper surface, and each flat PDMS surface. Root mean square roughness (R_{rms}) values were averaged over three surfaces.

3.2.4 Grain Threshold Processing

The AFM images acquired from the rough PDMS surface were analyzed using a grain height threshold measuring technique with Gwyddion 2.20 analysis software. Height thresholds of 3.5, 3.4, 3.3, 3.2, 3.1, 3.0, 2.9, and 2.8 μm were chosen for the z-axis of the AFM topography images with the lowest point of the image set as the 0 z-axis value. Surface area above the threshold was masked in red as seen in Figure 3.2. Height threshold surface area was measured on a minimum of four AFM images from the rough surface using the eight threshold values mentioned previously. The total surface area masked in red was calculated and then divided by

the total surface area of the image to give the ratio f_{afm} for each threshold value. The f_{afm} value is the average from all four topography images.

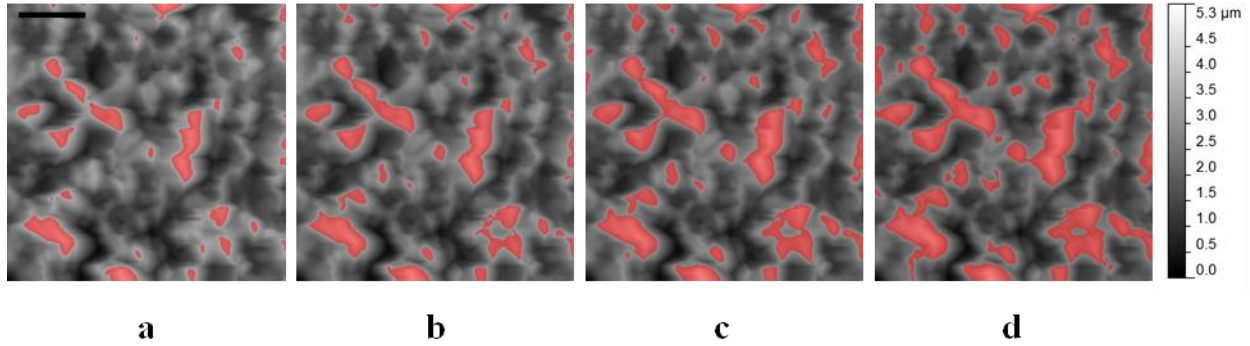


Figure 3.2. Example of grain height threshold processing using AFM of $45 \times 45 \mu\text{m}$ topography images of the rough PDMS surface. The lowest point of the image (colored in black) is set as the 0 z-axis value. Surface area above a specified threshold is masked in red. As the threshold decreases, more surface area in red is exposed. (a) $3.5 \mu\text{m}$ threshold. (b) $3.2 \mu\text{m}$ threshold. (c) $3.0 \mu\text{m}$ threshold. (d) $2.8 \mu\text{m}$ threshold. Scale bar = $10 \mu\text{m}$. Threshold images of 3.4 , 3.3 , 3.1 , and $2.9 \mu\text{m}$ are not shown.

3.3 Results and Discussion

3.3.1 AFM Characterization of Rough PDMS

Figures 3.3a and 3.3c show $45 \times 45 \mu\text{m}$ contact mode AFM images of clean SiC paper and a PDMS surface templated from SiC paper. The AFM image of the SiC paper shows a surface that is consistent with a randomly arranged grain structure. The AFM image of the templated, rough PDMS surface has features that mirror the structure of the SiC paper. The corresponding, randomly chosen line sections from the AFM images of the SiC paper and the rough PDMS are shown in Figures 3.3b and 3.3d respectively. Comparing the two cross sections, no feature size is lost. Peak height and width of the SiC paper are similar to the valley depth and width of the rough PDMS.

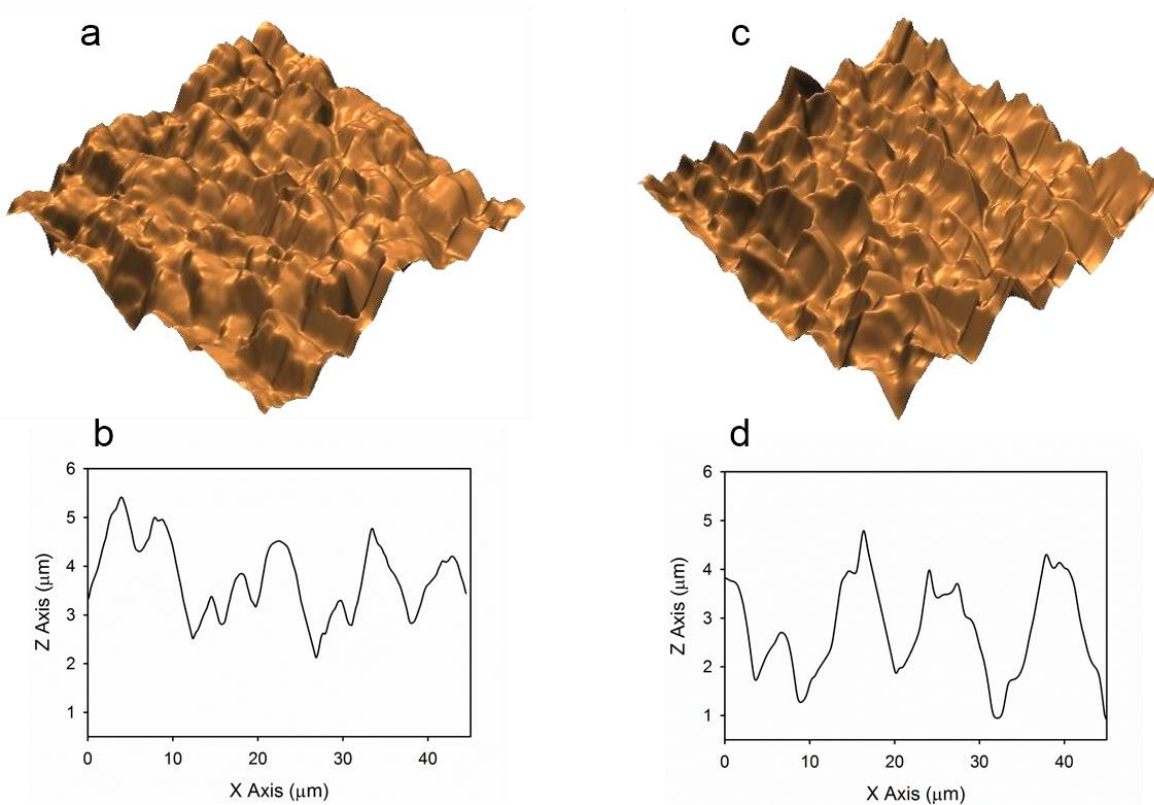


Figure 3.3. (a) 45 x 45 μm 3-D AFM image of the SiC template with a z-scale from 0 to 5.6 μm (b) Line section taken from image *a*. (c) 45 x 45 μm 3-D AFM image of the PDMS surface after removal from the template (rough PDMS) with z-scale from 0 to 5.3 μm . (d) Line section taken from image *c*.

To further analyze the feature size of the rough PDMS surface, the cross sections from three AFM images were evaluated. Seven cross sections were selected at random from each AFM image and the first seven features of each cross section were recorded to give a total of 147 measurements. Feature size was measured by taking the full width at half maximum (FWHM) of the PDMS features. These FWHM values were then plotted into a histogram (Figure 3.4), comparing the number of features in each half micron range as a percentage of the total features measured. The majority of the FWHM values fall between 2 and 6 microns. There is then a decline in frequency with increasing feature size, with no features observed greater than 16 μm .

Natural super-hydrophobic, high adhesion surfaces frequently show a nanoscale structure embedded on top of the microstructure with 200 - 700 nm dimensions^{167, 173}. No such nanostructure was observed in our templated surface (Figures 3.3c and 3.3d). This may be due to the larger feature size of the AFM tip (~10 nm) or possibly deformation of the PDMS while imaging with the contact force of the AFM. The heights of the PDMS microstructure are also seen in Figure 3.3d and range between 2.0 and 3.5 μm .

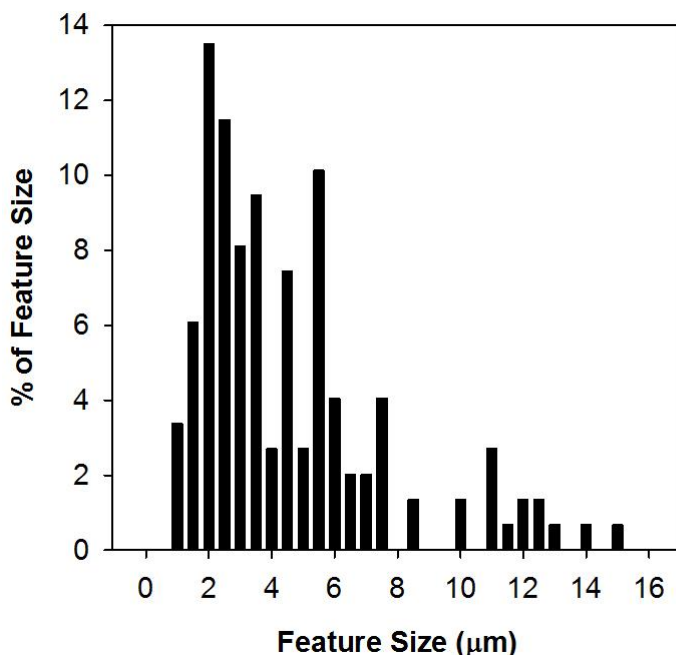


Figure 3.4. Histogram FWHM feature sizes as a percent of the total measurements of the rough PDMS.

3.3.2 Static Contact Angle and Roughness

Table 3.1 shows a summary of the static water contact angle measurements and root mean squared roughness (R_{rms}) as determined by AFM analysis. The R_{rms} value is a quantitative value of the surface topography feature size and is defined as the standard deviation of the distribution

of surface heights from a mean line. The R_{rms} combined with the 3-D AFM images provides a complete characterization of the rough PDMS surface to better understand the observed super-hydrophobic, high adhesive wetting phenomena.

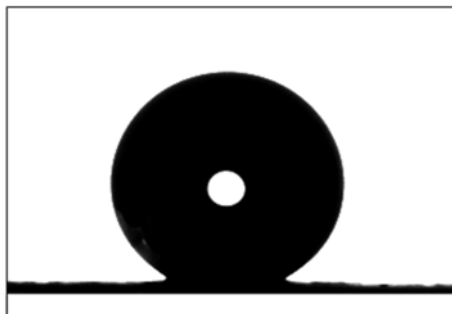


Figure 3.5. 6 μ L water drop on a rough PDMS surface with a static contact angle of 154°.

Table 3.1 Static contact angles and roughness values for flat and rough PDMS surfaces.

Surface	Static (°)	R_{rms} (nm)
Flat	112.5 \pm 1.3	2.7 \pm 0.7
Rough	153.5 \pm 1.8	1380 \pm 330

Data for rough PDMS templated from SiC paper was compared to flat PDMS templated on a polished silicon wafer. An AFM image of the flat surface and a horizontal cross section can be seen in Figure 3.6a and 3.6b. The flat PDMS gave a hydrophobic contact angle of 113° and the rough PDMS gave a super-hydrophobic contact angle of 154° as observed in Figure 3.5. Since the flat PDMS and the rough PDMS have the same chemical composition, the 40° increase in static contact angle can be attributed to the increase in roughness of the surface. As seen in the Table 3.1, the R_{rms} changes from a nanometer scale for the flat PDMS, to a micron scale for the rough PDMS. Further chemical modification of the rough surface was tested using hydrophobic SAMs with

fluoro and methyl head groups to increase the contact angle. This did not increase the contact angle of the surface, but decreased it to $\sim 130^\circ$ (data not shown). PDMS surfaces were exposed to oxygen plasma and then incubated in a dilute solution of alkoxy silanes for chemical modification. Although still hydrophobic the chemical moieties decreased the super-hydrophobic capabilities of the micro-roughness. It is hypothesized that the secondary chemical modification allowed the water to penetrate deeper in the micron pores, allowing the water to spread more on the surface, decreasing the contact angle. Oxygen plasma exposure was essential for the formation of hydroxyl groups on the surface for silane attachment, but it also increased the surface energy and increased the hydrophilicity. Although modified with hydrophobic molecules, the increase in surface energy had a greater impact on wettability than the chemical deposition. Therefore, the overall contact angle was decreased when compared to the unmodified PDMS.

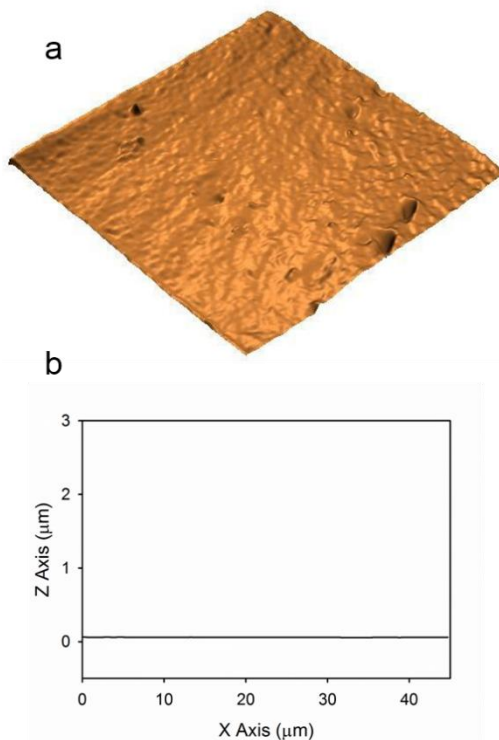


Figure 3.6. (a) $45 \times 45 \mu\text{m}$ 3-D AFM image of the PDMS fast on a silicon wafer with a z-scale from 0 to 60 nm (b) Line section taken from image *a*.

3.3.3 Solid-Liquid Contact

It is hypothesized that water drops on the micro-rough structure of the PDMS created air gaps left underneath the drop. These air pockets have the capability of holding drops as large as 25 μL , as seen in Figure 3.7. The ability for a surface to maintain super-hydrophobicity and high adhesiveness characterizes the surface a “rose petal” type substrate. Figure 3.7 demonstrates that smaller 2 μL water drops or larger 25 μL drops on the rough PDMS surface are capable of retaining their spherical shape when inverted. Minimal elongation of the 25 μL drop is noted due to gravity, but the drop still maintains a strong adhesion at the interface of the liquid and the surface.



Figure 3.7. Captured image of 2 and 25 μL water drops on an inverted rough PDMS surface.

The ability of a large water drop to rotate 180° on the rough surface indicates the drop has penetrated into the microstructure of the surface. The mechanism of adhesion for petal surfaces is due to the collective capillary force of the air pockets underneath the droplet during inversion or tilting^{163, 166}. The presence of air gaps between the water drop and the surface can be described by the Cassie-Baxter wetting model, even with partial penetration of the drop into the surface¹⁷⁴. The fraction (f) of the rough surface is in direct contact with the drop and solid-liquid interface can be modeled with a Cassie-baxter equation¹⁷⁵;

$$\cos \theta^* = -1 + f(\cos \theta_0 + 1) \quad \text{Equation 3.1}$$

where θ^* is the apparent contact angle on the rough surface and θ_0 is the apparent contact angle on a smooth surface of the same material. Using the contact angle values from Table 3.1, the value f for the rough surface was calculated to be 0.170. The value for f can now be used to define how deep the water drop was penetrating into the rough PDMS surface. Using AFM topography images of the rough PDMS surface, the surface area above a specific threshold was calculated and then divided by total surface area of the image (Methods, Section 3.2.4) to give the fraction f_{afm} . Eight threshold values were chosen and their respective f_{afm} values can be seen in Table 3.2.

Table 3.2. f_{afm} values calculated for different threshold heights. f_{afm} is equal to threshold area divided by total surface area. Each f_{afm} value is the average of four measurements from AFM images of the rough PDMS surface.

Threshold Height (μm)	Average f_{afm}
3.5	0.08 ± 0.02
3.4	0.09 ± 0.02
3.3	0.11 ± 0.02
3.2	0.13 ± 0.03
3.1	0.16 ± 0.03
3.0	0.18 ± 0.03
2.9	0.22 ± 0.03
2.8	0.25 ± 0.03

The f_{afm} values from Table 3.2 were plotted against the single f value calculated from Equation 3.1 (Figure 3.8). As the height threshold is increased, less surface area above the threshold is exposed

decreasing the value of f_{afm} . Comparing f , fraction of solid-liquid interface calculated from the Cassie-Baxter equation, and f_{afm} , fraction of surface above a specified height, the water drop sits only on the portion of the surface above $3.0\ \mu\text{m}$ (Figure 3.3c) and does not penetrate any deeper. The limited penetration of the drop into the surface leaves air trapped underneath the drop. These air pockets and the capillary force associated with them have the adhesive capability to hold inverted water drops as large as $25\ \mu\text{L}$ as seen in Figure 3.7, which is much greater than recent reports¹⁷⁴.

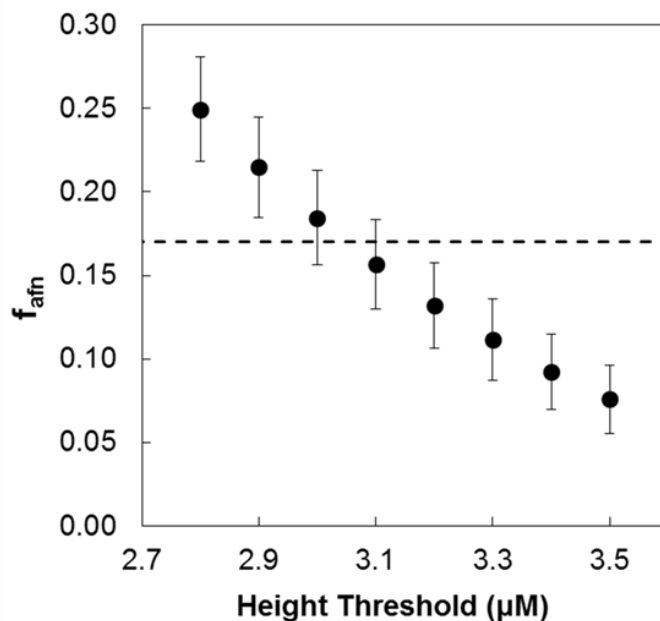


Figure 3.8. f_{afm} vs. height threshold for a rough PDMS surface. The f_{afm} values are taken from Table 3.2 and the dashed line indicates the value of f calculated from Equation 3.1 ($f = 0.170$).

3.3.4 Surface Free Energy

When a surface or interface is created there are disruptions of the intermolecular bonds and the surface becomes less energetically favorable than the bulk of the material. The surface free energy can then be defined as the excess energy of the surface when compared to the bulk. The surface free energy (γ_{total}) of the PDMS surfaces was determined using a method described by

Chibowski *et al*^{176, 177}. In these references an equation is derived by taking Young's equation for the static contact angle of a liquid on a surface and modifying it to include the involvement of liquid residue from the receding drop. This residual film effectively changes the solid surface free energy which is now related to the receding contact angle. By measuring the advancing and receding contact angle for a series of liquids of known surface tension, the surface free energy of the PDMS can be determined. The liquids used were de-ionized water, formamide, and DMSO. The surface free energy was calculated by taking the advancing and receding contact angle (θ_a and θ_r respectively) for each liquid and their respective surface tensions values (γ_l ; water¹⁷⁸, formamide¹⁷⁹, and DMSO¹⁸⁰) and applying them to Chibowski's equation (Equation 3.2).

$$\gamma_{total} = \frac{\gamma_l(1+\cos\theta_a)^2}{2+\cos\theta_r+\cos\theta_a} \quad \text{Equation 3.2}$$

The surface free energies of the flat and rough PDMS calculated from each liquid and the average value are shown in Table 3.3. The surface free energy of the flat PDMS is in good agreement to literature data (12.54 mN/m)¹⁸¹ obtained using contact angles for two solvents on spin coated flat PDMS. The low surface free energy for the rough PDMS surface is consistent with super-hydrophobic wetting¹⁸². The hydrophobicity arises mainly because of the chemical composition of the polymer and the presence of low molecule weight species at the surface¹⁸³.

Table 3.3. Surface free energy for each liquid used on flat and rough PDMS substrates.

PDMS Surface	Water γ_{total} (mN/m)	Formamide γ_{total} (mN/m)	DMSO γ_{total} (mN/m)	Average γ_{total} (mN/m)
Flat	11.0 ± 1.0	12.2 ± 0.6	13.9 ± 0.4	12.4 ± 0.1
Rough	1.3 ± 0.8	1.5 ± 0.4	6.6 ± 0.8	3.1 ± 0.7

Examination of the results in Table 3.3 reveals that the surface free energy of the rough PDMS obtained using DMSO is higher than might have been expected from Equation 3.1. This would indicate that the advancing contact angle is lower than might be expected from the model and the receding contact angle is higher. In fact, the calculation is more sensitive to the advancing contact angle than the receding. At present we consider that the most likely reason for this discrepancy is that the model is based on a modification of Young's equation which considers the surface free energy of the surface with and without a surface solvent film and the surface tension of the solvent. The surface topography and therefore the area of the surface in contact with the solvent are not taken into account. Given that the model gives a consistent result for the flat surface we conclude that the discrepancy is due to the rough surface. In a bid to investigate this phenomenon further grit paper with varying grain sizes were also used as templates for the PDMS cast. However, it was found that there was a much wider variation in the grain sizes than in the paper used in the present study, *vide infra*.

3.3.5 Contact Angle Hysteresis and Adhesion Measurements

The contact angle hysteresis (CAH, $\Delta\theta$) was obtained from the difference in the advancing and receding contact angles of water ($\theta_a - \theta_r$) and was measured on both flat and rough PDMS surfaces. These values are presented in Table 3.4 for the flat and rough PDMS surfaces. The CAH

for each surface is large and slightly larger for the rough surface than for the flat surface. By comparison, the CAH reported for the lotus leaf is $\sim 2^\circ$ ¹⁸⁴. In terms of adhesion, a low CAH indicates a low adhesion surface while a large CAH indicates a high adhesion surface. When a super-hydrophobic surface with low adhesion has the CAH measured, the drop is mainly sitting on air pockets and the small portion of solid in contact with the drop is a hydrophobic material. As a result, advancing and receding the drop the surface has a minimal effect. On a super-hydrophobic surface with high adhesion, the micro-structure is different and the drop has been allowed to partially penetrate the surface structure. When a drop on this surface is advanced or receded, the pull of the capillary action and larger solid-liquid contact underneath the drop create a greater CAH¹⁸⁵.

Table 3.4. Advancing, receding and contact angle hysteresis (CAH, $\Delta\theta$) values and the volume capacity at 60° for each PDMS surface measured using de-ionized water.

Surface	θ_a ($^\circ$)	θ_r ($^\circ$)	$\Delta\theta$ ($^\circ$)	Volume Capacity at 60° (μL)
Flat	125.0 ± 1.3	103.1 ± 2.8	21.8 ± 3.4	36.0 ± 2.5
Rough	156.4 ± 4.6	130.9 ± 5.7	25.8 ± 6.0	35.0 ± 1.3

As mentioned earlier, grit paper of different grain size were used as templates to investigate the effect of topography and feature size on the super-hydrophobic, adhesive properties of the PDMS cast as seen in Figure 3.9 SiC papers with 0.5, 1.0, 14, and 30 μm features (as described by the manufacturers Struers Inc. and Lee Valley Tools Ltd.) were tested as templates for PDMS and the wettability of each cast was measured (Table 3.5). Although a large CAH was found for each surface ($\geq 20^\circ$), no surface exhibited super-hydrophobic properties. Static contact angles for these surfaces were between 120° to 130° using de-ionized water. AFM analysis of the surfaces, as shown in Figure 3.9, displayed a large variation in feature size compared to the surface examined

in this paper. The 0.5 and 1.0 μm surfaces had features as large as 25.0 μm and overall had less uniformity in distribution of feature size and shape. The larger feature sizes on these surfaces decreased the static contact angle indicating water could impregnate the surface and spread more readily than it could on the 2 – 6 micron features of the rough PDMS surface. The CAH for the other PDMS surfaces in Table 3.5 was similar to the CAH observed to the rough and flat PDMS is in Table 3.4. This may signify the chemistry of the PDMS surface is more essential to the adhesion of the surface than the topography.

Table 3.5. Static contact angles and CAH ($\Delta\theta$) values for other rough PDMS surfaces.

Surface Features (μm)	Static ($^\circ$)	$\Delta\theta$ ($^\circ$)
0.5	130.4 \pm 1.5	20.6 \pm 1.9
1.0	125.4 \pm 1.4	24.6 \pm 4.1
14	126.6 \pm 1.9	23.6 \pm 3.8
30	121.3 \pm 2.9	21.1 \pm 3.2

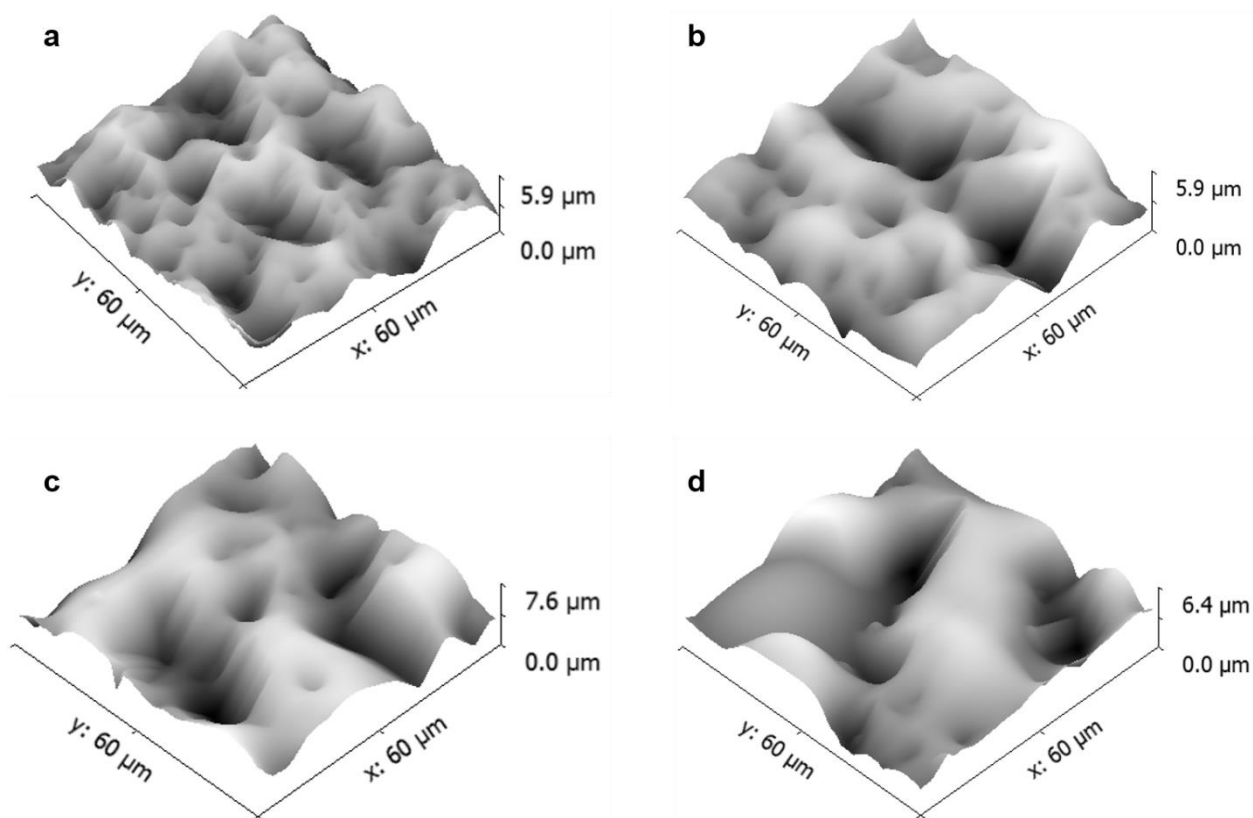


Figure 3.9. AFM 60 x 60 μm topography images of PDMS surfaces cast from a variety of SiC grit paper. Described by the manufacture as having (a) 0.5, (b) 1.0, (c) 14, and (d) 30 micron features. Distribution of feature size was not uniform for these templates.

To further characterize the adhesive properties of the flat and rough PDMS substrates, the volume capacity at 60° was measured using de-ionized water, as seen in Figure 3.10. The volume capacity was $36 \mu\text{L}$ for the flat PDMS and $35 \mu\text{L}$ for the rough PDMS. The volume held by each surface is similar, as might be expected from the values of CAH obtained for these surfaces (Table 3.4). Despite this, the mechanism of adhesion for each surface is thought to be different. A water drop on a tilted, flat surface and a water drop on a tilted, rough surface have their own distinct shapes. The drop on the tilted, flat substrate can spread across the surface to increase the liquid-surface contact area and therefore increases the amount of water adhered to the surface. The even distribution of spreading water allows the drop to have a symmetrical and uniform shape. On

the tilted, super-hydrophobic substrate the drop is “pinned” to the surface through capillary action (Figure 3.1c). The 2 - 6 μm structures (Figure 3.3c and 3.3d) allow water to partially penetrate the surface while leaving a substantial air pocket that renders the surface super-hydrophobic, giving the drop a unique asymmetric shape. The base of the water drop is immobilized on the rough PDMS and cannot spread across the surface even at a 60° angle. This forces the water to bulge over the base of the drop.

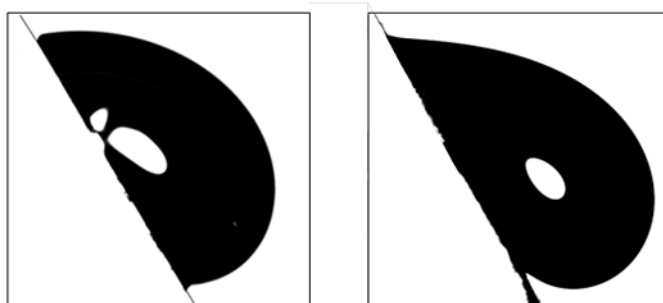


Figure 3.10. Adhesive properties of PDMS. (Left) 33 μL water drop on a flat PDMS at a 60° angle. (Right) 33 μL water drop on a rough PDMS at a 60° angle.

3.3.6 Impact of Surface Characterization

There have been previous studies that have cast super-hydrophobic surfaces from both synthetic surfaces. However this is the first study where a simple, reproducible templating procedure has been described and the resulting surface fully characterized. For example, Xie *et al*¹⁸⁶ cast a super-hydrophobic surface from SiC paper, but only a small CAH (5°) was observed. Limited physical and chemical surface characterization was completed and no adhesive properties were identified. The surface presented in this work is super-hydrophobic and highly adhesive. Surface properties have been thoroughly analyzed as well as the solid-liquid interface between water and the PDMS samples. This indicates the size, shape, and manufacturing of the grit is critical to the adhesive properties of the surface. Since the template is not fabricated in the

laboratory, the optimal grit template needs specific physical characteristics produced by the manufacturer to yield a super-hydrophobic and highly adhesive surface. The FWHM size of the of the grit paper peaks should fall between 2 and 6 μm with heights between 2 and 3.5 μm to achieve a surface with these unique wetting properties. The characterization provided will be beneficial in fabricating future surfaces that can hold a large inverted volume as well as maintain a super-hydrophobic wetting state.

The micro-roughness characterized in this report may be also be of use as a cell culture platform. The roughness has been extensively characterized and is simpler and less expensive to fabricate than a surface with ordered geometry or topography produced from photolithography⁵¹. Cells cultured on altered surface topography or surface roughness have exhibited differences in their biochemical behavior¹⁸⁷. The surface presented would be offers an opportunity for a unique cell culture system. The ease of the fabrication process allows for the possibility for commercialization of the surface and adaptability for many types of biological systems. Cells cannot be cultured on chemically unmodified PDMS, but silane or protein deposition onto the PDMS surface encourages cell adhesion. The roughness does not produce a 3-D scaffold for cell culture, as the cells are not completely surrounded by scaffolding, but provides a surface architecture that forces cells to behave differently than if they were cultured on 2-D. Therefore, our substrate could be designated as a *pseudo-3-D* surface for cell culture. The extensive characterization of the rough PDMS substrate will provide applications in the future of alternative cell culture platforms.

3.4 Conclusions

We have demonstrated a rapid, facile and inexpensive templating procedure to fabricate a super-hydrophobic, adhesive surface. The method described may be also applied to other polymers and castable materials. Characterization of this surface has shown microstructure features that mirror the features of the template. These features are unique to the manufacturer of the silicon carbide paper and they establish the wettability and adhesion of the polymer substrate. Ample surface characterization has identified the super-hydrophobic and adhesive properties of this surface which aid in the development and fabrication of future petal substrates. The super-hydrophobic and adhesive properties can be described by a hybrid Cassie-Baxter, Wenzel model that allows water droplets to partially penetrate into the rough surface. Applications for this surface include microdroplet transport and reactions for lab-on-a-chip systems.

4.0 Fibroblast extracellular matrix and adhesion on micro-textured polydimethylsiloxane (PDMS) scaffolds

4.1 Introduction

The role of the extracellular environment is vital in determining cellular behavior¹⁸⁸⁻¹⁹⁰ as cells are able to discern and respond to their local micro- and nano- scale surroundings¹⁹¹⁻¹⁹³. *In vivo*, cells sense and respond to their immediate support structure including other tissues, connecting cells, and their extracellular matrix (ECM)¹⁹⁴⁻¹⁹⁶. Controlling these physiological cell functions can be tailored by altering and modifying the chemical and physical properties of their culture scaffold to stimulate changes in the actin cytoskeleton and cellular integrin attachment¹⁹⁷.¹⁹⁸ Modification of surface topography has been shown to produce changes in differentiation¹⁹⁹, immunosuppressive properties²⁰⁰, adhesion²⁰¹ and proliferation²⁰² when compared to cells cultured on unmodified substrates. As mentioned in Section 1.2, conventional cell culture systems, such as tissue culture PS, lack significant, physical surface topography and often produce cells that do not model their native tissue²⁰³⁻²⁰⁵. Therefore, it is a necessity for culture scaffolds and matrices to mimic a native environment and provide a physiologically relevant system for investigating cells *in vitro*. Although there has been significant work in designing organized micro-topography, such as pillars²⁰² and groves²⁰⁶ for biomimetic scaffolds the majority of natural bio-interfaces have multiple feature sizes and are randomly oriented²⁰⁷. Research in developing textured or porous culture scaffolds is being pursued²⁰⁸⁻²¹⁰, but how surface morphology effects cells biochemical signaling pathways is still poorly understood. Fields that require control of cell function and guidance, such as tissue engineering, implantable biomaterials, and high throughput screening (HTS) assays^{211, 212} need a low cost and simple scaffold fabrication method for a culture platform.

The platform should provide an environment where cellular ECM and signaling can be driven by surface topography and customized to mimic an *in vivo* system.

This work seeks to design a low-cost, micro-textured, polymer matrix for cell culture and quantify cell response on substrate topography. The interaction of human fibroblasts with a chemically and physically modified PDMS substrate is investigated. The polymer surface was fabricated using an inexpensive templating technique, described in Chapter 3 and a previous literature report²¹³, to produce micro-scale peaks and valleys that have been extensively characterized. An amine terminated self-assembled monolayer (SAM) was deposited on the polymer to promote cell adhesion. Fibroblasts cultured on this substrate had their morphology, cell area, FN formation, and adhesion thoroughly investigated in terms of fluorescent microscopy and AFM adhesion force curves. Cells cultured on the modified scaffold exhibited significant differences in their biological properties when compared to cells cultured on unmodified PDMS. This chapter highlights how ECM and cellular adhesion can be customized by altering surface geometry and provides a valuable resource for the development of future biomaterials. Overall, this procedure has the ability to be applied to other biocompatible polymers and creates a facile method for a generating a reproducible, micro-scaffold for cell culture and controlled ECM.

4.2 Experimental Methods

4.2.1 AUTMS Modification

PDMS was cut into ~2.5 x 2.0 cm samples and sonicated in a 1:1 ethanol and de-ionized water mixture to remove any surface debris, dried in nitrogen, and baked at 70°C for 10 minutes

to remove any excess solvent. The PDMS surfaces were activated for 45 seconds with oxygen plasma and immediately incubated in a 1% v/v AUTMS solution in ethanol for 1 hour at room temperature. The PDMS was removed and sonicated for 1 minute in fresh ethanol, dried in nitrogen, and baked for 1 hour at 70°C. Figure 4.1 displays a schematic representation of the surface fabrication and AUTMS deposition.

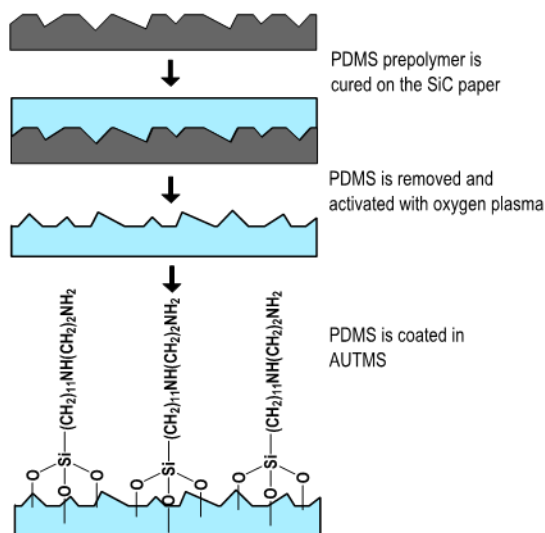


Figure 4.1. Schematic representation of PDMS surface fabrication and AUTMS deposition.

4.2.2 Static Contact Angle

Three, 4 x 1 cm sections were cut from rough and flat AUTMS modified PDMS surfaces. The reported static contact angle was the average of contact angle measurements made from three surfaces with a minimum of six measurements per surface. Static contact angle measurements were made with 1.5 μL de-ionized water drops.

4.2.3 Cell Seeding and Growth on PDMS Surfaces

Human fibroblast cells were seeded on surfaces at an initial 5×10^4 cells/mL in serum free DMEM/F12 media. The cells were allowed to adhere to the surface for 1 hour before the media was aspirated and replaced with 1% FBS and 1% P/S in DMEM/F12. Cells were cultured in a humidified atmosphere at 37°C and 5% CO_2 .

4.2.4 AFM Surface Characterization and Cell Adhesion Measurements

AFM imaging was completed using MikroMasch (San Jose, CA) DPE18/AIBS cantilevers with a resonant frequency of 64.4 kHz and a nominal force constant of 4 N/m. Three topography images ($50 \times 50 \mu\text{m}$) were taken in alternating contact (AC) mode for each type of surface and average roughness (R_a) values, representing the deviation of the surface height, were averaged over the three images. All surfaces imaged were coated with an AUTMS monolayer.

Cell adhesion measurements were completed using single cell force spectroscopy (SCFS)^{214, 215} on Bruker (Camarillo, CA) NP-O10 silicon-nitride, tipless cantilevers with a resonant frequency of 20 kHz and nominal spring constant 0.06 N/m. The real spring constant of each cantilever was calibrated using the thermal method²¹⁶. To enhance cell-cantilever adhesion, cantilevers were incubated in a 1.0 mg/mL concanavalin A aqueous solution for 30 minutes at room temperature, rinsed with water, and air dried. Within 20 minutes after cells were seeded on the sample surface, a non-adhered cell was identified using the Nikon Eclipse Ti-U optical microscope (MVI, Avon, MA) attached to the AFM. The functionalized cantilever was then positioned above the identified cell and brought into contact. After 5 minutes, the cantilever was withdrawn from the surface and the cell-cantilever adhesion was strong enough that the cell moved with the cantilever away from the surface. Cell-surface adhesion strength was measured by

engaging the cell-attached cantilever to the modified PDMS surfaces, holding for 1 second with a 1 nN force, and then pulling it away. The resulting force curves were used to calculate the adhesion of the fibroblast to the PDMS. Adhesion measurements were performed with a minimum of six cells on different areas of the PDMS substrates.

Force curves were analyzed individually using MATLAB (Mathworks, Natick MA) to determine the adhesion strength for each measurement, given by;

$$F_{adh} = k(d_{max} - d_0) \quad \text{Equation 4.1}$$

where k is the cantilever spring constant, d_{max} is the cantilever deflection corresponding to the maximum pulling force applied to the cell during retraction, and d_0 is the baseline cantilever deflection measured after the cell is completely detached from the substrate.

4.2.5 Morphology Analysis

Cells imaged by fluorescence for general morphology analysis were cultured 24 hours on the PDMS samples before being stained and fixed. Samples had their current media removed and were rinsed twice (2X) with PBS. The cells were then fixed by incubating the surface in 4% formaldehyde solution in PBS (pH 6.9, methanol-free) for 10 minutes at room temperature. The surfaces were washed 2X with fresh PBS, incubated in a 0.1% Triton X-100 solution in PBS for 3 minutes at room temperature, and washed 2X with PBS. Samples were then incubated in a 20 μ L/mL solution of rhodamine phalloidin in PBS with 1% w/v BSA for 25 minutes at room temperature to stain the cellular f-actin. Samples were washed 2X with PBS, and stored at 4°C in PBS until imaged. Cells were examined using wide-field microscopy. Quantitative analysis was done with ImageJ 1.45s software. Cell area was determined by cellular rhodamine phalloidin

fluorescence. Thresholding criteria distinguished cellular fluorescence from non-fluorescent non-cell areas. Overlapping cells or cell bodies that were not entirely contained in the image were not used. Each histogram and average area reported is data collected from ~150 cells. Data was collected over at least three different experiments.

4.2.6 Immunofluorescence Staining of Fibroblasts on PDMS Surfaces

Cells and surfaces to be imaged by confocal fluorescence microscopy (vinculin and actin stain) had their media removed and were rinsed 2X with warm PBS. The cells were fixed by incubating the surface in 4% formaldehyde solution in PBS for 10 minutes at room temperature. The surfaces were washed 2X with fresh PBS, incubated in a 0.2% Triton X-100 solution in PBS for 5 minutes, washed 2X with PBS, blocked with 5% normal goat serum in PBS for 30 minutes, and rinsed 2X with PBS. Cells were incubated in hVIN-1 anti-vinculin produced in mouse, diluted in PBS (1:266) for 1 hour at 37°C and washed three times (3X) with PBS. Cells were then incubated in diluted Alexa Fluor 555 Goat Anti-mouse IgG (1:1000) and diluted Alexa Fluor 633 phalloidin (1:200) in PBS for 30 minutes at 37°C and washed 3X with PBS. Samples were mounted on glass coverslips with mounting media containing fluorescence anti-quenching agent and observed using confocal microscopy.

Cells and surfaces to have FN, f-actin, and nucleus staining were incubated in a 1.0 µg/mL Hoechst 33342 trihydrochloride trihydrate solution in PBS for 20 minutes at 37°C and rinsed 2X with PBS. Cells were fixed by incubation in 4% formaldehyde solution in PBS for 10 minutes at room temperature, washed 2X with fresh PBS, incubated in a 0.1% Triton X-100 solution in PBS for 3 minutes, washed 2X with PBS, blocked with 5% normal goat serum in PBS for 30 minutes, and rinsed 2X with PBS. Cells were incubated in 3.5 µg/mL of H-300 fibronectin primary

antibody in PBS with 1.5% goat serum for 1 hour at room temperature. Cells were then incubated in fresh PBS for 15 minutes before incubation 3.5 $\mu\text{g}/\text{mL}$ goat anti-rabbit IgG-FITC secondary antibody in PBS with 2% goat serum in PBS for 45 minutes at room temperature. Cells were rinsed 2X with PBS, incubated in a 20 $\mu\text{L}/\text{mL}$ rhodamine phalloidin solution in PBS with 1% w/v BSA for 25 minutes at room temperature, and rinsed 3X with PBS. Samples were stored at 4°C until imaged. Fluorescent images were collected with a wide-field fluorescent microscope.

4.2.7 Immunofluorescence Staining of Fibronectin on PDMS After Fibroblast Extraction

PDMS surfaces to be imaged had media and rinsed 2X with PDMS. Fibroblasts were removed from the PDMS surface by addition of 2% Triton X-100 in Tris Buffered Saline (pH 8.0) for 10 minutes at room temperature. Surfaces were washed 2X with PBS and fixed by incubation in 4% formaldehyde in PBS for 10 minutes at room temperature. Surfaces were washed 2X with PBS, incubated in 5% normal goat serum in PBS for 30 minutes, washed 2X with PBS, and incubated in 3.5 $\mu\text{g}/\text{mL}$ of H-300 fibronectin primary antibody in PBS with 1.5% goat serum for 1 hour at room temperature. Cells were then incubated in fresh PBS for 15 minutes before incubation with 3.5 $\mu\text{g}/\text{mL}$ goat anti-rabbit IgG-FITC secondary antibody in PBS with 2% goat serum in PBS for 45 minutes at room temperature. Cells were washed 3X with PBS and fluorescent images were collected with a wide-field fluorescent microscope.

4.3 Results

4.3.1 Surface Characterization

The 50 x 50 μm AFM topography images of the flat (Figure 4.2a) and micro-textured (Figure 4.2b) PDMS surfaces are shown in Figure 4.2 and show marked differences in topography. Both the flat and textured PDMS surfaces are coated with the amine terminated silane, AUTMS, to promote cell adhesion. The flat PDMS has nano-scale cracks running over the surface due to the oxygen plasma activation combined with thermal stress²¹⁷, giving the flat substrate a R_a value of 2.65 nm (Table 4.1) and minimal surface architecture (Figure 4.2c). The textured PDMS surface is covered with 2 - 6 μm wide peaks that are 1 - 3 μm in height (Figure 4.2d), giving the substrate a much higher R_a value of 804 nm when compared to the flat PDMS. Static contact angles for each surface are also given in Table 4.1. The contact angles for the flat and textured AUTMS coated PDMS surfaces are 104° and 121° respectively. The surface composition and chemistry remained the same between the flat and micro-textured PDMS, therefore the increase in hydrophobicity on the rough PDMS is attributed to its higher surface roughness.

Table 4.1. Roughness average and static contact angle values for rough and flat PDMS.

Surface	Roughness Average (R_a)	Static Contact Angle
Flat PDMS	2.65 ± 0.2 nm	$104 \pm 4^\circ$
Micro-textured	804 ± 53 nm	$121 \pm 3^\circ$

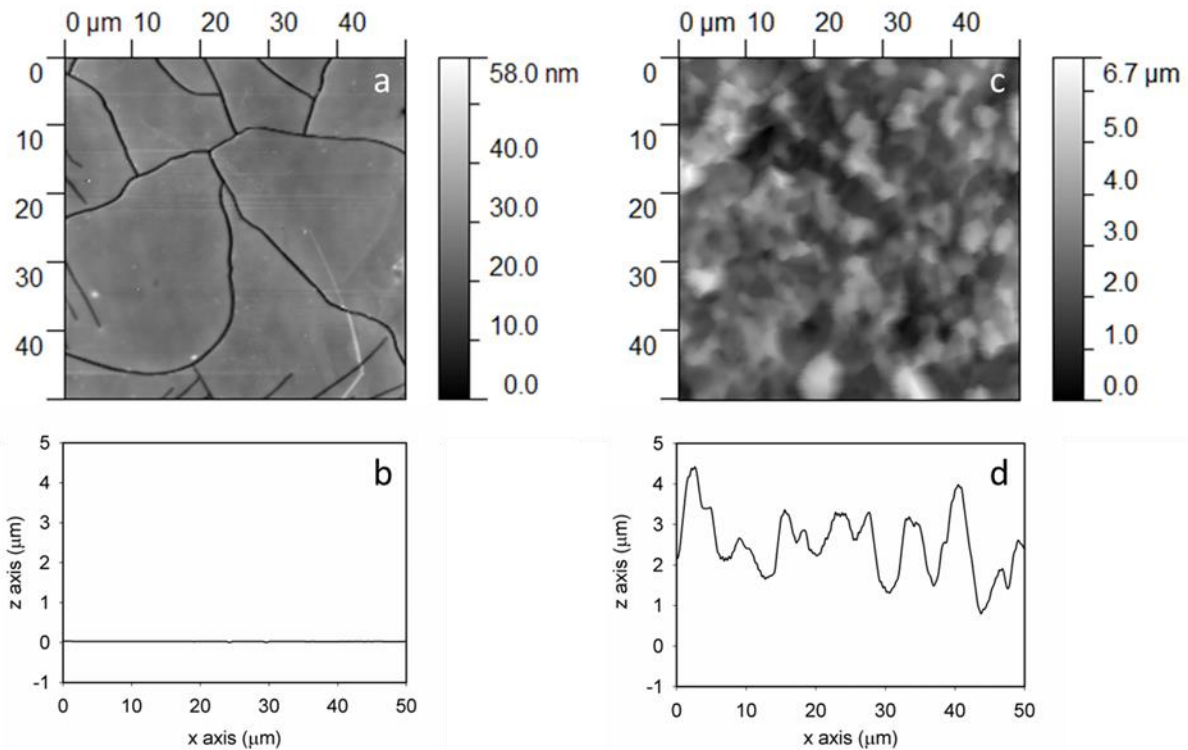


Figure 4.2. (a) 50 x 50 μm AFM topography image of AUTMS coated, flat PDMS and (b) a corresponding horizontal line section. (c) 50 x 50 μm AFM topography image of AUTMS coated, micro-textured PDMS and (d) a corresponding horizontal line section. Note difference in Z-scale between panels *a* (0 - 58 nm) and *c* (0 - 6.7 μm).

4.3.2 Cell Morphology and Adhesion Analysis

Initial observation of fibroblasts grown on PDMS surfaces reveals large differences in cell morphology and apparent cross-sectional area when comparing cells grown on each surface type. Qualitative and quantitative morphology analysis (Figure 4.3) demonstrates a much larger apparent cell area for fibroblasts grown on flat surfaces (Figure 4.3a) when compared to rough surfaces (Figure 4.3b). Cell area was calculated using fluorescence microscopy 24 hours after cell seeding and subsequent image processing. A representative frequency histogram of geometric cell area for fibroblasts cultured on flat and micro-textured PDMS is shown in Figure 4.3c. The cell

areas on the flat PDMS surface have a maximum value at $2,750 \mu\text{m}^2$, while cell areas on the roughened PDMS have a maximum at $1,750 \mu\text{m}^2$. Cell area distribution for the roughened substrate is much narrower when compared to cell areas on the flat substrate with the majority of the area distribution falling between $1,250$ and $2,250 \mu\text{m}^2$. Fibroblasts cultured on the roughened PDMS do not spread across the micron features on the surface, while fibroblasts on the flat PDMS are not restrained by surface topography and spread to have larger geometric areas as well as a greater range of areas; between $2,000$ and $4,750 \mu\text{m}^2$. The average cell area, in Figure 4.3d, for fibroblasts on flat and micro-textured PDMS is $3,410$ and $1,760 \mu\text{m}^2$ respectively.

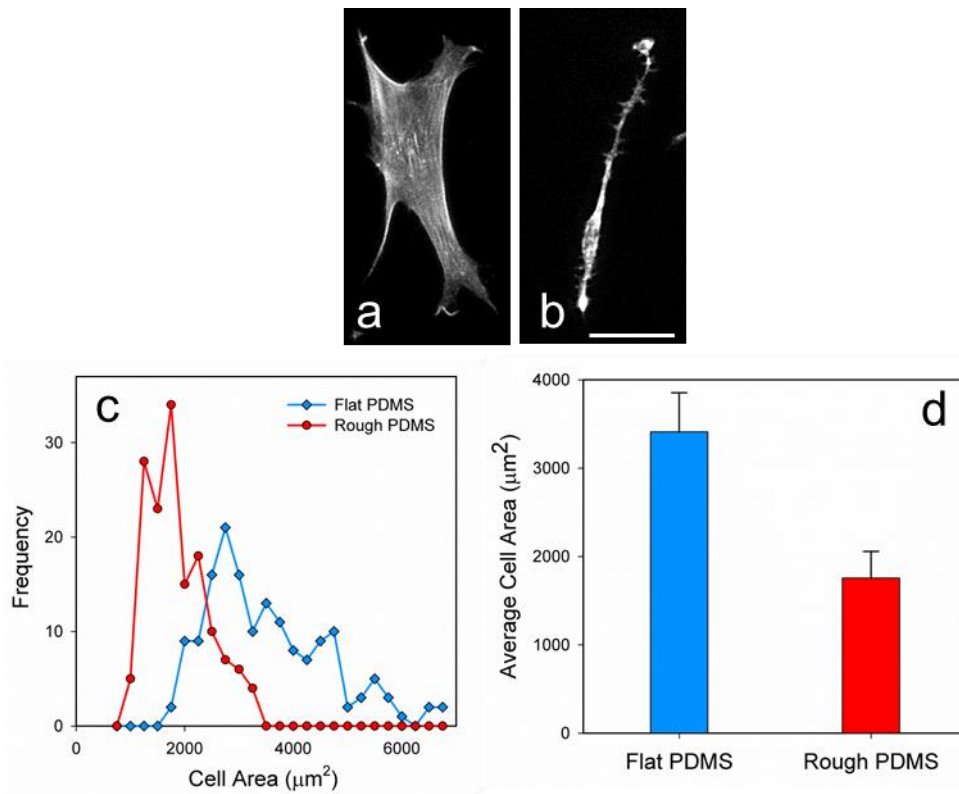


Figure 4.3. (a) Fibroblasts stained with rhodamine phalloidin on AUTMS coated flat and (b) micro-textured PDMS surfaces. Scale bar is equal to $50 \mu\text{m}$. (c) Frequency plot of cell areas from fibroblasts cultured on flat and rough PDMS surfaces. (d) The average cell area of fibroblasts cultured on flat ($3410 \mu\text{m}^2$) and micro-textured ($1760 \mu\text{m}^2$) PDMS surfaces. All area measurements were made 24 hours after cell seeding. All data is based on ~ 150 cells for each surface over three separate experiments.

To investigate the mechanism of this cell morphology difference, cells growing on each surface type were stained and imaged with confocal microscopy to observe the nature of the focal adhesion complexes and actin cytoskeleton within the cells. Focal adhesions were investigated by staining cellular vinculin, a common protein associated with adhesion sites to a surface. Fibroblasts in Figures 4.4a and 4.4b are shown as maximum intensity composite images, where each composite is composed of 165 images from a Z-stack that have been “flattened” into a single image. Figures 4.4c and 4.4d represent color-coded topography images generated by image analysis of Z-stacks from Figures 4.4a and 4.4b respectively for analysis of the cell’s vertical profile.

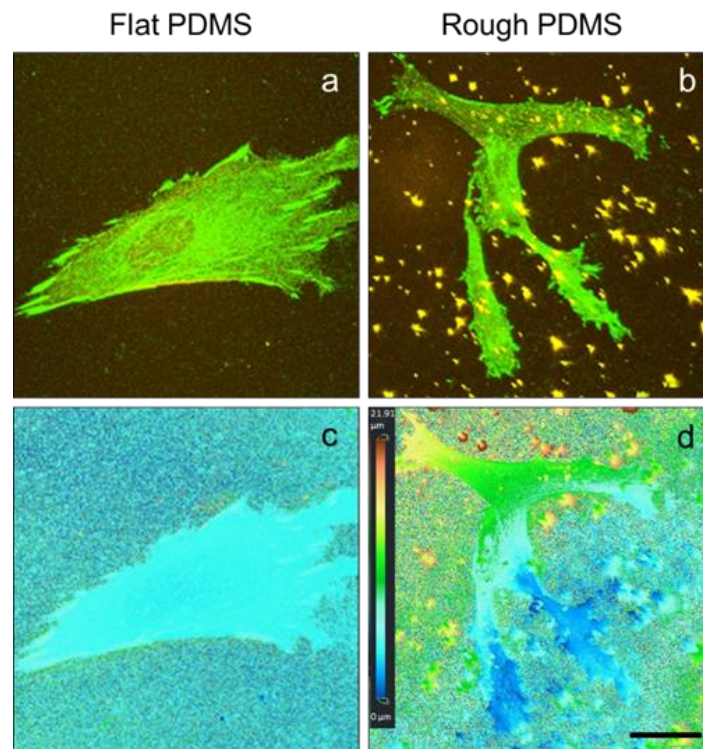


Figure 4.4. Fluorescent staining of fibroblasts grown on (a) flat and (b) micro-textured PDMS substrates. The top row of images are maximum intensity plots composed from confocal microscopy Z-stacks of vinculin (green) and actin (red) staining. Cells were fixed and stained 24 hours after seeding. Scale bar is equal to 25 μm .

For further analysis of cell adhesion on the modified polymer substrates, AFM was used to obtain force curve data from fibroblasts attached to a tipless cantilever as shown in Figure 4.5. The fibroblast attached to the cantilever was brought into contact with the surface for 1 second and then removed; the resulting force required to remove the cell from the surface was analyzed and is shown as a frequency plot in Figure 4.6. The inset shows an example of a force curve plot obtained from a cell removed from a flat PDMS surface. The force required to remove a cell from the flat PDMS was found to have a large distribution between 400 and 7,500 pN while the force to remove a cell from the rough PDMS is almost exclusively located between 50 and 300 pN.

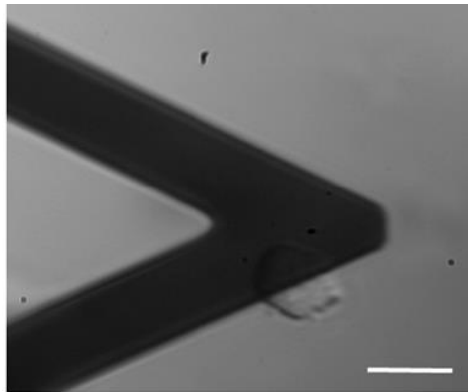


Figure 4.5. Fibroblast cell attached to tipless AFM cantilever. Scale bar equals 100 μm .

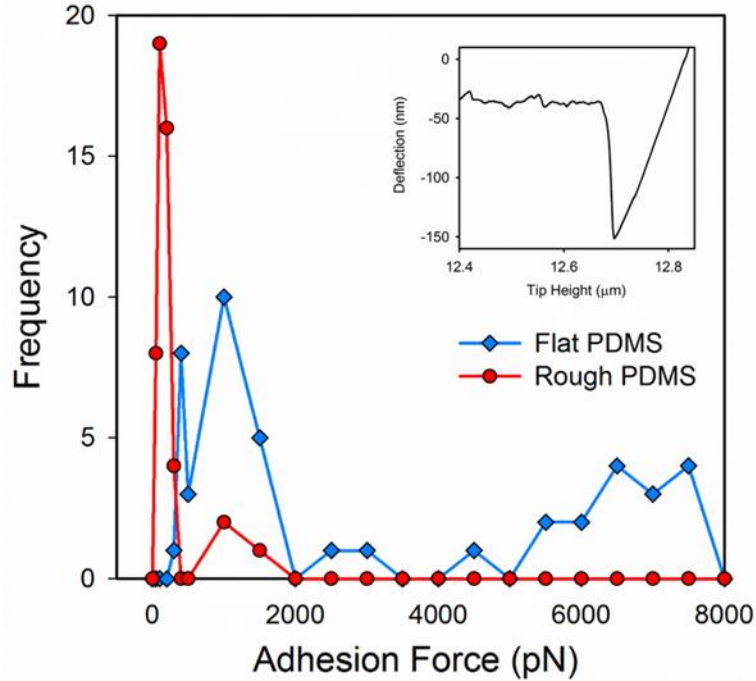


Figure 4.6. Frequency plot of AFM cellular adhesion measurements on flat and micro-textured PDMS. Inset contains an example of a force curve plot obtained from a cell removed from a flat PDMS surface.

4.3.3 ECM Arrangement

Fluorescent staining for f-actin, FN, and nuclei with cells attached to the surface and FN staining of the surface after their extraction is shown in Figure 4.7. Cells cultured on the flat PDMS (Figure 4.7a) displayed obvious, long actin stress fibers across the length of the cell. No actin fibers are observed in fibroblasts on the rough surface (Figure 4.7b), instead actin is distributed uniformly throughout the majority of the cell body. FN is observed in Figure 4.7a-d with the cell present and after detergent extraction from the surface. Complete removal of the cells from the surface was confirmed by staining for surface actin. No actin was observed on either the flat or micro-textured PDMS surfaces, indicating no intact cells remained on the surfaces (data not shown).

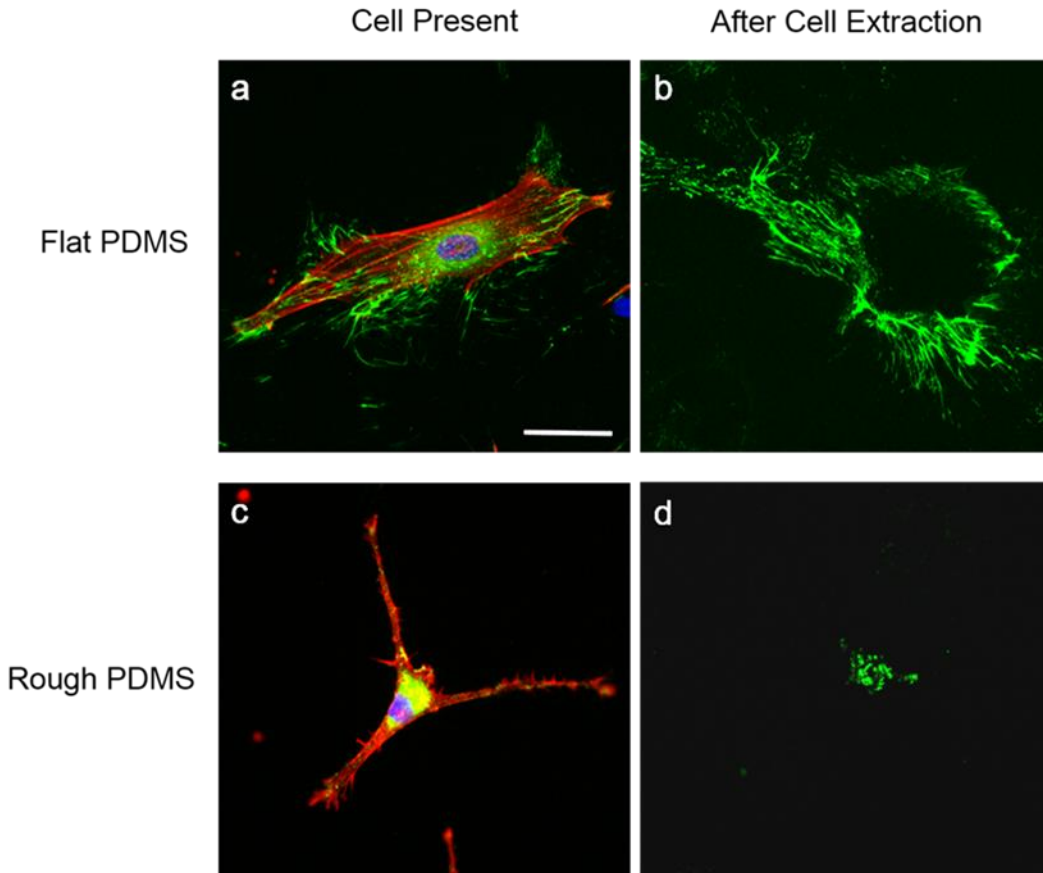


Figure 4.7. Fluorescent images of FN (green), f-actin (red), nucleus (blue) stain. (a) A fibroblast cultured on flat PDMS (b) and a flat PDMS surface after cell extraction. (c) A fibroblast cultured on rough PDMS, (d) and a micro-textured PDMS surface after cell extraction. Cells were fixed and stained 24 hours after seeding. Scale bar is equal to 50 μm .

4.4 Discussion

Initial characterization of the two different surface topographies observed in Figure 4.2 and quantified in Table 4.1 reveals two unique micro-environments for cell culture. The significant increase in surface roughness and hydrophobicity induces a morphology change when compared to the flat polymer substrate. The spindle like, slender morphology of the fibroblasts cultured on the rough surface has been noted in previous reports of cells on porous substrates²¹⁸ and is

drastically different from the fibroblast cultured on the flat PDMS where there is extensive cell spreading and less elongation, giving the cells a much greater surface area. The change in cell area is quantified in Figure 4.3c and 4.3d, with the cell area of fibroblasts on the micro-textured surface being almost half the value observed for cells on the flat PDMS. The 2 – 6 μm features of the PDMS limit cell spreading and produce cells comparable with the morphology of fibroblasts observed *in vivo*^{11, 219}. Fibroblasts on the flat substrate do not have their growth restricted and can have a large cell areas as well as a greater variety of cell areas as seen in Figure 4.3c.

To compare cell morphology with cellular adhesion, confocal microscopy was performed on fibroblasts with fluorescently labeled vinculin and actin (Figure 4.4). Fibroblasts cultured on flat PDMS are ringed with discrete focal adhesion complexes, as shown by vinculin staining, connected throughout the cell cytoplasm by an actin protein network to produce a stereotypical “fried egg” cell shape observed in cells cultures on conventional tissue culture plastic and flat growth surfaces^{220, 221}. Cell thickness for fibroblasts on the flat PDMS does not vary; rather it keeps a consistent $\sim 6 \mu\text{m}$ height as seen in Figure 4.4c. In contrast, fibroblasts growing on roughened PDMS display no discrete focal adhesion complexes, and thicker morphology (Figure 4.4d). The increase in Z-direction growth of the cells is the cause of the apparent decreased cell cross-sectional area of cells grown on rough surfaces. The increased cell thickness has been reported with fibroblasts cultured on coarsely etched and micron grooved titanium substrates^{222, 223}. An artifact associated with the PDMS substrate is apparent in some of the confocal images. Distinct yellow dots on the micro-textured PDMS images are apparent in Figure 4.4b. These dots do not appear on the flat PDMS substrates. Control experiments were performed where unmodified rough PDMS and AUTMS coated PDMS were exposed to actin and vinculin staining procedures in the absence of fibroblasts (Figure 4.8). The results indicate residual antibody stain

is captured in the micro-pits of the PDMS surface producing the fluorescent spots on the confocal images. These spots are not associated with vinculin or actin produced by the cell.

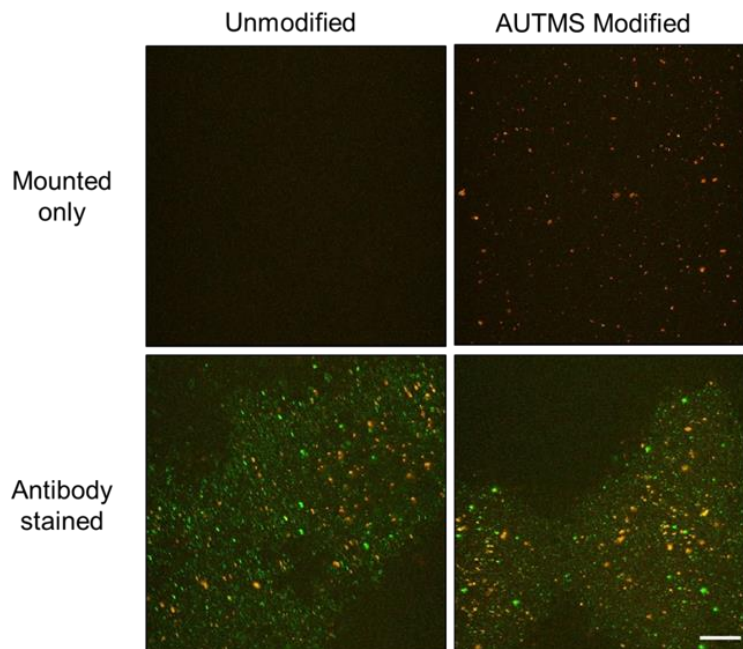


Figure 4.8. Maximum intensity plots of vinculin and actin staining of unmodified rough PDMS (left column) and rough PDMS modified with AUTMS (right column). Scale bar is equal to 25 μm for all images.

Cellular adhesion was further investigated with AFM SCFS as shown in Figure 4.6. Unlike the vinculin labeling after 24 hours of cell-surface contact, the SCFS data revealed information about the initial cell-surface interaction and adhesion forces associated with only a second of surface contact. Cell adhesion is the sum of formation of discrete ligand-receptor bonds and forces such as Van der Waals, electrostatic, and steric interactions^{224, 225} and a large change in adhesion is noted between cells on the two polymer substrates. The drastic difference in initial cell adherence can be attributed to the change in surface area the cell encounters when pressed against the polymer. The micro-textured PDMS surface would have a smaller surface area for the cell to

attach to than the flat PDMS allowing the cell to be removed with less force. Since the cell would make initial contact with the micron scale peaks on the roughened PDMS surface, the peaks would be regions where the beginning of the formation of focal adhesion complexes could occur. This would also correspond to the increase in cell volume on the rough surface noted with confocal microscopy. Cells cultured on the flat PDMS have the ability to immediately spread on the surface, decreasing their height and thickness. The ability to readily spread would increase their ability to adhere and increase the force needed for their removal. Fibroblasts on the rough surface, have their spreading ability hindered, so as they adhere their thickness decreases minimally then remains relatively constant. The lack of cell spreading and attachment reduces the force needed to remove them with the AFM.

Recent studies by Pierres *et al.*²²⁶ indicate that early cell-substrate interactions cause membrane fluctuations that induce mechanisms for cell behavior including adhesion and morphology. Although the data was observed at two different time points, a correlation can be drawn between the adhesion forces collected from the AFM and the fluorescent labeling of focal adhesion points in Figure 4.4. The large forces required to remove a cell from the flat PDMS are indicative of an increase of ligand receptor bonds. The subsequent enlargement of these adhesion focal points and recruitment of new adhesive molecules generates discrete vinculin islands as seen in Figure 4.4a. The initial lack of surface adhesion on the micro-textured PDMS could alter the cell membrane so that no isolated focal adhesion points occur and decrease the amount of force needed to remove the fibroblast from the PDMS. This could also explain the observed lack of cellular proliferation on the rough PDMS surface. Although not quantified, there was a decrease in the number of cells on the rough surface when compared to the flat PDMS when cells were observed with fluorescence microscopy. The limited cell adhesion during initial attachment and

replacement of culture media after one hour from cell seeding would decrease the number of cells on the rough surface. However, this has not been investigated.

Actin and ECM composition of cells on the two different surfaces are examined in Figure 4.7. Comparing the fibroblasts on the two surfaces an altered morphology is observed as described earlier, but a significant change is also observed in the actin cytoskeleton. Cells cultured on the flat PDMS (Figure 4.7a) displayed obvious, long actin stress fibers across the length of the cell. This is consistent with cells cultured on flat substrates that can induce cytoskeletal stress and promote multiple stress fibers²²⁷. Fewer actin fibers are observed in fibroblasts on the rough surface (Figure 4.7b), instead actin is distributed uniformly throughout the majority of the cell body. The lack of fibers is similar to fibroblasts observed *in vivo*²²⁸ making the micro-textured PDMS scaffold more similar to a native cell environment when considering cellular actin distribution. FN is observed in Figure 4.7a-d with the cell present and after extraction from the surface. Fibroblasts on the flat PDMS surface produce strands of FN inside and outside the cell body creating a large ECM surrounding the cell. On the micro-textured substrate, FN is centered around the cell nucleus with less distribution through the cell body and little or no FN is observed outside of the cell. This cellular FN can then be compared to FN left on the PDMS surface after cell removal. The FN deposited on the flat PDMS surface after cellular extraction, is a silhouette of ECM representing part of the original cell shape (Figure 4.7b). This cellular “footprint” on the flat PDMS contains individual strands of FN which are also seen in the fibroblast in Figure 4.7a. In contrast, the ECM deposition on the roughened PDMS, observed after cellular extraction (Figure 4.7d) displays discrete compact, islands of FN on the micro-features of the surface. Cellular extraction was confirmed by staining for surface actin. No actin was observed on either the flat or micro-textured PDMS surfaces, indicating no intact cells remained on the surfaces.

The strands of FN detected on the flat PDMS are indicative of tension generated by the cytoskeleton²³ which is also indicated by the actin stress fibers noted in Figure 4.7a. Generation of FN fibrils is completed by integrin binding and more importantly FN-FN binding²²⁹ signifying a significant decrease of FN-FN binding sites in fibroblasts cultured on the roughened PDMS compared to the flat. Under the experimental conditions described here, cells were seeded and allowed to attach to the substrates in serum free media that was subsequently replaced with media containing a low concentration of FBS (1% v/v). Lacking FN adsorption to the PDMS surface from solution deposition, the majority of FN observed can be assumed to be cell-derived. The two types of FN secretion depicted, fibrils and compact islands for flat and micro-textured PDMS respectively, can have dramatic effects on cell signaling²³⁰. By simply altering the surface features we have altered the ECM assembly and driven its development in two different directions. The ability to control and guide ECM development using surface roughness provides a powerful tool in creating biomaterials that can produce physiologically relevant cells and tissues.

Designing an artificial 3-D cellular environment to mimic a native cell system is complex and impractical for single cell studies, but research using 2-D environments is not ideal for physiological cell behavior. The surface presented offers an alternative system, where surface micro-roughness stimulates cells to exhibit responses that have been noted *in vivo*. The surface is not a 3-D matrix, but the distinctive topography provides similar results to cells in a 3-D system. The markers for monitoring cell behavior reported here can be compared to a study by Cukierman *et al.* where human fibroblasts were cultured on flat substrates and compared to *in vivo* environments²²⁰. Cukierman noted discrete islands of focal adhesion sites in cells cultured on flat substrates, but none in cells in a native environment. This is analogous to our focal adhesions observed by vinculin staining where no islands of vinculin were noted, but a uniform distribution

of focal adhesions throughout the cell body. Cells on our flat substrates spread to have large surface areas creating tension on the cell membrane, requiring anchors of focal adhesions to bind them to the surface. On the micro-roughened surface, cell spreading was hindered and bulky, discrete focal adhesions were not needed. As mentioned previously, actin stress fibers are another indicator of a cell environment. Actin stress fibers are indicative of cells on planar surfaces and are formed at the base of focal adhesion sites²³. Fibroblasts on our roughened substrate exhibit no actin fibers, but like vinculin, actin is evenly distributed throughout the cell. In an *in vivo* system, cells are constantly having their ECM remodeled and undergoing cytoskeletal rearrangement. Substantial actin stress fibers and focal adhesions would hamper cellular development in a living system²⁹. The rough PDMS surface mimics a native system by restricting significant cell adhesion and cytoskeletal actin filaments. ECM, adhesion, and cytoskeletal organization are mediated by integrin binding to their surroundings²²⁹. The micro-roughness fabricated created changes in the cell-surface interface and therefore integrin attachment and cell signaling. Compared to the flat PDMS, the rough PDMS generated significantly changed cell behavior that is analogous to cell behavior observed *in vivo* and other 3-D culture systems.

4.5 Conclusion

In this study, we have fabricated a polymer substrate with surface micro-roughness that has been thoroughly characterized. The rough surface was capable of altering fibroblast geometric area and adhesion when compared to fibroblasts cultured on a flat substrate; with cells on the micro-textured substrate having a smaller morphology and fewer discrete focal adhesion complexes. AFM SCFS was used to analyze the initial adhesion force of cells in contact with the

polymer substrates. Vinculin staining and AFM adhesion measurements indicate a decrease in cell adhesion on the rough PDMS surface. Actin formation and ECM deposition was also analyzed with cell present and after extraction from the surface. FN secretion left a partial cell “footprint” giving insight into the fibroblast-substrate interaction and valuable information on cellular behavior with polymer micro-topography. FN formation on each surface was driven in two different directions, with long FN fibril formation on the flat surface and compact islands of FN on the rough surface. This indicates a bottom-up approach, using surface topography will guide cell ECM formation and gives insight on the impact of micro-architecture on cell behavior. The templating technique described here can be applied to a number of tissue engineering or cell-surface studies to better replicate *in vivo* environment using low cost, *in vitro* surface fabrication methods. The cell-substrate relationship is complex and understanding how material interactions can alter and manipulate biochemical signaling will be critical for future *in vitro* cell analysis.

5.0 Fibroblast behavior on chemically patterned and micro-roughened PDMS surfaces

5.1 Introduction

In vitro studies of cell behavior are an essential prerequisite in modeling *in vivo* responses to, pharmacological agents, cell therapies, biomaterials, and implantable devices. Culturing mammalian cells in a polystyrene Petri dish or on a glass coverslip are widely used methods for cell analysis. However, as described in Chapter 3 and 4, a 2-D environment for cell culture is not an accurate representation of the *in vivo* environment of the cell^{188, 203, 204, 231}. The complexity of the *in vivo* domain cannot easily be imitated by 2-D substrates and therefore 3-D scaffolds must be designed to replicate the *in vivo* microenvironment. Cells grown in 3-D cultures have been shown to exhibit different morphology^{220, 232}, adhesion^{201, 233}, proliferation^{234, 235} and gene expression^{236, 237} as compared to cells cultured on flat substrates. Modifying surface roughness can create a *pseudo* 3-D platform for cell growth, allowing for the study of biological properties that may not be found using conventional 2-D cell culture. The influence of surfaces with ordered textures and random topographies on cell behavior has been widely studied^{196, 238}, but has yet to be combined with micro surface patterning. Previous work has studied cell viability exclusively on chemically patterned surfaces using self-assembled monolayers (SAMs)²³⁹⁻²⁴¹, or on micron – scale rough surfaces²⁴²⁻²⁴⁴. In this work we show how textured, rough surfaces may also be combined with biochemical patterns for directed growth of cells on micron-scale, surface-patterned substrates.

Structural organization and alignment of cells created by the surface micro-pattern combined with surface roughness facilitates applications in tissue engineering such as the co-

culturing of cells, high throughput screening (HTS) assays^{245, 246} and the fabrication of “organ on a chip” systems²⁴⁷. Current methods in surface tissue engineering lack organization of cell growth resulting in tissues that do not emulate the *in vivo* tissue they were made to replace^{248, 249}, while HTS assays are carried out on a 2-D surface raising concerns where the morphology of the cells differs from the cells observed *in vivo*²⁵⁰. The surface presented here has the potential to address both problems by producing directed cell growth on a micro rough environment. The cell alignment can mimic highly organized native tissue structure, such as blood vessels, while being cultured on a micro-rough surface topography. Other attempts at producing a pattern on a rough surface have been tested, but resulted in large, macro-scale patterns with inconsistent reproducibility and little cell viability analysis²⁵¹.

Fabrication of the surface presented uses a simple templating technique to produce a polymer microstructure that has been discussed thoroughly in Chapter 3²¹³. Chemical modification is done using photolithography processes combined with protein adsorption to produce 50 μm wide lines of FN on the surface as seen in Figure. 5.1. The technique described has the possibility of being assimilated onto a wide range of other 3-D platforms including; polymers, plastics, and commercially available scaffolds. The templating and patterning procedure described offers a simple and reproducible method for culturing cells with controlled, directional growth on a scaffold with defined architecture. The influence of the rough polymer scaffold is examined and compared to modified and unmodified tissue culture polystyrene for an in-depth analysis of the benefits of surface topography for cell culture.

5.2 Experimental Methods

5.2.1 Photoresist Pattern on Rough and Flat PDMS Surfaces

PDMS was cut into 3 x 3 cm squares and sonicated in a 1:1 ethanol: deionized water solution for 5 minutes, dried in nitrogen, and baked at 70° for 20 minutes to remove any excess solvent. The surfaces were activated for 45 seconds with oxygen plasma to allow a more uniform coating of photoresist²⁵². Before photoresist deposition the PDMS was baked on a hot plate for 3 minutes at 150° C and then cooled for 5 minutes at room temperature. Photoresist was spin coated (3000 rpm for 45 seconds) onto the PDMS surface and then baked at 115° C for 3 minutes. The photoresist coated PDMS was exposed to 400 nm light through a chrome mask using a Suss MJB4 Mask Aligner (Garching, Germany) for 6 seconds. The photoresist coated PDMS was incubated in developer for 1 minute before being rinsed with water and dried in nitrogen. Photoresist deposition and patterning was completed at Harvard University's Center for Nanoscale Systems (CNS, Cambridge, MA).

5.2.2 BSA and FN Patterning on PDMS Surfaces

PDMS with photoresist patterns were incubated in 10 mg/mL of bovine serum albumin (BSA) in Dulbecco's phosphate-buffered saline (DPBS, Cellgro, Manassas, VA) for 30 minutes at room temperature. The PDMS surfaces were washed with water, sonicated in acetone for 1 minute to remove remaining photoresist, washed again with water, and dried in a stream of nitrogen. The surface was then incubated in 25 µg/mL of FN in PBS for 1 hour at room temperature. The PDMS surfaces were sonicated in water for 30 seconds and dried in nitrogen. The fabrication of the surface, photoresist deposition, and FN/BSA patterning can be seen in Figure. 5.1.

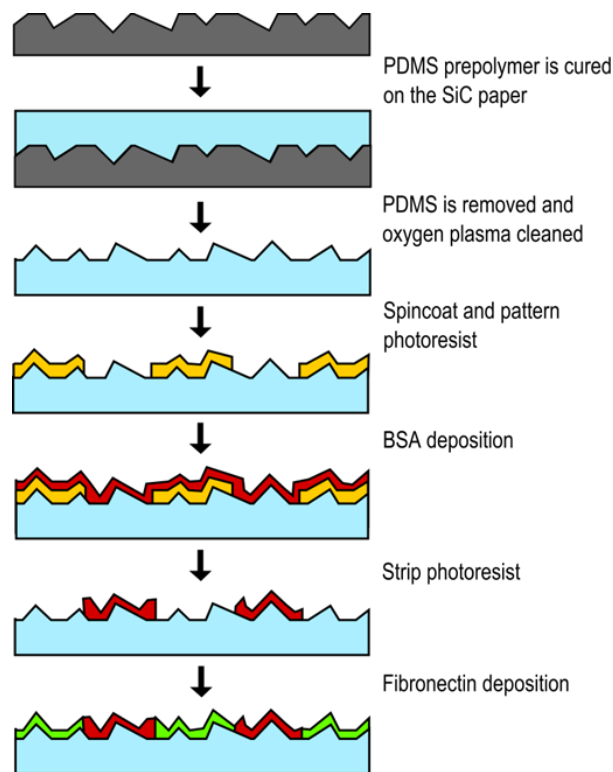


Figure 5.1. Cartoon representation of rough PDMS surface fabrication and BSA and FN deposition and patterning.

5.2.3 PDMS and Petri Dish Surfaces for Morphological and Gene Expression Analysis

Morphology and protein analysis experiments were carried out on un-patterned $_{FN}Flat$, $_{FN}Rough$, $_{FN}Petri$ dish, and $_{UN}Petri$ dish surfaces. FN deposition procedures for un-patterned surfaces were consistent with FN patterning procedures described earlier. Flat and rough surfaces PDMS surfaces were sonicated in a 1:1 ethanol: de-ionized water solution, dried in a stream of nitrogen, and baked at 70° C for 10 minutes. The surfaces were activated with oxygen plasma for 45 seconds before immediate incubation in 25 μ g/mL FN solution in PBS to produce $_{FN}Flat$ and $_{FN}Rough$ PDMS surfaces. PDMS surfaces were sonicated in sterile, de-ionized water for 30 seconds and dried in nitrogen. Petri dishes were coated with FN by activation with oxygen plasma and incubation in a 25 μ g/mL FN solution as previously described for PDMS surfaces. FN coated

Petri dish surfaces (_{FN}Petri dish) were rinsed 2X with PBS before cell culture. Petri dishes that had no FN coating were used without surface treatment or modification (_{UN}Petri dish).

5.2.4 Cell Seeding and Imaging

Human fibroblast were seeded on surfaces at an initial 5×10^4 cells/mL in serum free DMEM/F12 media. The cells were allowed to adhere to the surface for 1 hour before the media was aspirated out and replaced with 1% FBS and 1% P/S in DMEM/F12. Cells had media replaced every 2 - 3 days and were cultured in a humidified atmosphere at 37°C and 5% CO₂.

Cells and surfaces to be imaged with fluorescence had media removed and were rinsed twice (2X) with DPBS. The surfaces were then incubated in 1.0 µg/mL Hoechst 33342 trihydrochloride trihydrate (stain for cell nuclei) in PBS for 25 minutes at 37° C. The staining solution was aspirated off and the surfaces were rinsed 2X with fresh PBS. The cells were fixed by incubating the surface in 4% formaldehyde (methanol-free) solution in PBS for 10 minutes at room temperature. The surfaces were washed 2X with fresh PBS, incubated in a 0.1% Triton X-100 solution in PBS for 5 minutes at room temperature, and washed 2X with PBS. Samples were finally incubated in a 20 µL/mL solution of rhodamine phalloidin (stain for f-actin) in PBS with 1% w/v BSA for 20 minutes at room temperature, washed 2X with PBS, and stored at 4°C in PBS until imaged. FN patterns on PDMS were imaged by doping the FN deposition solution with 1.0 µg/mL Alexa Flour 488 WGA in PBS. Photoresist patterns were imaged using bright field microscopy. All images, excluding images for morphology analysis, were taken using a Nikon wide field fluorescent microscope.

5.2.5 Morphological Analysis

Cells were seeded on each surface as described earlier and were allowed to grow for 24 hours before being fixed and stained with Hoechst 33342 and rhodamine phalloidin as previously described. Cells were examined by an inverted Leica (Buffalo Grove, IL) DM IL fluorescent microscope with a Leica DFC420C camera and Leica Application Suite v2.5.0 R1 imaging software. Quantitative analysis was done with ImageJ 1.45s software. Cell area was determined by cellular rhodamine phalloidin fluorescence. Thresholding criteria distinguished cellular fluorescence from nonfluorescent non-cell areas. Cells analyzed were required to have a single, intact nucleus (determined by Hoeschst 33342 stain). Overlapping cells or cell bodies that were not entirely contained in the image were not used. Each histogram and average area reported is data collected from three separate experiments and at least 100 cells.

5.2.6 AFM Characterization of the Surfaces

AFM imaging was completed using MikroMasch (San Jose, CA) DPE18/AIBS cantilevers with a resonant frequency of 64.4 kHz and a nominal force constant of 4 N/m. Three topography images (60 x 60 μm) were taken in AC mode for each type of surface. All surfaces were prepared as described previously. Average roughness (R_a) values, representing the deviation of the surface height, were averaged over the three images for each surface as seen in Table 5.1. The height of the FN was determined on flat PDMS in AC mode by determining the difference in height between a FN coated area and a bare PDMS area.

Table 5.1. Roughness average (R_a) values for $_{FN}Flat$, $_{FN}Rough$, $_{FN}Petri$ dish, and $_{UN}Petri$ dish surfaces acquired from AFM images.

Surface	Roughness Average (R_a) (nm)
$_{FN}Flat$	3.1 ± 0.5
$_{FN}Rough$	730 ± 60
$_{FN}Petri$ dish	13 ± 1.0
$_{UN}Petri$ dish	5.1 ± 0.3

5.2.7 RNA Isolation and cDNA Synthesis

Cells were dissociated from various surfaces by exposure to 0.25% trypsin-EDTA. Trypsin was neutralized by addition of an equivalent volume of complete growth medium, and the cells were pelleted by a 5 minute centrifugation at 100 x g. The supernatant was aspirated and the cell pellet was washed in 1 mL DPBS and re-pelleted as above. The PBS was aspirated off, and the dry pellet immediately flash frozen in liquid nitrogen. Pellets were stored at $-80^{\circ}C$ for up to 2 weeks. RNA was isolated from frozen cell pellets using the Trizol® (Life Technologies) method according to manufacturer's suggested protocols. Purified RNA was resuspended in 20 μ L of nuclease-free water followed by the addition of 2 U RNase-free DNase I and incubated at $37^{\circ}C$ for 30 minutes, followed by a heat-inactivation incubation of $85^{\circ}C$ for 10 minutes. RNA concentration was quantified using a NanoDrop 2000 spectrophotometer (Thermo Scientific, Wilmington, DE), and adjusted to a final concentration of 1 μ g/ μ L in nuclease-free water if necessary. RNA quality was assessed by running 1 μ g of RNA on a 1% Tris-Acetate EDTA (TAE) agarose gel and visualizing the 28S and 18S rRNA bands *via* ethidium bromide staining using a ChemiDoc-It TS2 Imager (UVP, Upland, CA). cDNA was reverse transcribed from purified RNA using the qScript cDNA Supermix according to the manufacturer's suggested protocols. To

validate the reverse transcription reaction and to validate the absence of genomic DNA contamination, a 50 ng RNA equivalent of the cDNA reaction mix (positive control) or a 50 ng RNA equivalent without reverse transcriptase (negative control) was used in a 20 μ L PCR reaction with 10 μ L of 2X GoTaq Green Mastermix using 250 ng each of forward and reverse primers specific for GAPDH (Table 5.2). PCR were carried out by initial denaturation at 95°C for 5 minutes followed by 30 cycles of 95°C for 30 seconds; 60°C for 30 seconds; 72°C for 30 seconds, with a final 72°C extension of 7 minutes on a T100 Thermal Cycler (BioRad, Hercules, CA). Products were resolved on a 2% TAE agarose gel and visualized by ethidium bromide imaging as described earlier.

5.2.8 Relative / Real-Time PCR

The human Extracellular Matrix & Adhesion Molecules PCR Array was purchased from Qiagen and run according to manufacturer's suggested protocols on the RealPlex² real-time PCR system (Eppendorf, Hauppauge, NY). Briefly, a 500 ng RNA equivalent of the cDNA reaction in 100 μ L of molecular grade water was combined with 1350 μ L of 2x RT² SYBR Green Mastermix and 1250 μ L of molecular grade water. 25 μ L of the final reaction mix was pipetted into each well of the RT² PCR array plate, and the plate was centrifuged to remove air bubbles. The reaction was subjected to PCR with the following parameters: initial denaturation of 95°C for 10 minutes followed by 40 cycles of 95°C for 15 seconds and 60°C for 1 minute with a 35% ramp speed and image capture at the end of the 60°C incubation. A 20 minute melting curve from 60°C to 95°C was carried out following PCR to examine purity of double-stranded DNA species. Relative gene expression was calculated using the $\Delta\Delta$ Ct method using GAPDH as the reference gene. All data

are presented as fold-change assuming a 100% efficiency in product doubling using the equation $2^{(-\Delta\Delta Ct)}$.

To validate PCR array results, a separate real-time PCR reaction was carried out using independently-designed, intron-spanning primers (Primer Blast NCBI, Table 5.2). Accordingly, a 25 ng RNA equivalent of the cDNA reaction was combined with 10 μ L of 2X SYBR Green Supermix 250 ng each, of forward and reverse primer, in a 20 μ L final reaction volume. Real-time PCR was carried out on the RealPlex² real-time PCR system (Eppendorf) with the following parameters: initial denaturation of 95°C for 10 minutes followed by 40 cycles of 95°C for 15 seconds, 60°C for 20 seconds, 72°C for 20 seconds, 85°C for 15 seconds with a 100% ramp speed and image capture at the end of the 85°C incubation.

Table 5.2. Primer sequences used to validate expression levels from PCR array.

	Primer	Sequence 5'-3'	Amplicon Size (bp)
MMP14	Forward	GGTGGTCTCGGACCATGTCT	178
	Reverse	TGTGTGTGGGTACGTAGGTC	
CTNND2	Forward	TGCTCAAATCCAGACACGCT	120
	Reverse	GATGGGCAGGCCTTTCTCTT	
COL15A1	Forward	GGAGGGGGTTCATTCTGTGG	186
	Reverse	ATAGAGAGGGTTGGTCCCCC	
COL6A1	Forward	CACTCAAAGCAGCGTGGAC	140
	Reverse	GTCGGTCACCACAATCAGGT	
GAPDH	Forward	ACAGTCAGCCGCATCTTCTT	288
	Reverse	TGGAAGATGGTGATGGGATT	

5.3. Results

5.3.1 BSA and Fibronectin Patterning on PDMS

The patterning and fabrication of the PDMS surfaces is summarized in a cartoon shown in Figure 5.1. Topography images ($60 \times 60 \mu\text{m}$) of the final PDMS surfaces were acquired using AFM and are shown in Figure 5.2. PDMS patterned with $50 \mu\text{m}$ wide stripes of FN separated by $60 \mu\text{m}$ stripes of BSA are shown in Figure 5.3. The FN stripes encourage cell adhesion while the BSA stripes limit cell adhesion confining the cells to the FN regions. It is noted that the stripes are significantly wider than the dimensions of individual cells. The FN was fluorescently labeled for imaging on flat and rough PDMS surfaces, as seen in Figure 5.3b and 5.3d respectively. Figure 5.3 clearly shows that pattern dimensions are retained throughout the experiments, from the photoresist stripes to the FN stripes.

5.3.2 AFM Characterization of Surfaces

Topography images ($60 \times 60 \mu\text{m}$) of the FN coated flat (FN_{Flat}) and rough (FN_{Rough}) PDMS surfaces in Figure 5.2 were taken with AFM to determine surface topology and to discern nano- and micro- scale surface features. Nano-scale cracks on the FN_{Flat} PDMS surface contribute to its roughness (Figure 5.2a) as determined from the R_a value. These cracks are due to a combination of exposure to oxygen plasma²⁵³ and dried adsorbed FN on the surface. AFM images of PDMS surface before oxygen plasma exposure or FN deposition did not exhibit any surface cracks (data not shown). On the FN_{Rough} surface, $2 - 6 \mu\text{m}$ wide peaks and valleys, with heights of $1 - 3 \mu\text{m}$ (Figure 5.2b) give a much greater R_a . The R_a for the FN_{Flat} and FN_{Rough} PDMS surfaces was calculated to be $3.1 \pm 0.5 \text{ nm}$ and $730 \pm 60 \text{ nm}$ respectively (Table 5.1).

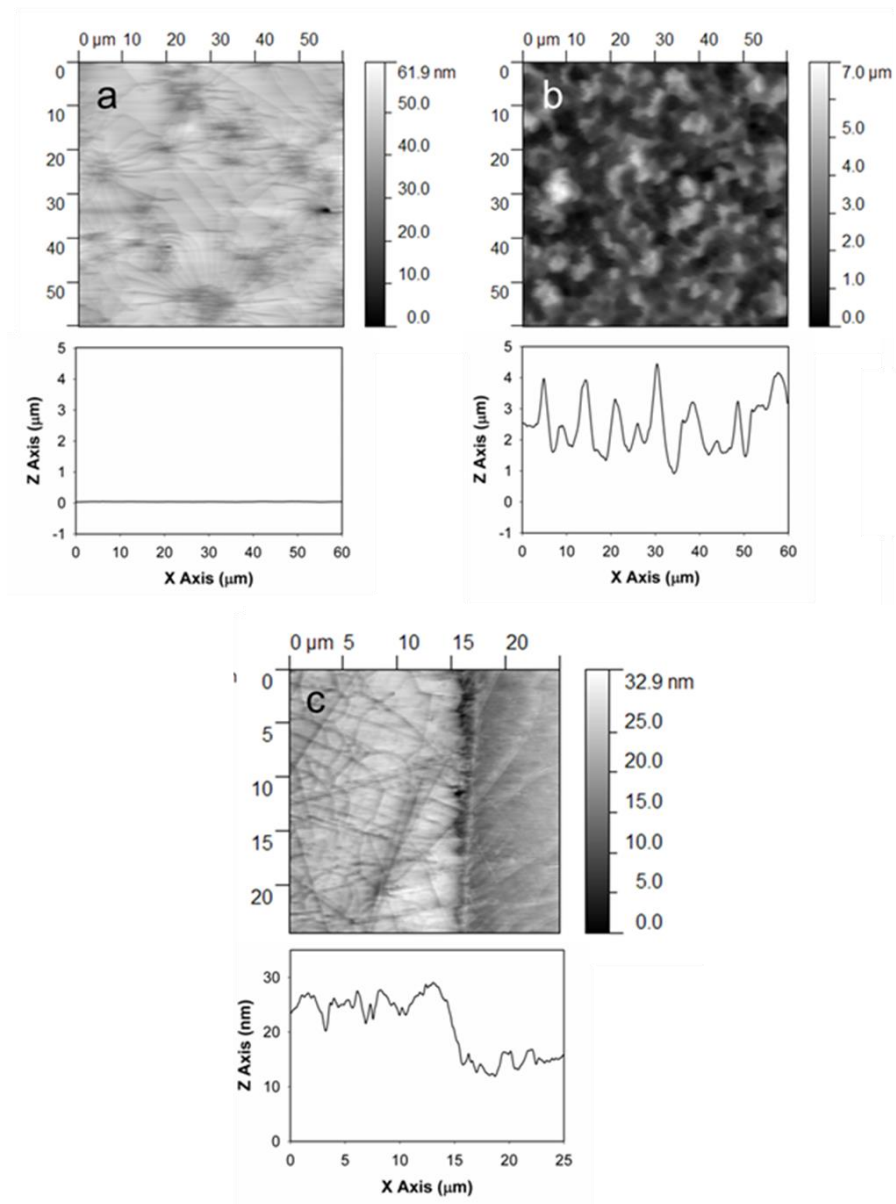


Figure 5.2. (a) 60 x 60 μm AFM image of flat PDMS coated in FN and a corresponding horizontal line section below. (b) 60 x 60 μm AFM image of rough PDMS coated in FN and a corresponding horizontal line section below. (c) A 25 x 25 μm AFM image of a FN stripe on top of a flat PDMS surface and a corresponding line section below. Note difference in Z-scale between panels *a* (0 – 61.9 nm), *b* (0 – 7.0 μm), and *c* (0 – 32.9 nm).

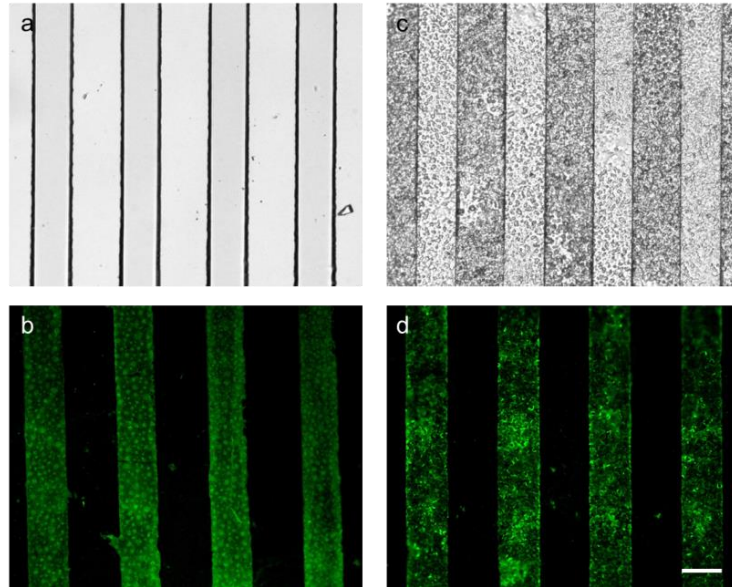


Figure 5.3. (a) A 50 μm stripe photoresist pattern with 60 μm spacing on flat PDMS (b) FN adsorbed on flat PDMS after photoresist removal and BSA deposition (c) A 50 μm stripe photoresist pattern with 60 μm spacing on rough PDMS (d) FN adsorbed on rough PDMS after photoresist removal and BSA deposition. Photoresist images were taken in bright-field. FN was labelled with Alexaflour 488 WGA and imaged with a fluorescent microscope. Scale bar is equal to 50 μm .

Determination of the thickness of the FN layer on the PDMS was found using AFM. The height of the FN was determined to be approximately 10 nm as seen in the 25 x 25 μm image in Figure 5.2c. The line section in Figure 5.2c clearly defines a FN coated area and non-FN area (bare PDMS) on the flat PDMS surface. Cracks in the FN and PDMS surface are noted and are similar to the cracks seen in Figure 5.2a. To quantify how surface topography impacts cell behavior of fibroblasts, cell area and protein expression were analyzed on the PDMS_{FN}Rough and PDMS_{FN}Flat surfaces as well as FN coated Petri dishes (FNPetri dish), and unmodified Petri dishes (UNPetri dish). The R_a values for the Petri dish surfaces can also be seen in Table 5.1. The R_a values for FNPetri dish and UNPetri dish are 13 nm and 5.1 nm respectively. The difference in the

R_a value between the two types of Petri dishes is most likely due to the FN structure on the $_{FN}$ Petri dish which would increase the apparent surface roughness compared to $_{UN}$ Petri dish. Taken together, these results describe the physical characteristics of our test surfaces, and demonstrate that a nanometer scale layer of FN can be efficiently patterned onto a micro-roughened surface.

The Petri dish surfaces were chosen to compare to PDMS because they are commonly used for cell culture experiments²⁵⁴, but there is a significant difference in the stiffness of both materials. The Young's modulus, a measure of elasticity of a material, of PDMS (made with a 10:1 ratio of elastomer:hardener) is 2.6 MPa²⁵⁵, and 3.7 GPa for polystyrene Petri dishes²⁵⁶. The large Young's modulus value for polystyrene is indicative of the high degree of cross linking in the polymer, making it more rigid and difficult to stretch. PDMS is flexible and therefore has a lower Young's modulus. When compared to $_{UN}$ Petri dish, the $_{FN}$ Flat and $_{FN}$ Rough PDMS surfaces are more pliable and have a protein coating, but when $_{FN}$ Petri dish is compared to the PDMS surfaces, there is only a change in material stiffness. This allows cell culture between conventional Petri dishes and our *pseudo* 3-D PDMS scaffold to be compared and analyzed. Further examination of material properties on cell behavior will be discussed.

5.3.3 Fibroblast Culture on Surface Pattern

Human fibroblast cells were cultured on the FN/BSA patterned surface and monitored over six days. Cells were fixed and stained with rhodamine phalloidin 1, 3, and 6 days after cell seeding (Figure 5.4). Cells adhered to the FN pattern after one day of culture and little or no attachment was noted on the BSA spaces. Fewer cells were observed on the rough surface than the flat PDMS surface, albeit not at statistically significant levels (data not shown). Even restrained to the 50 μ m lines, the cells on each surface still had a significantly different morphology. Over the entire six

day monitoring period, the cells on the flat surface retain a large cell area and extensive spreading. Cells on the rough surface maintain their spindle, elongated shape for the entire six days. The organization of cell growth is also maintained over the six day period, with cells on both surfaces following and growing on the 50 μm wide FN lines. After 3 to 6 days some cell growth off the pattern is noted, but the alignment is still preserved. As evidenced by rhodamine-conjugated phalloidin incorporation, this phenomenon is due, in part, to an altered actin cytoskeleton (Figure 5.4 and 5.5b), as it should be noted that cells on a rough surface are morphologically constrained to an area far narrower than the 50 μm FN lines. The preservation of cell alignment over an extended time frame on a 3-D scaffold offers new and exciting possibilities for more biologically relevant HTS assays and tissue engineering studies. Given that surface chemistry and topography are critical in determining cell behavior, new tissue and cell culture scaffolds must be developed to mimic *in vivo* environments¹⁹⁵. This requires directional cues for cell organization as well as a 3-D micro environment to imitate surrounding tissue and ECM. To achieve this goal, a micro rough scaffold with a biochemical pattern has been developed as seen in Figure 5.4.

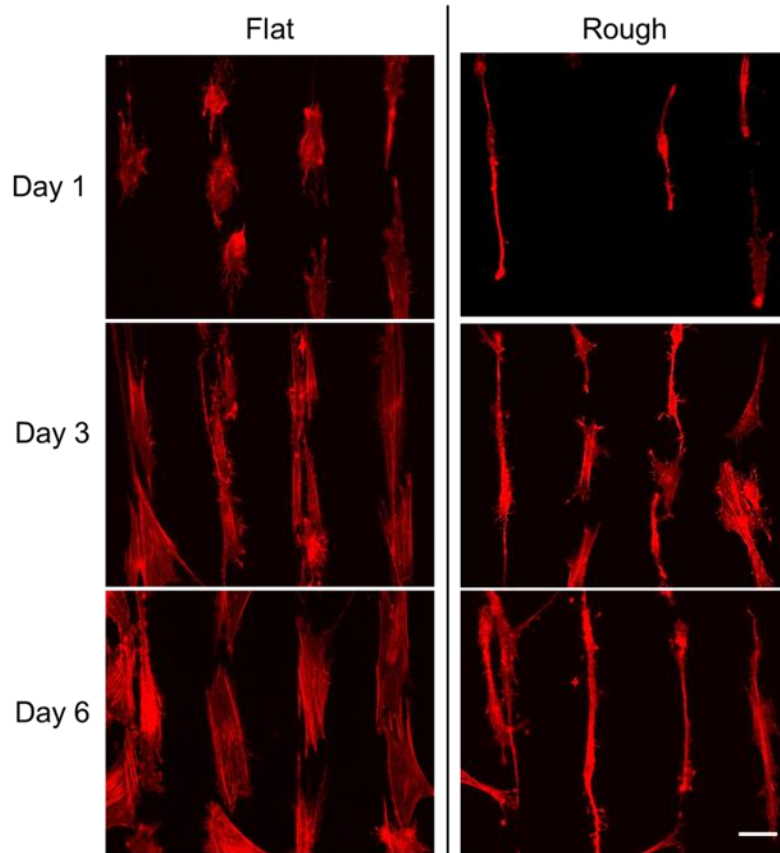


Figure 5.4. Fibroblast growth monitored at 24 hours, 3 days, and 6 days after cell seeding on 50 μm stripes of FN separated by 60 μm stripes of BSA on flat PDMS surface (left) and rough PDMS surface (right). Each image contains four vertical, FN stripes. Fibroblasts are fixed and stained with rhodamine phalloidin. Scale bar is equal to 50 μm .

5.3.4 Cell Morphology Analysis

To examine the effect of FN coated rough surfaces on cell phenotype, cell area on FN_{Flat} , FN_{Rough} , $\text{FN}_{\text{Petri dish}}$, and $\text{UN}_{\text{Petri dish}}$ un-patterned surfaces was compared and analyzed 24 hours after cell seeding (Figure 5.5). Cells growing on the FN_{Flat} surface (Figure 5.5a) had a significantly different shape compared to cells grown on FN_{Rough} (Figure 5.5b) surfaces. Fibroblasts on FN_{Rough} surfaces had a long, spindle shape while fibroblasts on FN_{Flat} were more rounded and had a greater geometric area. Cells grown on $\text{FN}_{\text{Petri dish}}$ (Figure 5.5c) and $\text{UN}_{\text{Petri dish}}$ (Figure

5.5d) surfaces also had a much greater area compared to cells on $_{FN}Rough$. Between the two Petri dish surfaces, fibroblasts on $_{FN}Petri$ dish had a larger area than cells on $_{UN}Petri$ dish.

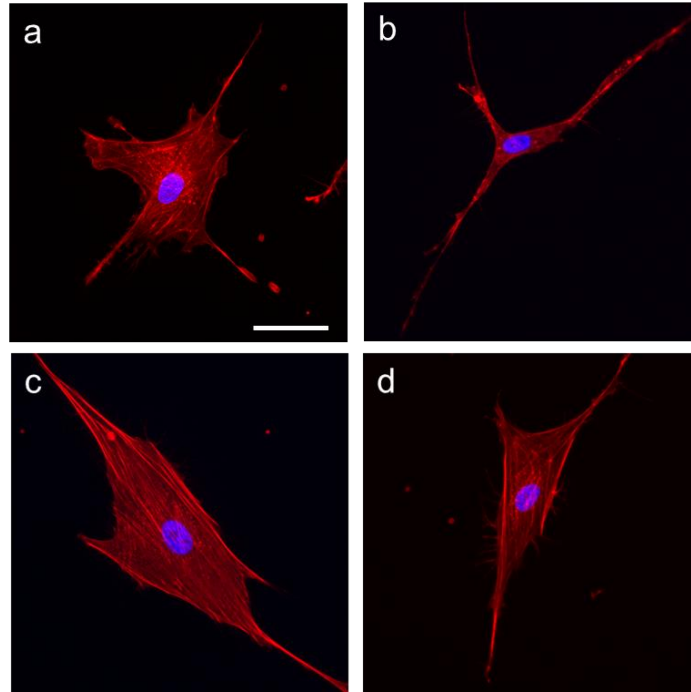


Figure 5.5. Human fibroblasts after 24 hours of culture on (a) $_{FN}Flat$, (b) $_{FN}Rough$, (c) $_{FN}Petri$ dish and (d) $_{UN}Petri$ dish. Cells are stained with rhodamine phalloidin (f-actin) and Hoechst 33342 trihydrochloride (nucleus). Scale bar is equal to 50 μm .

The FN coated PDMS surfaces ($_{FN}Rough$ and $_{FN}Flat$) are representative of the FN stripe pattern described earlier that encourages fibroblast adhesion. The large, round cell bodies in Figure 5.4 on the flat, patterned PDMS surface are analogous to the cell shape in Figure 5.5a on the $_{FN}Flat$ surface. Additionally, the spindle-like and elongated cells in Figure 5.4 on the rough, patterned PDMS surface are also equivalent to the cell shape in Figure 5.5b. The cell morphology of fibroblasts cultured on PDMS, Figure 5.5a and 5.5b, was compared to fibroblasts grown in polystyrene Petri dishes. $_{FN}Petri$ dish and $_{UN}Petri$ dish were chosen as comparisons because polystyrene is commonly used for mammalian cell culture. Fibroblasts cultured on $_{FN}Flat$

(Figure 5.5a) had a morphology that was comparable to fibroblasts on $_{FN}$ Petri dish (Figure 5.5c) and $_{UN}$ Petri dish (Figure 5.5d), even though there is a large difference in polymer stiffness between the PDMS and Petri dish substrates. The similarity in cell morphology between these cells (Figure 5.5a, 5.5c, 5.5d) can be assumed to be derived from the 2-D platform on which they were cultured and that there is no surface architecture to affect the cell shape.

Quantitative determination of cell area was calculated using fluorescence microscopy and image processing. A representative histogram of cell areas is shown in Figure 5.6 for the four different surfaces. The cell areas on $_{FN}$ Flat have a broad maximum range between 2,500 and 5,000 μm^2 . Cell areas on $_{FN}$ Rough surface have a single maximum at 2,000 μm^2 and a significantly narrower cell sized distribution compared to $_{FN}$ Flat PDMS. Fibroblasts cultured on $_{FN}$ Petri dish also had a wide size distribution with a maximum cell area between 3,500 and 6,000 μm^2 , but had only a single maximum of 3,000 μm^2 for cells cultured on $_{UN}$ Petri dish. The average cell area for each type of surface was compared in Figure 5.6b. The average area for the $_{FN}$ Flat and $_{FN}$ Rough was 4,170 μm^2 and 2,280 μm^2 respectively. The largest cell area, 5,320 μm^2 , came from cells cultured on $_{FN}$ Petri dish surfaces while fibroblasts on $_{UN}$ Petri dish surfaces had an average area of 3,840 μm^2 .

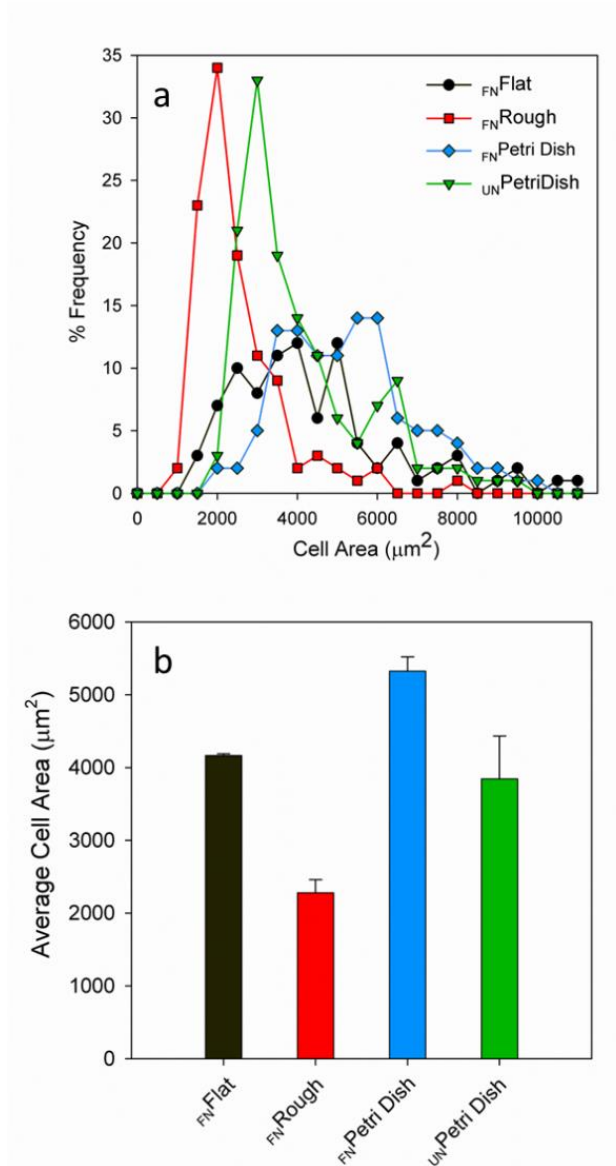


Figure 5.6. (a) Histogram analyses of cell areas and (b) average cell area for cells grown on FN_{Flat} , FN_{Rough} , $\text{FN}_{\text{Petri dish}}$ and $\text{UN}_{\text{Petri dish}}$ surfaces. All data is based on ~ 100 cells for each surface over three separate experiments.

Fibroblasts cultured on FN_{Rough} had the smallest average cell area compared to cells on the other three surfaces. FN_{Rough} also produced a narrow distribution of cell areas (Figure 5.6a). The thin and elongated cells seen in Figure 5.4 and 5.5b indicate the micro-roughness constricts

growth, reducing cell area. The micro-environment keeps the average cell area low as well as limits size distribution. Spindle morphology in fibroblasts has been observed in a previous report by Milner *et al*²⁰² where cells were cultured on micro-pillars, further demonstrating surface topography is vital to cell behavior. The _{FN}Flat surface had a distribution of cell areas that was similar to cells cultured on _{FN}Petri dish. The _{FN}Petri dish plot in Figure 5.6a is shifted towards larger cell areas, but has a comparable broad spectrum to _{FN}Flat. The large distribution of cell areas and increase in high cell area fibroblasts when compared to _{FN}Rough and _{UN}Petri dish can be attributed to the 2-D, protein coated surfaces²⁵⁷. _{FN}Flat and _{FN}Petri dish surfaces allow cell bodies to spread and grow unhindered by surface roughness. The decrease in average cell area from _{FN}Petri dish (5,320 μm^2) to _{FN}Flat (4,170 μm^2) in Figure 5.6b may be due to a change in the stiffness between PDMS and the Petri dish substrates²⁵⁸. The distribution of cell areas on _{UN}Petri dish is narrow, but wider than the distribution of cell areas on _{FN}Rough giving _{UN}Petri dish a larger average cell area. The narrow distribution of cell areas on _{UN}Petri dish when compared to _{FN}Petri dish can be attributed to the lack of protein coating on the surface keeping cell areas smaller as mentioned before.

5.3.5 Roughened Substrate Modulates ECM and Adhesion Molecule-Associated Gene Expression

To examine the molecular basis for the observed alterations in human dermal fibroblast phenotype described above, we compared the relative expression profiles of ECM and adhesion molecule-associated gene transcripts using Qiagen's RT² *Profiler* PCR Array system. Cells grown on _{FN}Rough substrates were directly compared to cells grown on _{FN}Flat PDMS as well as _{FN}Petri

dish and U_N Petri dish. Interestingly, for both F_N Flat and F_N Rough substrates, the act of changing the substrate from polystyrene to PDMS induced downregulation of the majority of transcripts on the array, with the exception of most of the matrix metalloproteinase transcripts. However, the expression levels of several transcripts that were modulated (up or down) by altering the growth surface material were either attenuated or exacerbated by roughening the surface. To limit the number of genes of interest, we set a threshold limit for those transcripts either up- or down-regulated by approximately 2-fold. Using this criteria, we identified five transcripts up-regulated (CTNND2, COL15A1, CNTN1, MMP14, and COL6A1) as a consequence of modifying only surface roughness. The relative gene identifier, name, ontology, and fold change for these transcripts are presented in Table 5.3. These results were corroborated by three independent biological replicates. Taken together these data indicate that modulating surface topography has a marked impact on the expression of the ECM and adhesion-associated genes, notably several of the matrix metalloproteinases (MMPs).

Table 5.3. Relative changes in extracellular matrix / adhesion molecule transcript expression as a function of surface roughness. Absolute values of fold change differ due to differences in primer efficiencies and specific experimental conditions.

Gene ID	Gene Name	Function	Fold Change (Range) on PCR Array	Average Fold Change on Array	Average Fold Change with Independent Primers
CTNND2	Catenin (cadherin-associated protein), delta 2 [Delta Catenin-2]	The protein encoded by this gene promotes the disruption of E-cadherin based adherens junction to favor cell spreading upon stimulation by hepatocyte growth factor.	1.8 - 4.6	3.1	5.0
COL15A1	Collagen, type XV, alpha 1	May adhere basement membranes to underlying connective tissue stroma.	1.7 - 3.7	2.5	2.0
CNTN1	Contactin 1	A GPI-anchored neuronal membrane protein that functions as a cell adhesion molecule.	0.8 - 4.8	2.3	N/D
MMP14	Matrix metalloproteinase 14 (Also known as MT1MMP)	A member of the membrane-type MMP (MT-MMP) subfamily; each member of this subfamily contains a potential transmembrane domain suggesting that these proteins are expressed at the cell surface rather than secreted.	1.0 - 4.8	2.3	5.8
COL6A1	Collagen, type VI, alpha 1	The protein encoded by this gene is the alpha 1 subunit of type VI collagen. Mutations in the genes that code for the collagen VI subunits result in the autosomal dominant disorder, Bethlem myopathy.	1.0 - 3.3	2.0	1.3

5.4 Discussion

We have described phenotypic alterations in morphology and ECM/adhesion molecule gene expression of dermal fibroblasts grown on surfaces with modulated topography patterned with biological matrices. While growth of mammalian cells has been extensively demonstrated on both coated surfaces as well as micro- and nano-textured surfaces²⁵⁹, and whereas tunable elastic PDMS substrates have been used to study cell behavior²⁶⁰, our approach of patterning biological substrates on micro-roughened PDMS allows for interrogation into the effect of surface roughness on cell behavior in conjunction with unidirectional cell growth. The deposition of patterned photoresist created a uniform pattern on the micro-textured surface as well as create defined sections of cell adhesive and non-adhesive areas. As a model of study, we chose to derivatize the surface structure of PDMS template from microgrit SiC paper. This approach has a number of advantages over conventional photolithographic techniques including ease of fabrication, and a well-defined surface with a level of randomness that mimics biological substrates²⁶¹, a property absent from surfaces fabricated with geometric features²⁶².

It must be mentioned, that unlike other reports of aligned cell growth using microcontact printing¹²³ or irradiated surface patterns⁵⁵, we chose to pattern the FN using a lift-off technique using photoresist. This may seem an odd choice since both of the previously mentioned techniques are well documented to produce chemical or biochemical patterns that can govern cell direction and adhesion. Both microcontact printing and photo irradiation were tested on our PDMS surfaces and both techniques generated reproducible FN patterns on the flat PDMS substrate, but this was not the same case for the roughened PDMS. PDMS stamps with 60 μm lines and 50 μm grooves “inked” with FN were stamped on both surfaces, but the micro rough surface did not receive an even transfer of the pattern and no uniformity was established. Photo irradiation of a UV sensitive

nitrobenzyl alkoxy silane SAM was also tested for producing a surface pattern. In a method developed by Nakanishi *et al*⁵⁵ the SAM modified PDMS surface was exposed to UV irradiation through a chromium mask. Here the nitrobenzyl group was removed leaving a carboxylic acid using a Norrish-type II photo-cleavage mechanism. This protocol did generate a pattern on the rough PDMS, but the minor change in surface chemistry induced no alignment or direction from the cells. The photoresist patterning technique produced the most reliable pattern that generated micron sized lines of cell adhesive and non-adhesive areas. FN was chosen because it is a major component of native ECM and cells readily adhere and migrate to FN coated surfaces. Surface bound FN, contains the peptide sequence RGD that is recognized by most transmembrane integrins for cell adhesion²⁴ making FN patterning ideal for controlled cell directionality. The BSA regions were used as non-adhesive regions for cell growth. BSA adsorbed to a surface prevents further protein modification or binding including FN, making it difficult for cells to adhere their ECM to these regions²⁶³.

The growth of primary neonatal human dermal fibroblasts onto patterned, _{FN}Rough PDMS surfaces generated two marked morphological and phenotypic alterations, respectively, in comparison to patterned, _{FN}Flat PDMS surfaces. Most notably, the appearance of the cells changed from that of a flattened phenotype with visible spreading of the actin cytoskeleton to that of an elongated spindle-like shape, suggesting that surface topography influences contact guidance of cells. To this extent, it should be noted that the elongation of the cells was independent of FN patterning, as we observed a similar phenotype on unpatterned _{FN}Rough PDMS surfaces. Second, cellular proliferation appeared to be markedly decreased (by approximately half) on roughened surfaces during the one week culture (data not shown). However, we did not investigate as to whether this was due to decreased rates of initial attachment. While these observations are contrary

to that of the typical phenotype expected from conventional tissue culture regimes, the cells grown on micro-roughened/patterned surfaces more closely resemble the elongated spindle-like fibroblasts found in the native human dermis²⁶⁴.

To interrogate the molecular mechanisms responsible for the observed morphological changes on rough substrates, we employed a commercially available PCR-based screen for predominant ECM proteins and cellular adhesion molecules. The data generated revealed a number of findings into the potential regulation of cell behavior by substrate mechanics. In particular, changing the culture surface from polystyrene to PDMS induced an upregulation of the majority of MMPs on the array (MMP1, MMP3, MMP16, and MMP13 were the top four upregulated genes in response to surface material) with a concomitant downregulation of ECM structural constituents (COL15A1) and adhesion molecules (LAMA3, ICAM1, and CTGF) as shown in Figure 5.7. As all groups incorporated a 10 nm FN coated surface, this observation perhaps indicates that substrate elasticity and not chemistry, is responsible for modulating the majority of expression levels of these gene transcripts. Gene ontology analysis suggests that the more pliant PDMS substrate is reducing overall cell adhesion properties and increasing cell migration properties. This may be of interest in examining potential micro environmental cues responsible as tumor metastasis in tissues with varying elastic moduli for guiding cellular processes such as lymphocyte extravasation in arteriosclerotic vessels as well. The genes with significant changes in regulation (two-fold change or greater) between the two types of PDMS (rough and flat) are highlighted in yellow in Figure 5.7 and described in more detail in Table 5.3. The gene with the largest average change using the independent primers, MMP14 (also known as MT1MMP, enclosed in red box in Figure 5.7) is a transmembrane protease that is responsible for cleavage and remodeling of cellular ECM proteins. Cell motility in tissue is dependent on MMP14

to degrade surrounding ECM so the cell can migrate throughout the tissue unhindered²⁶⁵. MMP14 derived cell migration is also essential for wound healing and remodeling of damaged connective tissue²⁶⁶. Although, cell migration and wound healing are not a focus of this report, the subtle change in surface topography generated fibroblasts that have the capability of being more active in wound repair than cells cultured on a flat Petri dish surface or flat PDMS surface. This holds exciting implications for this surface in the field of tissue engineering.

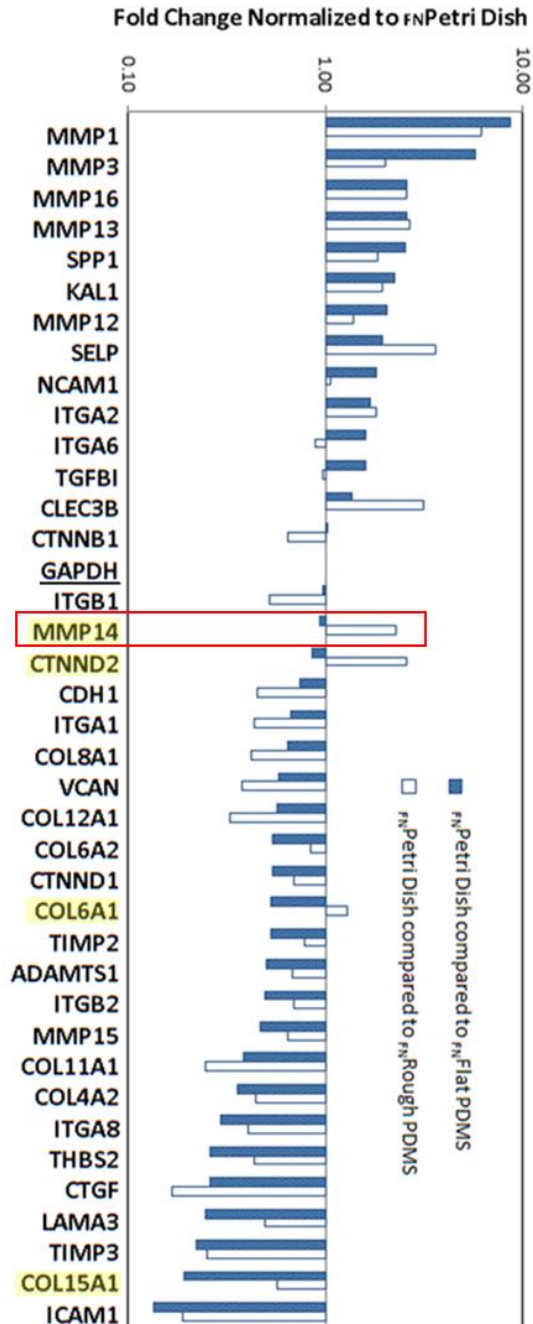


Figure 5.7. Fold change in ECM and adhesion molecule gene expression by fibroblasts in comparison to FN-coated tissue culture dishes on flat (blue) and roughened (white) FN coated PDMS normalized to gene expression on a Petri dish. Data represents the average of two independent biological replicates. Gene's that expressed a two-fold change or greater between rough and flat PDMS are highlighted in yellow. MMP14 outlined in red. GAPDH (underlined) was the reference gene.

One of the most striking observations was the elongated phenotype of the fibroblasts grown on rough PDMS surfaces. As described above, this elongation was independent of the space constraints of the patterned FN, as this same morphology was observed on un-patterned surfaces (however, the cells did not grow unidirectionally), and resulted in an altered actin cytoskeleton. The spindle-like fibroblast cultured on the rough FN pattern did not fill the width of the line (50 μm) as the fibroblast did on the flat, patterned PDMS surface. It is apparent that the surface roughness contracted the cytoskeleton which may have been induced by altered cell adhesion and ECM arrangement on the micro-roughness. While gene expression analysis did not demonstrate large paradigm shifts in the levels of ECM-associated transcripts, several interesting candidates did arise. For example, where there was virtually no change in the expression of MMP14 and CTNND2 between flat polystyrene and PDMS surfaces, roughening the PDMS surface induced a consistent 2 – 3 fold increase in the expression levels of these two transcripts across three independent biological replicates. Additionally, while a flat PDMS substrate grossly downregulated the expression of COL15A1 in comparison to polystyrene culture dishes, roughening the PDMS substrate appears to have ‘rescued’ this effect by bringing the expression levels of this gene closer to typical cell culture systems. These results suggest that subtle variations in substrate mechanics and topography may dramatically regulate cell behavior, even if by only subtle perturbation of ECM and cellular adhesion-associated gene expression. Accordingly, care should be exercised when designing bioinspired/biomimetic tissue culture systems, but also in the design and fabrication of implantable medical devices, specifically percutaneous implants such as prostheses, which must establish a long-term compatibility with the surrounding dermal tissue²⁶⁷. While we have focused primarily on dermal fibroblasts in this study, this technique also extends

to cell systems where directional growth is critical to functionality, such as motor neurons and skeletal myocytes.

5.5 Conclusions

This study has described the fabrication of a rough polymer surface with a protein micro pattern that produces aligned cell growth on a micro-rough substrate. The surface roughness provided a micro environment in which the morphology of the cells appears to be more relevant to that observed for fibroblasts *in vivo*. At the same time the surface pattern facilitates control of cell organization and alignment of growth. Cell alignment and altered morphology on the patterned, rough substrate was shown to last for at least six days. A quantitative comparison of cell morphology, cell area, and gene expression between the rough PDMS surface and cells on Petri dishes showed significant differences in cell behavior that indicate the modified surface as a possible option for replication of a native 3-D environment. Large changes in gene expression between PDMS and polystyrene surfaces indicate substrate stiffness is vital in cell signaling for ECM and adhesion molecule formation. Gene expression changes were also noted between rough and flat PDMS, specifically MMPs. This signifies surface roughness is imperative for ECM formation and degradation. The simplicity of the fabrication method allows for this process to be applied to tissue engineering studies, HTS assays, and other commercially available 3-D substrates.

6.0 Thermo-responsive, micro-roughened cell culture surface with controlled extracellular matrix and cytoskeleton

6.1 Introduction

The thermo-responsive polymer, polyisopropylacrylamide (PIPAAm), is a well-established smart biomaterial capable of sustaining adherent cell cultures at 37°C, but releasing cells and their extracellular matrix (ECM) when cooled below 32°C²⁶⁸⁻²⁷¹. At warmer temperatures, above PIPAAm's lowest critical solution temperature (LCST), the polymer dehydrates and collapses at the surface and when cooled, the polymer rehydrates and expands²⁷² (Figure 6.1). As a result, cells cultured on the thermo-responsive polymer are gently released into media when cooled²⁷³. Common methods of releasing cells from a culture substrate use the enzyme Trypsin or mechanical scraping but both methods damage the cells and ECM as well compromise cellular function^{274, 275}. These methods also release the cells individually or in clumps, and many of the cell-cell bonds are broken. PIPAAm surfaces avoid these problems by releasing the cells and ECM intact, and if cells are confluent, they are released as a single sheet²⁷⁶⁻²⁷⁸. The single sheets have the possibility to be combined with other cell sheets for more complex tissue engineering²⁷⁹. The retained ECM layer with the detached cell sheet supports the cell sheet shape and can ensure re-attachment of the sheet onto other cells or surfaces. The cell sheet layer contains no other scaffolding or inorganic material once detached, so it is readily incorporated into *in vivo* systems with no loss of biocompatibility²⁸⁰.

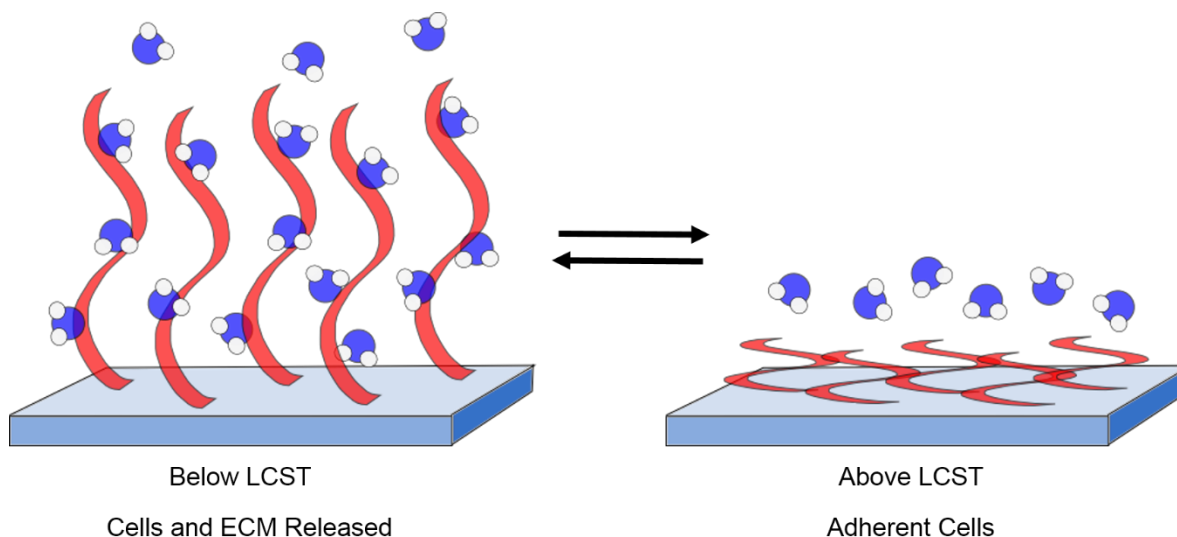


Figure 6.1. Schematic example of PIPAAm polymer chains attached to a surface in water. Below PIPAAm’s LCST, PIPAAm chains remain hydrated, but after a temperature increase above the LCST, the polymer rapidly dehydrates and the polymer chains fold in on themselves at the surface.

PIPAAm has been adapted for cell culture on the surface of biomaterials by a number of research groups. The polymer has synthesized with other monomers for copolymerization to induce differences in surface wettability and changes in the LCST²⁸¹ or terminated with biomolecules for increased cell adhesion^{282, 283}. Although research with PIPAAm is extensive, there have been few reports on the using thermo-responsive polymers in combination with 3-D or surface modified scaffolds^{284, 285}. None of these reports have investigated the impact of surface micro-structure or 3-D scaffolding on ECM formation for cell sheets. Surface topography has been well documented to control cell adhesion, morphology, gene expression, and ECM deposition^{5, 286, 287}. Combined with PIPAAm, altered surface architecture can be used to generate cell sheets with different biochemical properties and user defined ECM profiles. One of the main components of ECM, fibronectin (FN), is arranged into fibrillar matrix networks using synthesized cellular FN in a process known as fibrillogenesis. FN fibrillar assembly is mediated by transmembrane integrin binding which is crucial for cell growth and survival²⁸⁸ and vital for

facilitating wound healing²². The cell-material interface can be engineered for control of the fibronectin fibrils in a cell sheet. Micro surface topography alters cytoskeletal rearrangement and integrin binding²⁸⁹ and therefore directly influences ECM composition and arrangement. Cell sheets with controlled ECM would be beneficial for complex tissue formation or a tissue graft to aid in closing a wound.

The research presented has exploited PIPAAm's thermo-responsive properties to engineer a defined micro-rough surface on polystyrene (PS) for cell sheet formation and control of cellular ECM. The micro topography is produced using a simple templating technique to generate 1.5 – 5.5 micron wide features on the surface. The rough PS surface is modified with an amine terminated alkoxy silane, followed by secondary modification and UV initiated grafting of PIPAAm to the surface. The PIPAAm grafted PS surface (PIPAAm-PS) was characterized with AFM and infrared (IR) spectroscopy. The chemically and physically defined surface was used for cell culture with human fibroblasts to generate cell sheets with a unique ECM structure that was compared to cell sheets cultured on physically unmodified PS. Analysis of cellular f-actin and FN of the sheets was performed with fluorescence microscopy. Surface topography has fabricated two significantly different types of cell sheets from the same cell type and presents a new bottom-up approach for cell sheet engineering. To the best of our knowledge, this is the first report using a thermo-responsive surface in combination with surface micro-roughness for generating fibroblast sheets with specific cytoskeleton and ECM profiles.

6.2 Experimental Methods

6.2.1 Fabrication of PS surfaces

Micro roughened PS was fabricated with a modified protocol developed by Isenberg *et al*²⁹⁰. The rough PDMS was clamped, modified side down, into a commercially available tissue culture Petri dish between two aluminum plates. The PDMS, dish, and plates were heated to 110°C for 1 hour, removed, and allowed to cool to room temperature. The PDMS and metal plates were removed leaving the roughened PS. The complete fabrication procedure can be seen in Figure 6.2. The rough PS was then pressed with a heated, metal punch to generate PS discs 1.5 cm in diameter. Unmodified PS underwent no templating procedure, but was punched into discs. Templating the PS was tried by pressing the SiC paper into the PS directly, but few features were transferred using this method. The compression of the rough PDMS layer in-between the aluminum plates and the PS dish was more successful at producing micro-roughness on the PS surface.

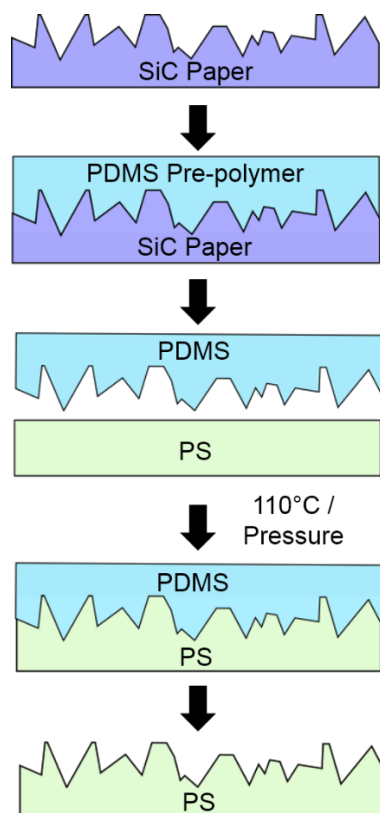


Figure 6.2. Fabrication process of micro-roughened PS. PDMS pre-polymer was cured on SiC paper. The physically modified PDMS was then used to template tissue culture PS using heat and pressure. The final PS substrate had micron surface size features.

6.2.2 PIPAAm- PS

The PS discs were cleaned by sonication in an ethanol bath for 5 minutes and dried in a stream of nitrogen. The substrate surfaces were incubated in a 50% v/v APTMS solution in ethanol for 20 minutes. APTMS-PS was rinsed with ethanol, dried in a stream of nitrogen, and incubated in a 0.5% v/v GA solution in PBS for 30 minutes for formation of imine Schiff base⁹⁰. The GA-PS discs were removed, rinsed with water, dried in a stream of nitrogen and immediately incubated in a 12% w/v NIPAAm, 0.5% w/v bis-acrylamide, 0.5% v/v benzyl alcohol, 3% w/v benzophenone, and 0.5 mM NaIO₄ (taken from aqueous 0.1 M NaIO₄) solution in methanol. The system was

placed on an ice bath and irradiated with a 5.1 mV/cm^2 UV lamp (RPR-3000Å lamp, S.N.E. Ultraviolet Co., Branford, CT) for 1 hour. Lamp power was measured at the distance of sample irradiation using a Gentec-EO (Lake Oswego, OR) Solo2 Laser Power and Energy Meter. The PIPAAm-PS discs were removed, rinsed with methanol, ethanol, sonicated in ethanol for 1 minute, and dried in a stream of nitrogen. The discs were soaked in water for 3 hours with water replaced every hour to remove any residual NIPAAm not grafted to the surface, rinsed with ethanol, and dried in a stream of nitrogen. An illustration of the chemical surface modification can be seen in Figure 6.3.

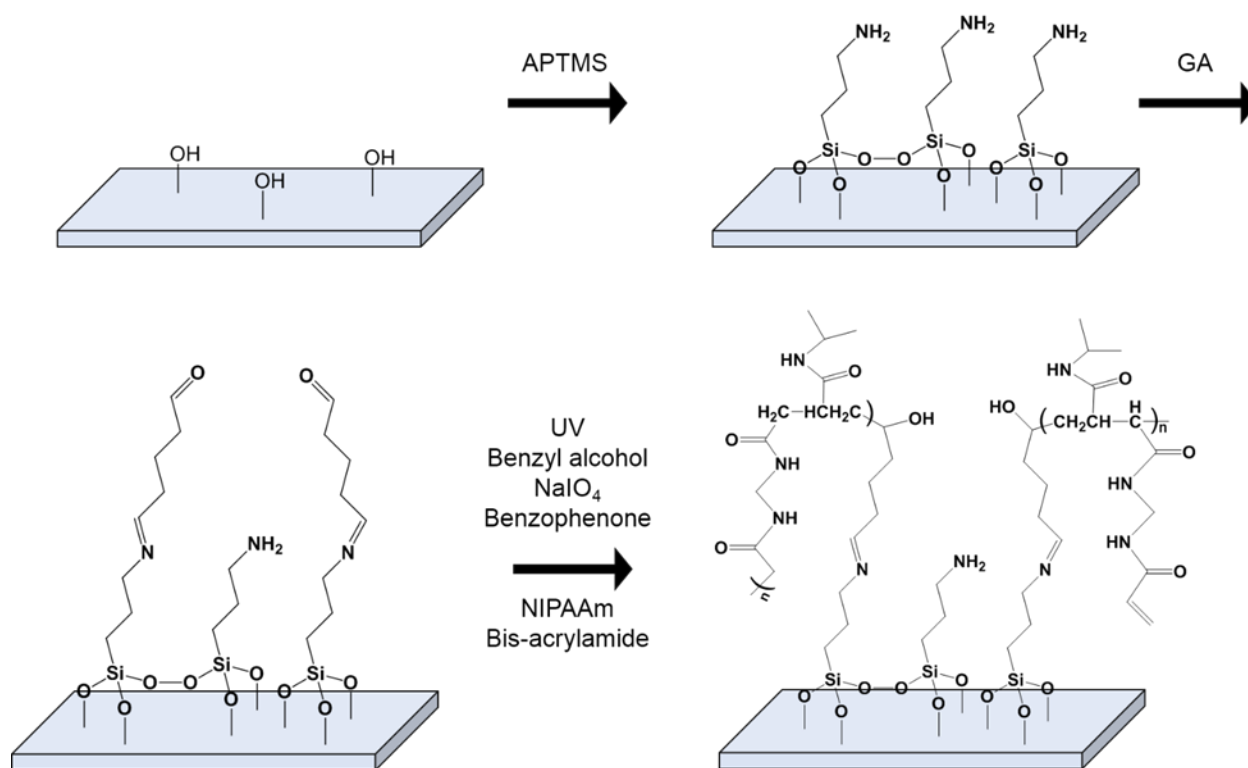


Figure 6.3. Schematic illustration of PIPAAm chemical attachment to a PS surface.

6.2.3 AFM Characterization of the surfaces

AFM imaging was completed with NanoWorld (Lady's Island, SC) NCSTR-10 cantilevers with a measured resonant frequency of 134 kHz and a nominal force constant of 7.4 N/m. A minimum of three topography images (40 x 40 μm) were taken in AC mode for each type of surface. All surfaces were prepared as described previously. Average roughness (R_a) values, representing the deviation of the surface height, were averaged over the collected images for each surface. Full width half maximum (FWHM) values were calculated by obtaining horizontal cross sections from five separate, 60 x 60 μm AFM topography images of the rough PIPAAm-PS surface. Cross sections were taken every 10 μm for every image for a total of 35 cross sections. The FWHM was taken for each complete feature contained within the cross section. PIPAAm surface grafting was confirmed by 1.0 x 1.0 μm topography images taken in AC mode on unmodified flat PS discs and comparing them to topography images of flat PIPAAm-PS discs.

6.2.4 ATR-IR Spectroscopy

FT-IR spectroscopy was performed with a Bruker Hyperion 3000 microscope equipped with a 20x ATR objective at 21°C. An atmospheric background was collected prior to the sample runs and a total of 1024 scans were collected for each sample. Scans were repeated a minimum of three times on each surface or sample type.

6.2.5 Cell Seeding

PIPAAm-PS discs were sterilized in 70% ethanol for 5 minutes and dried in a stream of nitrogen. PIPAAm-PS discs were incubated in PBS for 1 hour at 37°C followed by immediate incubation in FBS for 3 hours at 37°C. FBS was aspirated immediately before seeding human fibroblasts on surfaces at an initial 5×10^5 cells/mL in DMEM/F12 media with 10% FBS, 1% P/S,

and 0.1 mM MEM non-essential amino acids. Cells were cultured in a humidified atmosphere at 37°C and 5% CO₂ and media was removed and replaced every 1 - 2 days.

6.2.6 Detachment of cell sheets and Immunofluorescence Staining

After two days of culture, cells were confluent on PIPAAm-PS. Media was aspirated and replaced with fresh media at 4°C. After full detachment of cell sheets from the PIPAAm-PS surface, cells were immediately fixed and stained. Whole cell sheets were imaged with a Leica (Buffalo Grove, IL) S6 D stereo microscope equipped with a Leica DFC290 camera and a Schott (Southbridge, MA) 150 W Ace 1 light source. Bright-field imaging of cell sheets were taken with a Nikon E600 microscope.

Cells were fixed by incubation in 4% formaldehyde solution in PBS (pH 6.9) for 15 minutes at room temperature, washed twice (2X) with fresh PBS, incubated in a 0.1% Triton X-100 solution in PBS for 5 minutes, washed 2X with PBS, blocked with 5% normal goat serum in PBS for 30 minutes, and rinsed 2X with PBS. Cells were incubated in 4.0 µg/mL of H-300 fibronectin primary antibody in PBS with 1.5% goat serum for 1 hour at room temperature. Cells were then incubated in fresh PBS for 15 minutes before incubation 4.0 µg/mL goat anti-rabbit IgG-FITC secondary antibody in PBS with 2% goat serum in PBS for 45 minutes at room temperature. Cells were rinsed 2X with PBS, incubated in a 20 µL/mL rhodamine phalloidin solution in PBS with 1% w/v BSA for 25 minutes at room temperature, and rinsed 3X with PBS. Samples were stored at 4°C until imaging. Stained cell sheets were examined using confocal microscopy. In a maximum intensity composite image, each image is composed of multiple images from a single Z-stack that have been “flattened” into a single image. Single focal plane images represent a single image removed from the corresponding Z-stack.

6.3 Results

6.3.1 Characterization of surface topography with AFM

The topography of the PIPAAm grafted PS can be seen for the flat and micro-roughened surfaces is shown in Figure 6.4. Each image is a 40 x 40 μm section of the surface with a horizontal cross section of the image also shown. On the flat PS substrate the nanometer threads of the PS can be made out on the surface, but adds little to the surface architecture as seen in the corresponding cross section. On the rough PS, the templated micron features are easily identified, significantly increasing the roughness of the surface. The roughness average (R_a), calculated with AFM, of the PS flat and rough surfaces were averaged at 4.3 ± 0.6 and 283 ± 60 nm respectively.

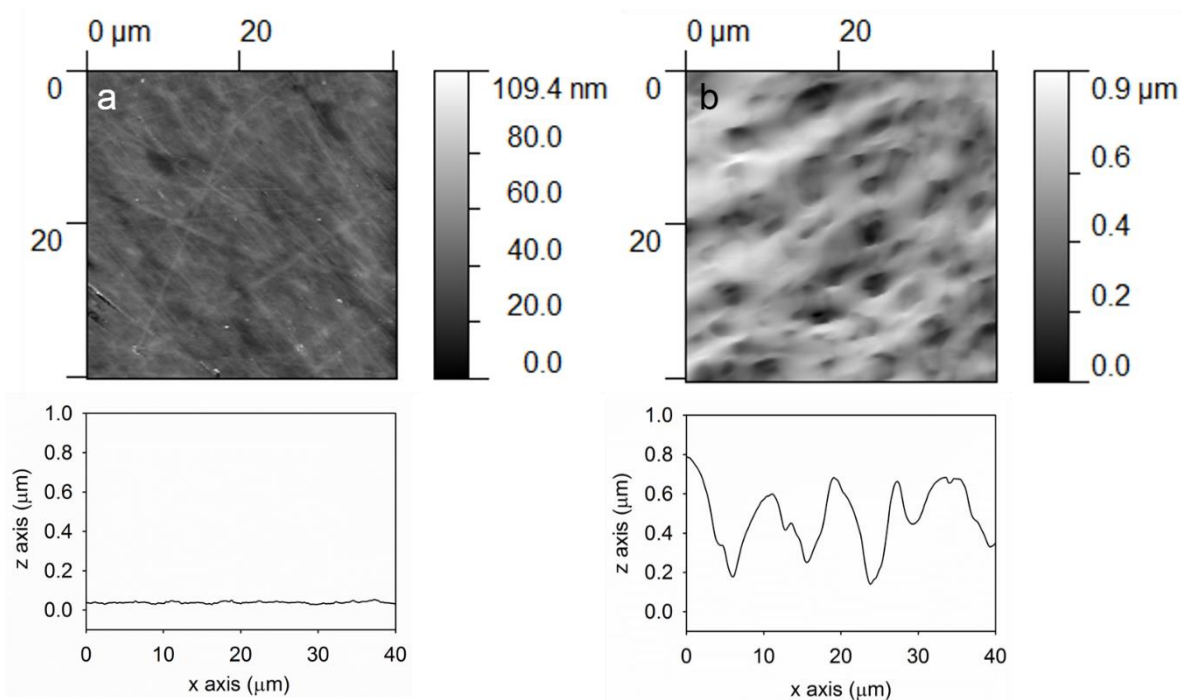


Figure 6.4. 40 x 40 μm AFM topography images of PIPAAm grafted (a) flat PS (color scale 0 – 109.4 nm) and a corresponding line section below and (b) micro-roughened PS (color scale 0 – 0.9 μm) and a corresponding line section below.

The height of the micron features of the rough PS range from 400 to 600 nm, but the feature widths are more variable. To quantify the surface topography, multiple cross sections were taken from AFM images of the rough PS surface, and the FWHM of each feature in the cross section was analyzed. The collected FWHM feature sizes were plotted as a frequency diagram as seen in Figure 6.4. Although FWHM sizes greater than 8 microns were noted, the majority of the feature FWHM range between 1.5 and 5.5 μm . This creates a significantly different cell culture platform when compared to cells on flat PS. The R_a of the micro-roughened PS surface is lower than the R_a value of the rough PDMS template (730 nm) that has been characterized extensively in Chapter 3 and our published reports^{44, 97}. Although the feature FWHM values are similar, 2 – 6 μm for the PDMS, the height of the micron features on PDMS are much larger, ranging between 1 and 3 μm . The change in feature height is most likely due to the heated, templating process. The 110°C temperature needed to press features into the PS may also deform and shrink the PS surface feature resulting in a reduced feature height.

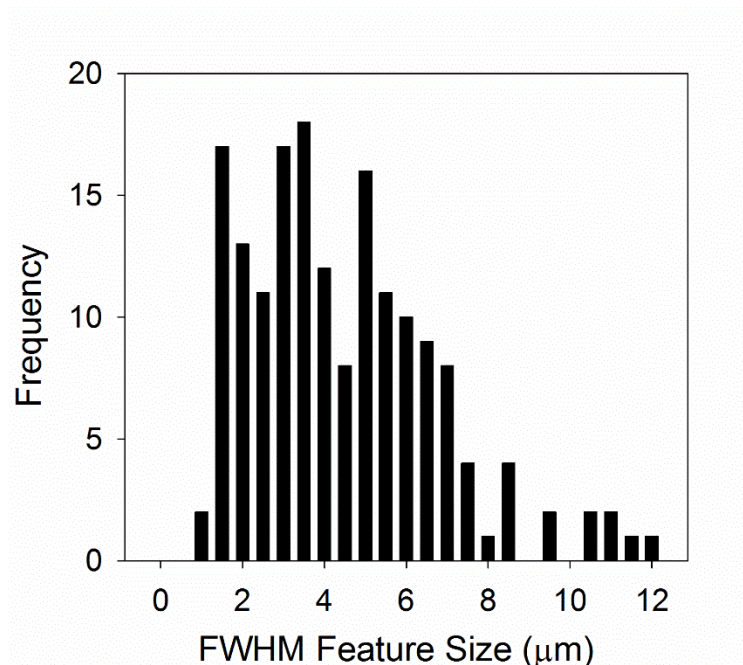


Figure 6.5. A frequency plot of the FWHM feature sizes collected from the topography of micro-roughened PS.

6.3.2 Confirmation of PIPAAm surface grafting

AFM and FT-IR were used to confirm that PIPAAm had been deposited on the PS surface. The 1.0 x 1.0 μm topography images of flat unmodified PS and PIPAAm grafted PS, as seen in Figure 6.6, exhibit the nanometer changes in height from PIPAAm grafting. The unmodified surface has no finite surface markers, but the polymer grafted surface has discrete islands of polymer covalently bonded to the surface. These islands represent the copolymer blend chains, polymer brushes, of PIPAAm and bis-acrylamide tethered by the amine terminated SAM to the PS. The polymer islands are approximately 20 – 40 nm in diameter and 5 - 15 nm in height and are similar to PIPAAm polymer brushes observed on silica substrates²⁹¹. AFM images of unmodified and polymer grafted surfaces were acquired at 21 °C therefore the thermo-responsive polymer would be in its extended, hydrated state.

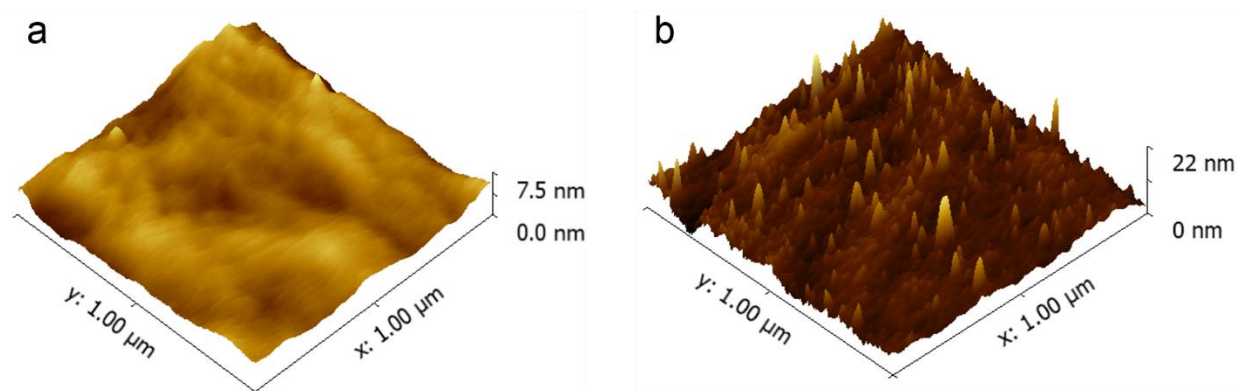


Figure 6.6. 1.0 x 1.0 μm AFM topography images of flat (a) unmodified tissue culture PS (b) and PIPAAm grafted tissue culture PS.

FT-IR analysis of the PIPAAm modified and unmodified PS surfaces were compared to IR spectra of the pure NIPAAm compound (Figure 6.7). The complete IR absorbance spectrum of NIPAAm, PS, and PIPAAm-PS are shown in Figure 6.7a. The overlap of absorption bands in PS and PIPAAm-PS are almost identical except in the region between 1570 and 1510 cm^{-1} as shown in Figure 6.7b, where overlap of NIPAAm bands are observed. NIPAAm exhibits a strong amide associated band at 1546 cm^{-1} . This band was not detected in the unmodified PS samples, but was in PIPAAm grafted PS. This band represents partial contributions from N-H bending and C-H stretching of the amide group in the polymer bound to the surface²⁹². Combined with the AFM topography data in Figure 6.6 the IR spectra of the modified PS confirms PIPAAm grafting to the PS surface.

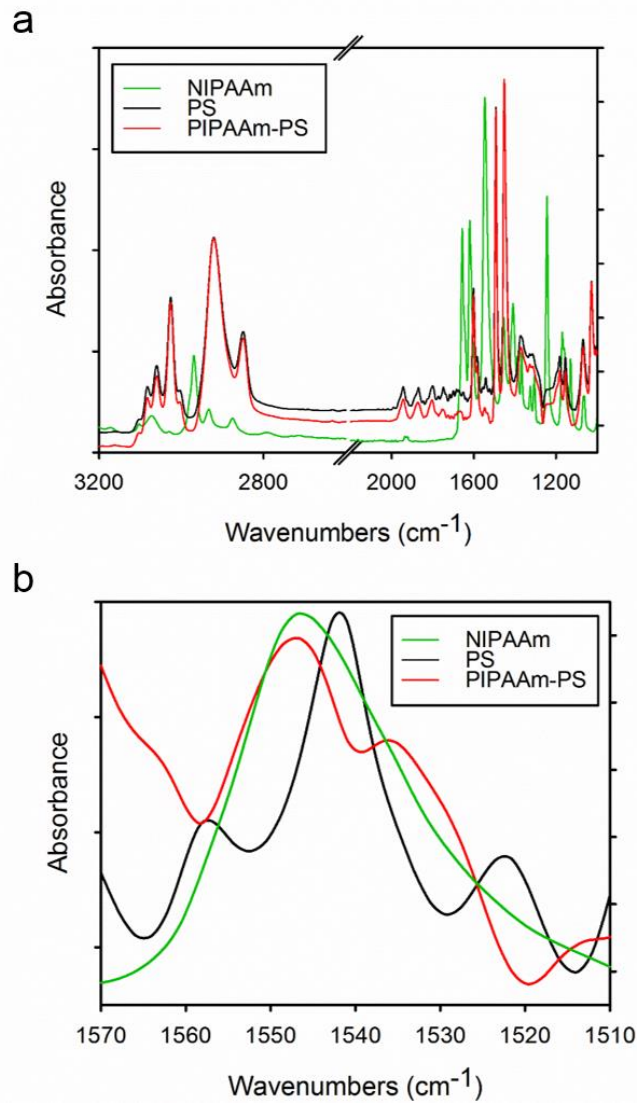


Figure 6.7. (a) ATR FT-IR spectrum of the surface of unmodified PS, the surface of PIPAAm derivatized PS, and NIPAAm. (b) Zoomed in region of spectra in *a* between 1570 and 1510 cm^{-1} .

6.3.3 Cell sheet formation on PIPAAm-PS

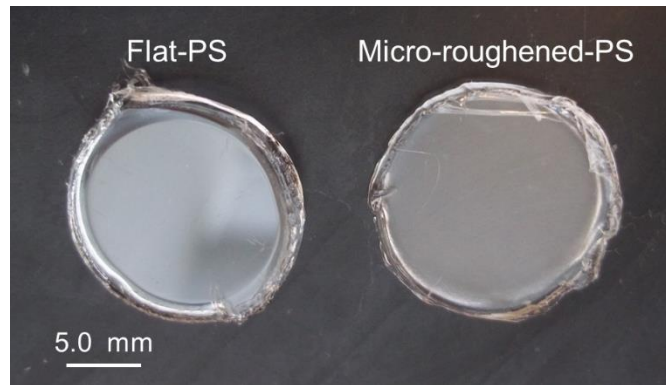


Figure 6.8. Flat and micro-roughened 16 mm diameter PS discs.

After cells were confluent on flat and rough PIPAAm grafted 16 mm PS discs (Figure 6.8), their culture media was aspirated and replaced with media that was chilled to 4°C. After submersion in the chilled media, the system was allowed to warm to room temperature. Cell sheets on the flat PIPAAm surface detached completely in less than 5 minutes, but cell sheets on the micro-rough PS surface took 40 minutes. An example of the cell sheet detachment from a flat PIPAAm-PS surface can be seen in Figure 6.9. Cells on the flat PIPAAm-PS contracted into circular, ~3.0 mm diameter sheets after detachment as seen in Figure 6.10. Sheets on the rough PS had less overall contraction and were larger than sheets generated from the flat surface even though the PS disc diameter was the same for both types of substrates. Fibroblast sheets on the rough surface were also more oblong and oval in appearance, with the longer diameter measuring between 6 – 8 mm.

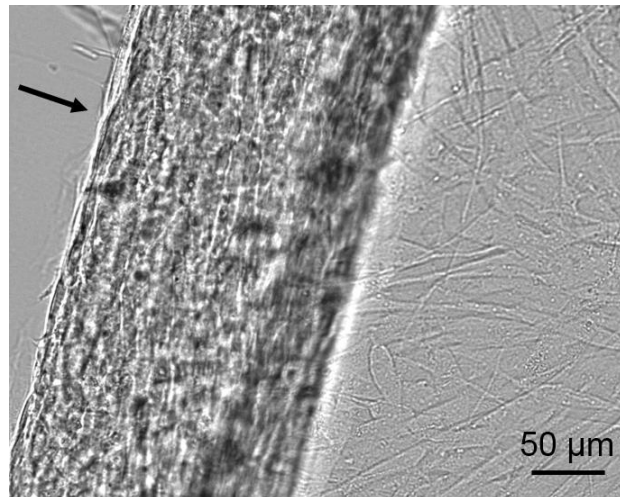


Figure 6.9. Bright field image of human fibroblast cell sheets detaching from a flat PIPAAm-PS surface. Arrow indicates edge of cell sheet and the direction in which the sheet is detaching.

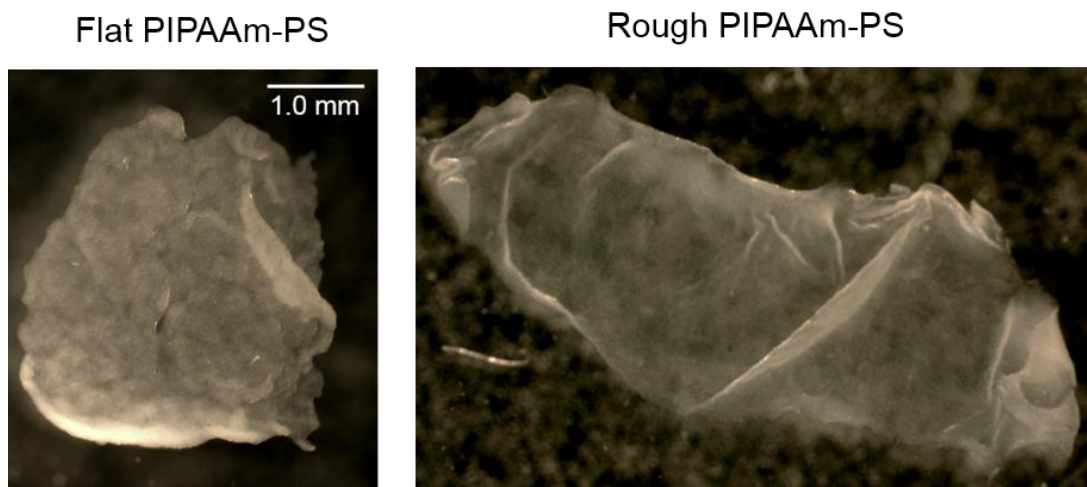


Figure 6.10. Human fibroblast cell sheets detached from a flat PIPAAm-PS and rough PIPAAm-PS surfaces. Scale bar is accurate for both figures. Note large difference in size between the two types of cell sheets.

6.3.4 Cell sheet analysis with fluorescent microscopy

Immediately after cell sheet detachment from the surface, the cells were fixed and stained. Intracellular f-actin and cytoskeleton was labelled with rhodamine phalloidin as shown in Figure 6.11. The ECM was quantified by labelling fibroblast FN using an antibody stain as shown in Figure. 6.12. After cell sheet detachment from the two types of PS surfaces (Figure 6.10) there is an obvious difference in sheet size and shape between the sheet from the flat and rough PS. Cells cultured on PIPAAm surfaces are known to contract into smaller shapes once detached due to the mechanical release of the cell from the surface. Strain and stress of the cell spreading and adhering to the surface are no longer holding the cell shape and so the cell sheets can shrink. The differences between the two cell sheets can be better compared at the micron level by analysis of the cell's actin cytoskeleton and ECM. Maximum composite confocal images of the f-actin in cell sheets from flat and micro-roughened PIPAAm-PS are observed in Figures 6.11a and 6.11c respectively. Images obtained from a single focal plane in the corresponding maximum composite image are shown in the lower row, Figures 6.11b and 6.11d. In the maximum composite obtained from cells cultured on flat PS (Figure 6.11a), unidirectional actin stress fibers are prominently displayed throughout the entire cell sheet. Individual cells from the same surface, observed in the single focal plane (Figure 6.11b), also contain bundles of actin stress filaments running across the entire cell body. The distinct actin fibers are not observed in the cell sheet from the rough surface (Figure 6.11c) and there is a more uniform distribution of actin throughout the cell sheet as observed in Figure 6.11b. In both images of the single focal plane, cells from each sheet are outlined with f-actin, displaying the border of the individual cell bodies and cell-cell junctions, but this is more defined on the cell sheet cultured on the rough substrate (Figure 6.11d). Here, the f-actin is localized at the cell border only and few actin filaments are seen within the cell bodies.

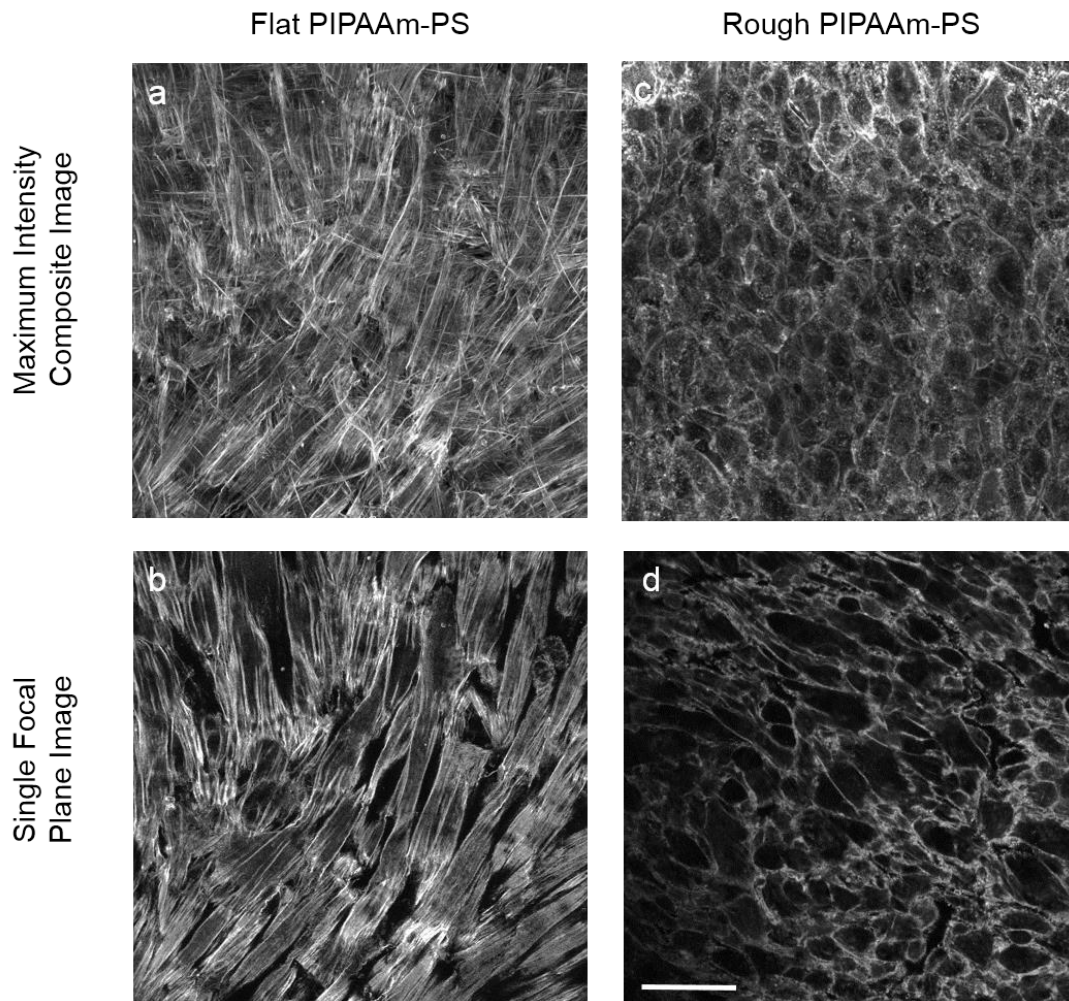


Figure 6.11. Confocal images of fibroblast cell sheets with rhodamine phalloidin labelled f-actin. (a) Cell sheet detached from flat PIPAAm-PS in a maximum composite image and (b) a single focal plane image obtained from the composite in *a*. (c) Cell sheet detached from rough PIPAAm-PS in a maximum intensity composite image and (d) a single focal plane image obtained from the composite in *c*. Scale bar is equal to 50 μm .

FN antibody staining combined with f-actin staining is observed in Figures 6.12a and 6.12b. The actin labels the cell body outline and shows where FN fibrils have formed in relation to the cell. Fibroblasts from the flat surface have fibrils rimmed around the edge of individual cells, while cells from the rough substrate have a matrix of fibrils that span the cells and combine with adjacent cell fibrils. In Figures 6.12c and 6.12d the FN matrix is observed without the actin

in cell sheets from the flat and rough PIPAAm-PS surfaces respectively. The overall density of the FN fibrils from cells on the rough surface is higher and a more extensive FN matrix is noted in contrast to the cell sheet from the flat surface. It is also observed in Figure 6.11 and 6.12 the actin highlights the significant difference in size and morphology of the cells. Cells from the flat PS are much larger and more round when compared to cells cultured from the rough PS surface. We have reported morphology changes for single cells when using altered surface topography compared to planar surfaces⁹⁷. This chapter focuses on the growth of confluent sheets of cells on the flat and rough surfaces and individual cell morphology was not studied.

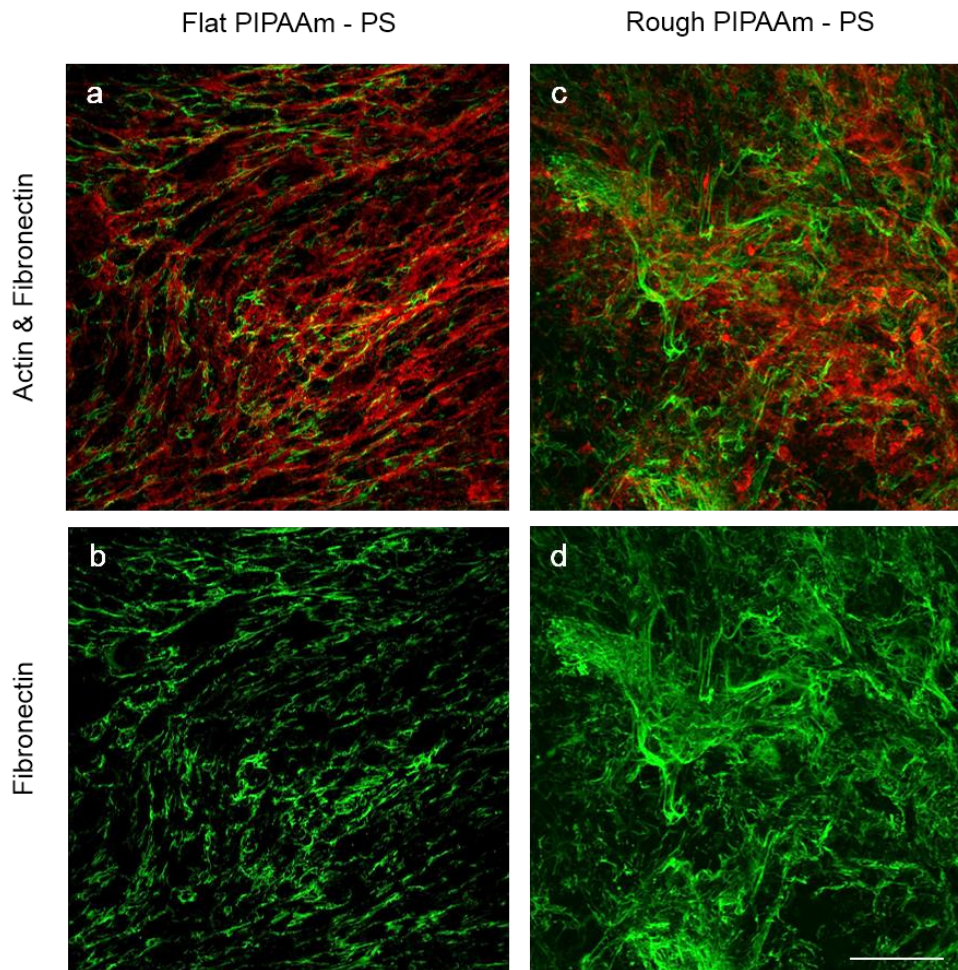


Figure 6.12. Confocal maximum composite images. (a) Cell sheet detached from flat PIPAAm-PS with f-actin and fibronectin labelled (b) and image *a* with only fibronectin. (c) Cell sheet detached from rough PIPAAm-PS with f-actin and fibronectin labelled (d) and image *c* with only fibronectin. Scale bar is equal to 50 μm .

6.4 Discussion

Multiple protocols for grafting PIPAAm onto a polymer surface were tested to fabricate a thermo-responsive substrate. All protocols were successful in this goal as documented by FT-IR spectroscopy (data not shown) of the surfaces, but the experimental procedure described here was chosen because of cell adhesion to the PIPAAm-PS. Other PIPAAm surface deposition protocols

did not promote cell adhesion or cell adhesion was sparse and not adequate for cell sheet formation. The lack of cell attachment to these surfaces may be due to the thickness of the PIPAAm layer which has been documented as hindering cell adhesion^{268, 270}. This PIPAAm-PS surface was chosen because it met three important criteria for cell sheet formation: (1) The cells must adhere to the surface after 24 hours, (2) cells will form a continuous sheet in less than 48 hours, (3) and cell sheets will detach from the surface in less than two hours when the thermo-responsive system is cooled below 20°C. The polymer grafting protocol described in the methods section was the only experimental method to meet all of these criteria for generating fibroblast cell sheets. The time frames of the three point criteria were chosen to achieve healthy cell sheets in a short period of time to have applicability as tissue grafts.

For formation of the PIPAAm-PS surface, UV/benzophenone graft polymerization was utilized to create radicals to initiate covalent linkage of a polymer or monomer to the PS substrate. Benzophenone photochemistry was chosen for our system because it is chemically stable in normal atmospheric conditions and only forms an active triplet-state ketone when exposed to UV light⁹¹, even in the presence of water or bulk nucleophiles²⁹³. The triplet state abstracts a hydrogen to create a radical and initiate the polymerization process. Benzophenone photopolymerization has also been accomplished by absorbing the molecule at the polymer surface for surface grafting of PIPAAm^{294, 295}. Since PS does not absorb most solvents, benzophenone was added in solution to react at the surface. Our polymer grafting also included the addition of NaIO₄ and benzyl alcohol. NaIO₄ was used to remove oxygen from solution as oxygen is an inhibitor of radical polymerization²⁹⁶. In the presence of a monomer and UV light, the periodate ion generates hydroxyl radicals that react with the monomer and consume oxygen. Benzyl alcohol was used to increase the efficiency of the polymer surface grafting by acting as a chain-transfer agent during

polymerization²⁹⁷. A chain-transfer agent slows the growth of primary polymer chains and facilitates chain termination keeping polymer chains from building and forming a gelatin in solution²⁹⁸. Overall, the experimental protocol was successful at creating a uniform fibroblast sheet on both the flat and micro-roughened PS.

When PIPAAm is in an environment below the LCST the hydrophilic moieties within the polymer interact with water through hydrogen bonding, but as the temperature increases these bonds break and the hydrophobic interactions become stronger forcing water molecules out of the polymer²⁹⁹. This phenomenon is reversible, so when the polymer is cooled, it will re-expand. For cell sheet engineering, the expansion of PIPAAm at the surface releases the cells and their ECM into solution. Our fibroblasts were cultured on two types of PIPAAm grafted PS, flat and micro roughened. The flat PS surface has nanometer sized features as seen in the AFM topography, but is effectively flat when compared to the templated micro features of the rough PS establishing two significantly different environments for fibroblast culture. The first noted difference between the two surface topography-cell systems was the rate at which the cell sheets detached from the PIPAAm-PS. Fibroblasts from the flat surface detached in 5 minutes while cells on the rough surface took 40 minutes after exposure to media at 4°C. PIPAAm hydration and chain expansion is rapid and instantaneous with a decrease in temperature below the LCST, but cell sheet detachment is delayed. Cell detachment from a thermo-responsive surface is described in is a two-step process involving the surface hydration and an active cell detachment³². Once the PIPAAm chains swell on the surface, passive cell adhesions through van der Waals forces and electrostatic interactions become weaker or non-existent forcing the cells to round and change shape. This initiates an active cell detachment, where in the case of a confluent cell sheet, the shared ECM is simultaneously contracted and the cell sheet detaches. The relatively short time between system

cooling and sheet detachment on the flat PIPAAm-PS surfaces indicates that the passive step governs the majority of the removal process. It can be hypothesized that the increased detachment time for cell sheets on the rough PIPAAm-PS is due to the fact that after the electrostatic interactions are broken there is no rapid relaxation of the stress fibers as there is on the flat surface. Here, because of surface topography, the ECM is not instantaneously contracted and the complete sheet detachment is prolonged. The micro-cavities of the rough surface allow cells to permeate into the PS altering the cell cytoskeletal and ECM arrangement. On a flat substrate cells can spread into large, stressed morphologies, and so when released there is a large amount of contraction back into a relaxed state. A cell on a rough surface topography does not experience the stressed morphology and its shape is constrained by surface micro features⁹⁷. Cell sheets on the micro-roughened PIPAAm-PS feel less strain on the surface. When the system is cooled and the cells encounter the PIPAAm hydration, the sheet contracts less, forcing the cells to more actively disengage their ECM from the surface.

Fluorescent microscopy of cell sheets was used to image the cell actin cytoskeleton and FN in the ECM. The cell FN matrix, cytoskeleton assembly, and cell adhesion are linked through integrin signaling³⁰⁰. Changes in the actin cytoskeleton generate inside-out signals to integrins and alter ECM formation³⁰¹. As noted earlier, cell sheets cultured on the flat substrate had actin stress fibers that are indicators of cells cultured on flat, stiff surfaces, where the cell can spread without restriction. The continued and increased cell spreading on 2-D surfaces leads to integrin clusters and large focal adhesion complexes, anchored by actin stress fibers^{27, 28}. The extended actin filament network in cell sheets cultured on the flat PS had limited FN fibrils that only surrounded the cell bodies. Culturing fibroblasts on the micron rough surface forced cells to change their integrin arrangement, morphology and actin cytoskeleton and therefore also changed

the ECM FN formation. On the rough PS, surfaces the limited actin formation resulted in a high density of FN fibrils that spanned multiple cells. The micro-environment of the rough PS created a spatial arrangement for fibroblasts to engage in altered cell signaling for cell sheets with distinctive properties³⁰². The two types of PS surfaces have stimulated the fibroblasts sheets to exhibit two significantly different types of cell response.

FN was chosen because it is one of the main proteins that composes the ECM and regulates a variety of cell behavior through interactions with cell integrins²³. FN fibrillogenesis is required for the deposition of other ECM proteins and ECM remodeling³⁰³. This makes FN an essential component for wound healing as it is a natural cellular adhesive. Cell sheets with a well-developed FN matrix are more likely to adhere and attach to sites that need a tissue graft²⁰. Mao *et al* showed stimulated fibrillogenesis and a higher FN density in human lung fibroblasts when cells were cultured on a pre-made mesh of FN matrix³⁰⁴. Their results yielded similar FN fibrils that are observed in cells on our micro-roughened surface, although instead of depositing a complex framework of FN, our system has utilized micro surface topography to induce changes in the FN-ECM assembly. Fibroblast cell sheets from this system have shown an increase in FN fibril density compared to cell sheets on a flat substrate making them potentially more beneficial for wound repair. By making a simple change in the surface roughness, integrin activation, ECM composition, and cytoskeleton arrangement can all be simultaneously and drastically altered when compared to cells on a planar surface. Surface topography offers a simple bottom-up method for controlling cell behavior and response. Our research has expanded the analysis of physical surface roughness on single cell systems to cell sheet engineering. The given experimental protocol presents a simple method for modifying physical surface topography that alters the cellular cytoskeleton and can provide cell sheets with increased fibronectin fibrils when compared to cell

sheets from 2-D substrates. Increased control of fibroblast ECM will lead to the design of cell sheets more capable of replacing damage tissue and aiding in wound repair.

6.5 Conclusions

We have developed a protocol for grafting the thermo-responsive polymer, PIPAAm, onto micro-roughened PS that is capable of sustaining fibroblast cell culture. The micron surface topography and chemistry of the PIPAAm-PS was extensively characterized. Fibroblasts cultured on the surface became confluent and could be released as a single sheet with an intact ECM when the media temperature was cooled. These cell sheets were compared to sheets cultured on physically unmodified, flat PIPAAm-PS. Significant differences in cell sheet size, f-actin orientation, and FN density were observed. Fibroblast sheets cultured on the roughened PS had a greater abundance of FN fibrils and less actin stress fibers when compared to sheets generated from the flat substrate. The changes in ECM make cell sheets exposed to altered surface topography potentially more useful wound healing and tissue graft applications. This research provides a bottom-up method for designing thermo-responsive, cell engineering technology for more complex cell-surface systems and cell sheets with user defined ECM parameters.

7.0 Final Discussion

7.1 Introduction

The work in this thesis describes a super-hydrophobic surface that was further modified with various methods for cell culture. The micro-roughness of the surface stimulated cell response analogous to cells *in vivo* and other 3-D cell culture matrices. This section is designated to compare and analyze the results between the past chapters and how they relate to the overall theme of the thesis. A discussion of topics that overlap or complement each other are presented here as well as a discussion of the topics in relation to cell biology.

7.2 PDMS vs. PS

In Chapter 3 – 5 the fabricated surfaces were designed with PDMS. PDMS was chosen because it can easily be molded and the polymer surface can easily be modified with silanes or proteins¹²⁷. In these chapters, PDMS surface micro-structure was created by templating PDMS on SiC grit paper. Chapters 4 and 5 use the rough PDMS surface for cell culture and compare the cell behavior to cells on flat PDMS substrates or cells cultured in PS well plates. The differences in material stiffness are significant, the elastic modulus is 2.6 MPa for PDMS¹²¹ and 3,500 MPa for PS¹¹⁹. As a result of the substrate stiffness change, cells alter biochemical signaling. This is most evident in Chapter 5, where fibroblast behavior on flat PDMS substrates is compared to cell behavior on PS Petri dishes. Between the two, 2-D flat substrates there is a significant change in gene expression. Cells cultured on the PDMS had continuous upregulation of matrix metalloproteinases (MMPs) and down-regulation of ECM adhesion molecules. In Chapter 6, surface micro-roughness is combined with PS instead of PDMS. The micro-roughened PDMS

was used as a template and pressed into tissue culture PS dishes to generate PS surface topography. Although, not discussed in Chapter 6, PDMS was tested for as a candidate for a thermo-responsive surface for cell sheet formation. Similar protocols and methods that were successful for grafting PIPAAm to PS were initially tested with PDMS. Grafting of PIPAAm onto PDMS surface was confirmed with AFM and FT-IR, but the surface did not provide confluent cell growth. Altering fabrication variables, such as chemical concentrations, irradiation times, and protein incubation periods could not produce a surface for uniform, confluent cell culture. Cells that did attach to the PIPAAm grafted PDMS, formed tight knit islands or bundles on the surface, as seen in Figure 7.1. Even after a few days in culture media, the bundles did not grow out onto the surface and cells remained in the bundled state. The clumps of cells on the surface varied in size, ranging between 20 and 100 cells per group. These islands of cells would detach from the surface when cooled, but were not capable of forming a cell sheet.

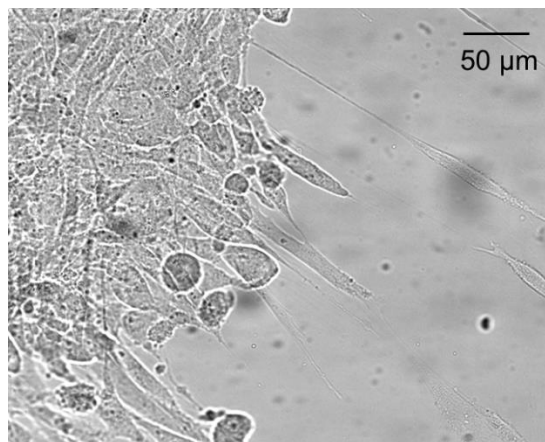


Figure 7.1. Bright field microscopy image of fibroblasts cultured on PIPAAm grafted PDMS. Cells banded into islands instead of growing out onto the surface.

Literature reports of PIPAAm on PDMS have shown confluent cell attachment²⁹⁵ but this may have been due to the different cell type used (smooth muscle cells). Cell adhesion using

smooth muscle cells in a specific culture system does not ensure cell adhesion of other cell types in the same system. The protocol for UV grafting of PIPAAm requires the hydrophobic molecule, benzophenone, but the porosity of PDMS makes the polymer capable of absorbing hydrophobic molecules into the bulk of the material¹²⁴. Grafting of PIPAAm onto a surface may be hindered or difficult to replicate because of benzophenone absorption below the surface of the PDMS. Benzophenone is also toxic to living cells, and residual material absorbed in PDMS could result in cell death with concentrations as low as 0.25 mM³⁰⁵. This may explain why PDMS was not an adequate material for supporting the thermo-responsive polymer and cell sheet formation. PS does not have these problems. The highly cross linked polymer is less porous and less likely to allow benzophenone absorption. In our experiment PS-PIPAAm presented a more suitable surface for confluent cell sheet culture than PDMS. The change from PDMS to PS is an example of how material properties can alter surface chemistry and cell-surface interactions. For future research, PS may be a more useful choice than PDMS for studying surface roughness. Although PDMS is a widely used biomaterial, PS perhaps has more commercial applications because it is commonly used for cell culture lab ware. Assimilating rough PS into current cell culture protocols would be easier than PDMS since well plates, culture flasks, and culture dishes are already made of PS. There would be no change in the material or bulk properties such as stiffness. Chapter 6 has demonstrated that surface roughness can be applied to two polymers and still influence cell behavior.

7.3 Actin Cytoskeleton Organization and Adhesion

In all the chapters that examine cell-surface interactions (Chapters 4 – 6), a constant marker for fibroblast behavior is analyzed: the cell actin cytoskeleton. As mentioned in the introduction, the actin cytoskeleton is linked to cell adhesion, integrin binding, and ECM. Changes in these factors can alter cytoskeletal rearrangement and *vice versa*. In Chapters 4 and 5, fibroblasts are cultured on roughened PDMS and in Chapter 6, roughened PS. The culture controls used were tissue culture PS and or flat PDMS. Fibroblasts on all flat, control surfaces, whether PDMS or PS, had visible actin stress fibers running across the cell bodies (Figure 7.2 a, c, and e). On the physically altered surfaces, even with the changes in surface chemistry, there are no significant stress fibers noted (Figure 7.2 b, d and f).

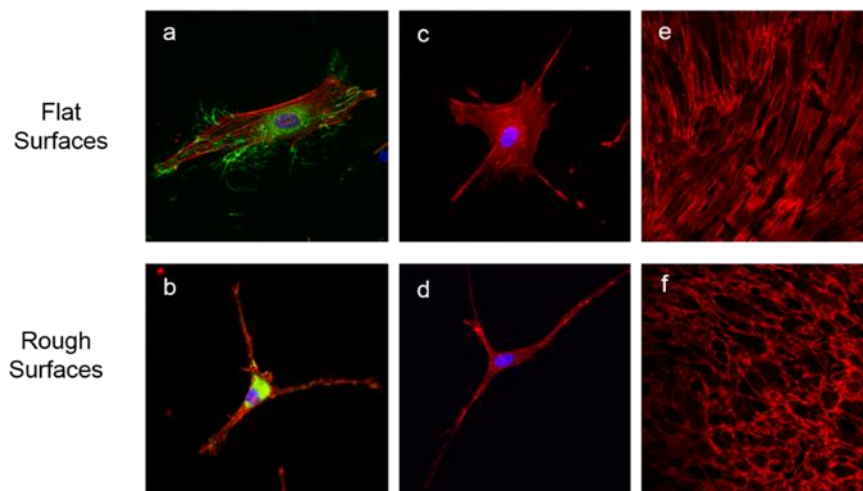


Figure 7.2. Examples of cytoskeletal actin. Figures a and b reprinted from Chapter 4, figures c and d reprinted from Chapter 5, and figures e and f reprinted from Chapter 6.

The change in actin fibers also correlated with cell area. Cell area was greater on planar surfaces when compared to cells cultured on the rough surface. The smaller, spindle like cells observed on

the rough substrates with minimal actin fibers is similar to cells observed *in vivo* or 3-D matrices^{11, 302}. An example fibroblast with spindle morphology in a 3-D matrix is shown in Figure 7.3. Actin stress fibers increase the tension of cell membranes and as a cell continues to spread on a surface the tension increases forcing the cell to anchor itself to the surface with bulky focal adhesions. A more slender cell that cannot spread to such a large due to surface topography area does not need such anchoring. Focal adhesion complexes are known to be located at the end of large actin stress fibers, composed of integrin aggregates, and are sites of tight adhesion to the underlying ECM²³. In Figure 7.2f the fibroblasts cultured on the rough PS do not exhibit a spindle morphology, but we believe this is because they have detached from a surface and the cell shape is not exclusively controlled by surface features. Culturing the cells to confluency on the PIPAAm-PS also changes cell morphology, as cells alter their growth once cell-cell contact is established. However, cells cultured on the rough PS still have a smaller geometric area than cells cultured on the flat PS (Figure 7.2e), indicating even after surface detachment, cell morphology can be altered by topography.

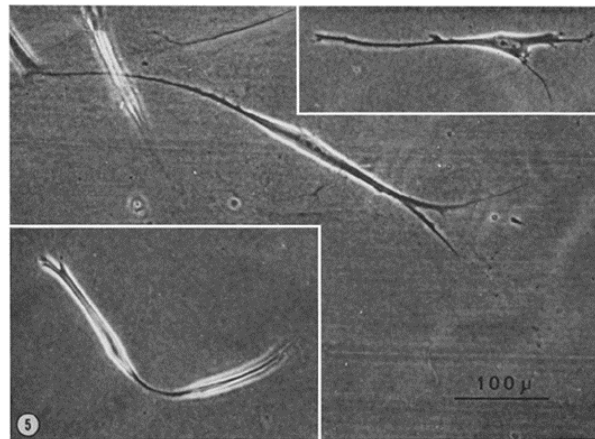


Figure 7.3. Examples of fibroblasts embedded in a 3-D collagen fiber matrix with a spindle like morphology¹¹.

Focal adhesion complexes are visualized in Chapter 4 with vinculin staining, reprinted in Figure 7.4. On the flat PDMS, discrete islands of vinculin are observed, but vinculin is evenly distributed throughout the cell on the rough PDMS surface. This is similar to the distribution of labeled actin in fibroblasts cultured on rough surfaces in Chapters 4 – 6. Cells on the roughened substrates are not forming discrete focal adhesions because they do not contain prominent actin stress fibers. The formation of localized focal complexes are features that have only been observed in classical, 2-D cell culture systems²⁹. *In vivo*, cells are not capable of containing large actin filaments and large focal adhesions because it would hamper essential mechanisms such as motility, ECM rearrangement, and mitosis required for a healthy organism³⁰⁶. The rough surface topography described in each chapter hinders the development of actin fibers and discrete focal adhesions, creating a more native like cellular environment. By making minor alterations to the substrate a *pseudo* 3-D surface environment can be artificially induced to produce cells similar to a physiological system.

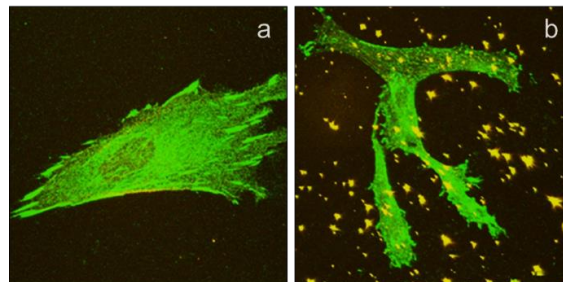


Figure 7.4. Examples of focal adhesions labelled with fluorescently labelled vinculin. Fibroblasts cultured on a (a) flat surface and (b) rough surface. Figures reprinted from Chapter 4.

7.4 ECM Assembly: Single Cell vs. Cell Sheet

The cellular ECM is one of main focal points of Chapters 4 and 6. FN was chosen as a marker for the organization and quantity of ECM in these systems because it is a main component of the ECM and is directly linked to integrin binding, adhesion, and cytoskeleton organization^{23, 300}. In Chapter 4, the FN matrix of individual fibroblasts was examined on micro-roughened PDMS and compared to cells cultured on flat PDMS (Figure 7.2a and 7.2b). Fibroblasts were cultured in a low serum, 1%v/v FBS system to minimize protein attachment to the surface and force cells to act more directly with the topography. In Chapter 6, fibroblasts were seeded on a micro-roughened, PS surface and allowed to become confluent in a sheet. These cells were compared to cells on a flat PS substrate and were cultured in a 10% v/v FBS system. The experimental protocols in each chapter vary in material and culture system FBS concentration, but the cells can be compared. The fibroblast in each system are cultured on similar surface roughness. Cells in both chapters exhibited significant actin stress fibers on their respective flat, control surface. These fibers ran across the entire body of the cell when examined individually or in a sheet, indicating that the differences in PS and PDMS material stiffness had no bearing on the cytoskeletal arrangement on the surfaces (Figure 7.2a and 7.5a) Fibroblasts on both materials were stressed, producing actin fibers to help them anchor to the flat surfaces³⁰⁷.

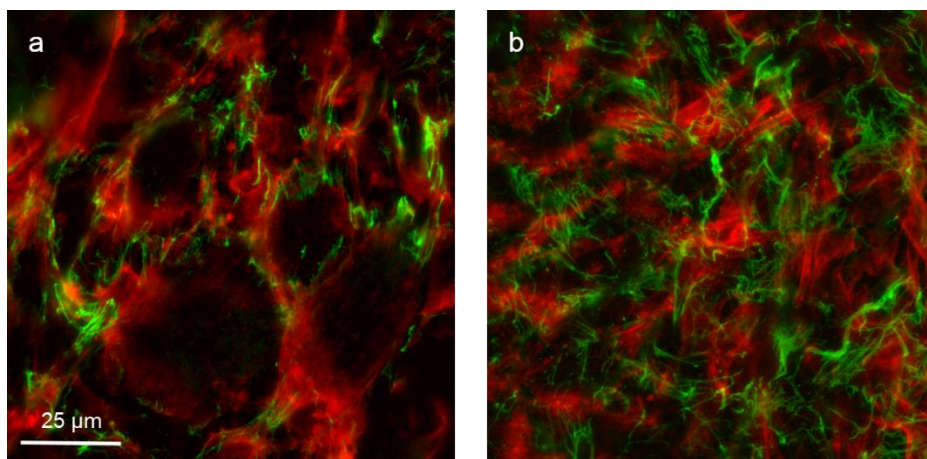


Figure 7.5. Examples of fluorescently labelled FN fibrils (green) and f-actin cytoskeleton (red) on cell sheets detached from (a) flat surface and (b) rough surface PIPAAm-PS surfaces.

FN composition and deposition was also similar between these two flat substrates. Cells on the flat PDMS generated FN fibrils that are comparable to the FN fibrils in the cell sheets in Chapter 6 (Figure 7.5a). On the two types of rough surfaces, the FN matrix is drastically different. On the rough PDMS, islands of FN are visible, but no fibrils are evident. On rough PS, there is significant secretion of FN fibrils in the fibroblast sheets that span individual cells and even jump between cells (Figure 7.5b). The formation of FN fibrils is known as fibrillogenesis and is initiated and mediated through integrin binding to secreted FN on the outside of the cell membrane³⁰³. Fibrillogenesis is almost non-existent in fibroblast cultured on the rough PDMS surface, but is amplified in the cells sheets cultured on rough PS. The limited FN fibril formation on the PDMS rough surface contradicts past literature reports where an increase in ECM FN was noted on surfaces with physically altered topography³⁰⁴, even in low FBS conditions³⁰⁸. In the reports with high FN fibril concentrations, cells were seeded at a density large enough to allow cell-cell interactions. In our work, fibroblasts on the rough FN were seeded so no cell-cell contact would be observed. Given this, it can be hypothesized that the lack of FN fibrils on the rough PDMS

surface is a result of limited cell-cell interactions. On the rough PS surface, cells were confluent and even overlapped allowing fibrillogenesis. Cell to cell contact is capable of altering integrin and cytoskeletal rearrangement, so it is possible that it would have a large impact on cellular ECM. This may be an important argument for tissue design and single cell model systems; that in order to truly imitate an *in vivo* environment, other cells may need to be present for a bio-mimic culture scaffold.

7.5 MMP14 in Relation to Cell Sheet FN and Actin

This section compares gene expression data from Chapter 5 and cell sheet ECM and actin from Chapter 6. The gene expression was completed with fibroblasts harvested from roughened and flat FN coated PDMS and compared to FN coated PS Petri dishes. Relative expression profiles of ECM and adhesion molecule-associated gene transcripts were compared between cells cultured on the different surfaces (Table 5.3 and Figure 5.7). Large changes in gene expression were noted between flat PDMS and PS surfaces indicating the change in substrate stiffness had a large impact on cell signaling. Between the rough and flat PDMS there were also differences in gene expression as shown in Figure 7.6. On the rough PDMS the matrix metalloproteinase (MMP), MMP14 (also known as MT1MMP) had an increased average fold change of 2.3 with PCR arrays and an average fold change of 5.8 using independent primers when compared to flat PDMS. MMPs are protease enzymes catalyzed by zinc ions to degrade the proteins of the ECM and other surface bound proteins³⁰⁹. MMP degradation and remodeling of the ECM is essential for cell survival and growth as well as inducing natural apoptosis in adherent cells³¹⁰. While the mechanism for the increase in MMP14 in cells cultured on a rough surface is unclear, it can be established that it was induced

by the surface micro-topography. The increase in expressed MMP14 could have exciting impacts in the field of tissue engineering and cell sheet formation on roughened substrates.

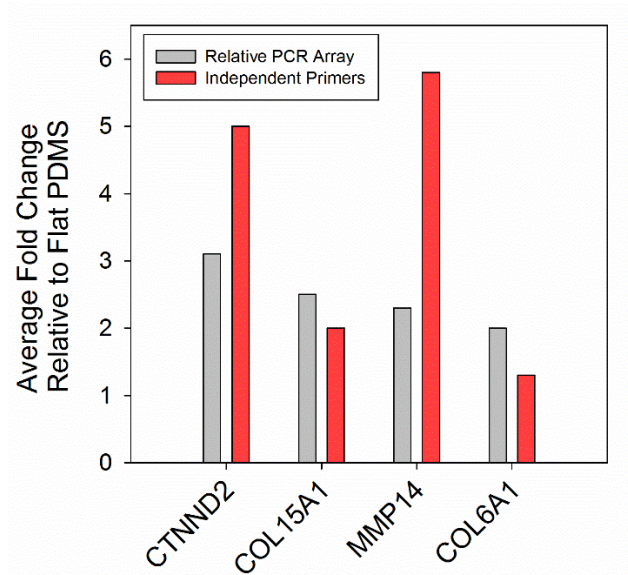


Figure 7.6. Average gene expression fold change of fibroblast cultured on rough PDMS using PCR arrays (grey) and independent primers (red) relative to fibroblasts cultured on flat PDMS. Data reprinted from chapter 5 in Table 5.3.

MMP14 is one of the most well studied MMPs and is a transmembrane associated protein that is capable of degrading ECM collagen, laminin and FN. When cells migrate in a tissue, degradation of the ECM is needed for motility, but ECM is also important scaffolding. To degrade only specific ECM the cell localizes MMP14 at the cell edge with f-actin²⁶⁵. As mentioned previously, f-actin is used as a marker for cell sheet behavior in Chapter 6 and is seen in Figure 7.2e and 7.2f. The confocal images of the f-actin stress fibers across the fibroblasts cultured on the flat PS are clearly visible, while actin in cells from the rough surface is located at the cell edge. The localized actin at the edge of the cells from the rough PS is in agreement with literature reports linking MMP14 and actin arrangement³¹¹. Changes in the actin cytoskeleton correspond to

changes in the expression of MMP14 and actin localized at the edge of the cell would assist MMP14 in ECM remodeling. The stress fibers noted in the fibroblasts cultured on flat PS, may delocalize MMP14 formation from the cell edge²⁶⁵. The surface roughness increases fibroblast MMP14 expression but it may also localize the MMP14 better than a flat substrate. Since MMP14 degrades ECM FN, the increase in FN fibrils in cell sheets cultured on the rough surface (Figure 7.5b) are perhaps due to a more organized actin cytoskeleton and MMP14 arrangement, where MMP14 only degrades at necessary sites. The lack of FN fibrils on the cell sheets cultured on the flat PS surface can therefore be attributed to delocalized MMP14 with less specificity for ECM FN degradation. For tissue engineering the increase in FN density would be advantageous for wound healing as FN acts as an adhesive for tissue grafts. MMP14 is also associated with wound healing as it is essential for instigating remodeling of damaged ECM and restoration of connective tissue²⁶⁶. The combination of high density FN and increased expression of localized MMP14 in cells sheets indicates surface topography could be a major future influence for designing thermo-responsive surfaces for cell sheet engineering.

MMP14 has also been a focus for cancer formation for the past two decades. It has been observed that invasive cancer cells have an overexpression of MMP14 enabling them to quickly degrade ECM and proliferate faster, promoting tumorigenesis³¹². As a result, MMP14 inhibitors have been investigated as a source to slow cancer development. However, significant evidence has shown the surrounding cellular environment yields different results in MMP and MMP inhibitor activity; inhibitors have a greater effect on tumor cell growth *in vivo* than *in vitro*. In a report conducted by Hotary *et al.*, tumor cells exposed to MMP14 inhibitors (TIMP-1 and TIMP-2) were cultured on 3-D protein matrices and compared to tumor cells on 2-D surfaces³¹³. Under the 2-D growth conditions, with tumor cells overexpressing MMP14, there are no changes in

proliferation between cells exposed to the inhibitors or cultured without the inhibitors as a control. In the 3-D matrices there is a significant increase in proliferation and the ability of the inhibitors to restrict tumor cell growth when compared to the control tumor cells. Hotary did not describe a mechanism, but hypothesized, that in a 2-D environment MMP14 activity and expression is subdued, but in a 3-D system cancer cells exploit the increased expression of MMP14 to increase their proliferation rate. The observed increase in MMP14 expression in fibroblasts on our micro-rough surface indicates that our substrate performs like a 3-D protein matrix. Combined with the other observed cell behavior described in this thesis the rough surfaces may be more relevant to an *in vivo* system. The comparison of our work to the experiments completed by Hotary *et al* also presents possible applications of our surface with tumor cells and cancer research. If the surface topography of the rough surface replicates the cell response achieved in 3-D matrices, then the substrates presented in this thesis could provide a simpler alternative. The formation of surface roughness with a template offers a less complex culture matrix for physiological cell behavior.

8.0 Conclusions and Future Work

Polymers have become integral materials in the field of biomaterial design and have been used for biomedical devices and tissue engineering applications. The bio-interface at the polymer surface is an essential junction for providing environmental cues for cell signaling. This thesis has demonstrated that chemical and physical surface modifications to polymers are a bottom-up method to alter and control cell behavior. A templating method generated polymer surfaces with micron sized features for well-defined and characterized surface roughness. The rough substrates were used for cell culture with human fibroblasts and cell responses were compared to cells cultured on flat surfaces, such as tissue culture PS. Throughout the thesis chapters, complex surface modifications were performed for control of a cell's biochemical fate and an understanding of the cell-surface interactions. Initially, a super-hydrophobic surface was fabricated with PDMS that displayed unusually high adhesion, similar to a rose petal. The roughness of this surface was used for single cell studies by modifying the surface chemistry with silanes or a thin film of protein. Finally, the surface roughness was templated on PS and derivatized with a layer of thermo-responsive polymer for cell sheet engineering.

The research highlights in this work are:

- 2 – 6 μm features on PDMS induced a super-hydrophobic contact angle of 154° , but was also highly adhesive
- Fibroblasts cultured on the rough substrate PDMS had a smaller geometric surface area when compared to cells on a 2-D substrate
- FN fibrillogenesis deposition can be increased or decreased based on surface topography

- Surface roughness decreases cell adhesion at the initial cell-surface contact and limits focal adhesions 24 hours after attachment
- Surface patterning and roughness can be combined for a novel cell scaffold with a directed cell alignment
- Differences in gene expression of cells was noted between cells cultured on different material stiffness as well as different surface topography
- Surface roughness was fabricated on PDMS and PS
- A thermo-responsive film was attached to surface roughness to generate cell sheets with an altered ECM and actin cytoskeleton.

At present, it is established that physical and chemical properties of biomaterials profoundly impact cell behavior, but detailed mechanisms that affect cell biological performance are just beginning to be understood. The goal of cell culture surfaces and scaffolds is to provide an *in vitro* environment that generates *in vivo* cell response. Design variables such as topography feature size, bulk material properties, and surface chemistry or biochemistry deliver an endless number of combinations that may produce different responses based on the cell type. This thesis used a simplified strategy by fabricating a surface with features in a narrow range and using it as a base for further modification (Figure 8.1). Cell studies with this surface were intentionally completed with a single, commonly used cell type. By keeping two design variables constant, surface roughness and fibroblasts, different projects observing fibroblast behavior could be quantitatively compared. The collected summary of cell response is now a thorough and comprehensive analysis of fibroblasts cultured on defined surface features, including single cell and cell sheet research. This work has shown the large range of bio-substrate applications that rough polymer surfaces can influence for altered cell biological response.

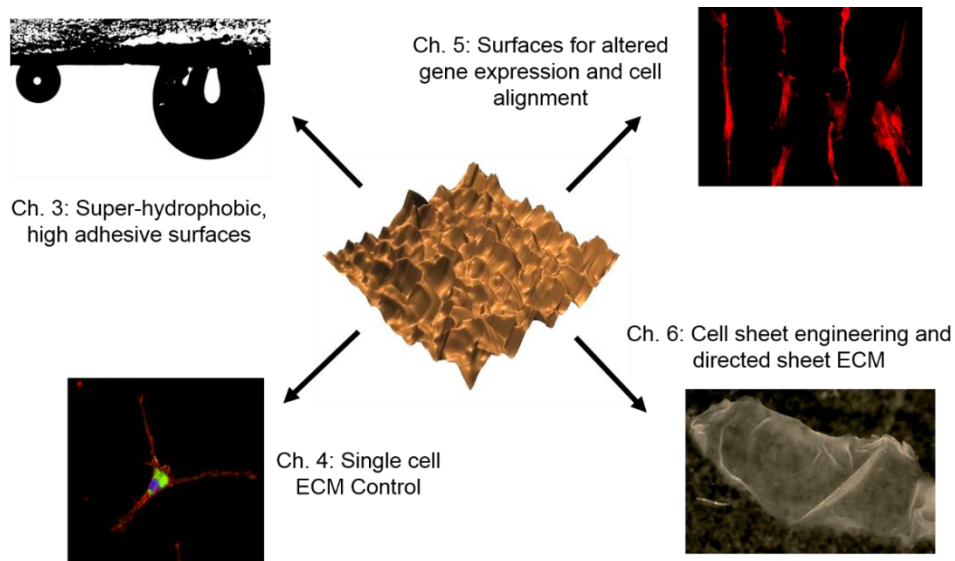


Figure 8.1. Research projects completed using the micro-rough polymer surface.

The micro-roughness has been described as a *pseudo* 3-D surface. An ideal *in vitro* system for physiologically relevant cells would replicate a 3-D, highly ordered native cellular environment. Literature reports of 3-D matrices have included scaffolds with micro- or nano-engineered pores, fibers, or gels. Cells in these systems impregnate the matrix and become surrounded in the scaffolding. For the majority of these reports, the cells exhibit *in vivo* behavior and the matrix was a successful biomimic, but these matrices require complex fabrication protocols and assaying the cells within the matrix can be difficult. Throughout this thesis we have compared the results of cells on polymer rough surfaces to cells cultured in 3-D matrices and *in vivo* and have found our cells have analogous behavior. The surface 2 – 6 micron topography has also proven to be a successful biomimic, but is much simpler to fabricate than current 3-D matrices. The micron features force the cell to alter its adhesion, cytoskeleton, and ECM without cell permeation into the substrate, labeling the rough surface a *pseudo* 3-D environment for cell culture. Equivocating surface roughness to a 3-D scaffold bridges the gap between analysis of cells on 2-D glass or polymer systems and analysis of cells in a complex 3-D matrix. In the 2-D systems,

physiological relevance of cell behavior is lost, but the surfaces are inexpensive and accepted culture systems for cell comparison. In the 3-D matrix, physiological relevance is returned, but there is no fabrication standard and cell behavior is difficult to quantify between different systems. One of the most significant findings of this work is that surface roughness may provide the key for combining the simplicity of 2-D culture surfaces and *in vivo* cell behavior. The mechanism for how surface roughness replicates a 3-D scaffold is hypothesized through the cell-surface interaction. Fibroblasts cultured on the micron features have delocalized focal adhesions and transmembrane integrin binding. Without significant focal adhesions, actin stress fibers are not needed and the cell morphology becomes contracted and spindle like. Inside-out signaling from the compact actin cytoskeleton to the integrins results in changes in FN fibrillogenesis and other ECM secretions. The cascade of cell signaling events induces upregulation and downregulation of specific genes, including MMPs and adhesion molecules. Although the cell is not completely surrounded in a 3-D scaffold the 2 – 6 micron surface topography has enough depth and feature dimensionality to imitate a cellular 3-D system.

Chapter 5 and 6 of the thesis prove the successful applications of the rough polymer in the field of biomaterials for complex systems. In each of the chapters the goal was to address two problems in cell culture using one surface. For Chapter 5, the rough PDMS delivered controlled cell adhesion and altered gene expression. In Chapter 6, the rough PS generated cell sheets and increased FN ECM. Both chapters offer combinations of surface properties that are more advantageous for cell culture than the individual surface property used alone. In Chapter 5, rough PDMS was patterned with FN and BSA for aligned cell culture. Cell alignment and controlled cell adhesion on 2-D surfaces has been reported for almost 30 years, but had yet to be tested with surface micro-roughness. This project was the first of its kind to do so. The bioactivity of the

cells was controlled with patterned surface biochemistry and surface topography. In Chapter 6, the rough PS was modified with a multi-step chemical process followed by UV grafting of a thin film of PIPAAm. Previous reports of cell sheet formation have consistently used flat surfaces. Without changing the objective of cell sheet formation, Chapter 6, took the thermo-responsive surface fabrication process a step further using micro-roughness as a culture platform. The resulting cell sheet had unique biochemical behavior that could aid in wound healing. Both Chapter 5 and 6 demonstrate that bioactive or environmentally responsive surfaces combined with micro-roughness offer solutions to problems that cannot be addressed by a single surface property. With a greater understanding of the cell-surface interface, the next generation of biomaterial surfaces will need to address increasingly complex issues with single cell analysis, cell behavior and signaling, and tissue integration into *in vivo* systems. This will include adopting different strategies of surface design, combining bulk material properties, surface chemistry, and micro- and nano- topography. The work presented in this thesis is the next step for surface science and offers an interdisciplinary approach for tailored cell behavior using micro-roughened polymer substrates.

Future research applying the surface technology presented in this thesis will be essential for the development of new substrates for controlled cell behavior. The rough substrates presented use surface topography to generate micron sized features that offer an alternative culture system. This thesis has demonstrated proof of concept methodology that surface roughness can alter human fibroblast behavior for biomaterial applications. Cells cannot grow into the substrate like a 3-D culture system, thus our substrate is designated as a *pseudo* 3-D surface for cell culture. Future projects will branch from this research and incorporate more cell types. The *pseudo* 3-D platform can be analyzed in conjunction with neuron, skeletal muscle, and stem cell cultures. The biochemical and morphological differences noted in these cells when compared to cells on a Petri

dish would not only create a library of micro-topography influence but initial parameters for designing individual cell culture templates for specific cell types. The goal of building an inexpensive, polymer scaffold to mimic an *in vivo* system has been explored here, however, it cannot be a universally accepted culture system if more cell species are not tested and analyzed. It will be essential that one of the future projects will involve cataloging cell behavior using different cells on our micro rough surfaces and comparing them to one another and other currently accepted culture methods.

As noted in the introduction, this thesis has followed the characterization, chemical modification, and thin film modification, in relation to cell culture. The development and fabrication of the surface increasingly grew more complex, with the addition of a SAM, then a biochemical pattern, and finally a thermo-responsive film. Additional surface alternations were able to address certain issues such as fibroblast adhesion, alignment, and cell sheet transfer. One of the goals of these research projects was to aid in the design of future biomaterials for tailored cell behavior. With the observations and results derived from this thesis, future research projects can customize and build new surfaces. Examples of possible future surface designs are given below.

Example 1:

Only a single cell type was explored in this thesis, but to advance biomaterial development, co-cultures of cells should be incorporated. As an example of a future design process, the fibroblast we have investigated could be co-cultured with epithelial cells on a rough PDMS surface. Epithelial cells are commonly used in research and observation of their behavior would be beneficial for a majority of bio-related disciplines. Interactions of epithelial cells and fibroblasts

are commonly found in the lung and their interactions are investigated for patients with asthma. The pattern of FN and BSA described in Chapter 5 could be modified. Removing BSA from the pattern and allowing alternating spaces of FN and bare PDMS, two cell types could be seeded. Fibroblast would be seeded first and migrate towards the FN. After a few hours, protein from the culture solution would adsorb onto the bare PDMS regions, allowing a second cell seeding of epithelial cells. The epithelial cells would fill the gaps between the fibroblast, organizing both cell types on the surface based on the FN pattern. Observations in cell-cell junctions and co-culture could be made in response to the surface roughness.

Example 2:

The surfaces for cell sheets generated in Chapter 6 could have localized surface roughness. The PS discs fabricated in Chapter 6 were either exclusively flat or rough. The embossing procedure described could be modified to only press roughness into specific areas of the discs. A single PS disc would contain regions of roughness and flatness. This type of mixed surface topography would be ideal for tissues for implants and would utilize osteoblasts, fibroblasts and skeletal muscle cells. Prosthetic implants that span multiple tissue types, such as bone, muscle, and skin need specific surface properties for each of the tissues. The portion of implant embedded in the bone would be rough and porous to encourage osteoblast growth onto the surface. Regions of the implant into muscle and skin need to be smoother for less integration so those tissues can keep their flexibility. If the PS is kept thermo-responsive, tissue grafts can be harvested to cover wounded areas that span multiple tissue junctions or they could be placed on prosthetics before implantation into the body to encourage tissue integration.

Example 3:

The micro-rough scaffold has been fabricated with PDMS and PS only, but there are many more possible materials to choose from. The elastic modulus of the two polymers has been discussed, however this is simply two ends of a spectrum of soft and hard. Investigating the mechanobiology of the scaffold by adjusting the polymer's elastic modulus in a gradient or defined series has great promise in understanding the effect of surface stiffness on cell morphology and genetic profiles. As discussed in Chapter 4, large changes in gene expression profiles were noted between fibroblasts cultured on flat PS and flat PDMS. The different genetic profiles are credited to the different material stiffnesses. To build off of this observation, a study could be done to gradually increase the stiffness on a flat and rough substrate and find when genetic differences are attributed to material properties or to topography. Biopolymers, such as polyacrylamide, can have their stiffness adjusted with minor changes to the chemistry and would be ideal for monitoring cells on a stiffness gradient. By knowing when a cell is responding to either material properties or surface properties, biomaterials for specific cell types could be designed that stimulate a desired cell response, such as increased fibrillogenesis or adhesion.

The above examples represent a small portion of the design possibilities using the rough surface, but offer ideas use of the rough surface in more biomaterial applications. Other future projects recommended entail research that does not use surface topography or chemistry to study cell behavior. In Chapter 3, the micro-roughness was utilized as a super-hydrophobic surface with high adhesion. Unlike the lotus leaf or rose petal, the rough PDMS surface exhibits no nano-features on top of the micro-structure. Secondary physical modification of the micron surface roughness with nano particles to mimic natural systems such as gecko feet or leaf surfaces could

drive the surface to become super-hydrophobic without high adhesion. This could have applications for self-cleaning surfaces or micro-fluidic channels.

The simplicity and low cost of the protocol for fabrication of the rough surface topography allows the surface to be utilized in a multitude of scientific fields. This leaves the door open for innovative and novel research that has possibilities beyond the laboratory. Commercialization and industry applications using our technology can easily be envisioned. Since the polymer was fabricated with two commonly used biomaterials, PDMS and PS, the rough surface could be assimilated into many current cell culture systems without significant changes to the manufacturing process. Multi-well plates that are used for single cell studies in rapid analysis techniques, such as high throughput screening (HTS) assays, could be modified with roughness. Initial response of cells cultured in HTS systems are used for precursors for future drug discovery research. Cells cultured on rough PS well plates would be more physiologically relevant than cells on conventional flat, plates offering a greater advantage for finding effective medicines. Cell sheet engineering on rough surfaces for tissue grafts could also be pursued for biomedical applications. Currently, commercially available cell sheets are only cultured on thermo-responsive, flat PS. The rough PS surface has demonstrated increased FN formation that would be more advantageous for wound healing applications than the sheets grafted from the flat surface.

This thesis has extensively examined the interaction of cell behavior with our micro-topography. Chemical modification, surface topography, and bulk material properties and their impact on cell biology have been researched in-depth. The future research presented offers opportunities for specific projects that will branch off from this body of work. The building blocks for future biomaterial studies and development have been established, so more complex surface

and material modification can be pursued. With this in mind, the surface may also be integrated into other fields outside of the life sciences to broaden the laboratory's research scope.

List of Figures

Figure 1.1. Focal points of substrate influence on cell behavior	14
Figure 1.2. Schematic representation of the cell-ECM interactions	18
Figure 1.3. Actin filaments of the cytoskeleton.....	20
Figure 1.4. Focal adhesion points and fibrillar adhesion sites	21
Figure 1.5. SEM images of natural surface topography	23
Figure 1.6. Graphical example of roughness average (R_a)	24
Figure 1.7. Cells aligning with grooves	26
Figure 1.8. Examples of self-assembled monolayers (SAMs).....	29
Figure 1.9. Hydrolytic deposition of alkoxy silane.....	32
Figure 1.10. EDC/NHS amide bond formation.	34
Figure 1.11. Schiff base formation between GA and amine.....	35
Figure 1.12. Protein deposition at a surface.....	36
Figure 1.13. Example of microcontact printing.....	37
Figure 1.14. Example of traction force of migrating cells.....	42
Figure 1.15. PDMS chemical structure.....	43
Figure 1.16. PS and tissue culture PS chemical structure.....	44
Figure 2.1. Schematic of PDMS casting process.	50
Figure 2.2. Example of ATR objective.....	52
Figure 2.3. Example of evanescent wave formation.....	54
Figure 2.4. Static contact angle schematic.....	55
Figure 2.5. Force balance at the three phase contact line.. ..	56
Figure 2.6. Advancing and receding contact angles.	57
Figure 2.7. Example of AFM tip for imaging.....	58
Figure 2.8. Schematic diagram of AFM tip, cantilever, and sample.	59
Figure 2.9. Graphical representation of the AFM force distance curve.....	61
Figure 2.10. Jablonski diagram.....	62
Figure 2.11. Illustration of wide-field fluorescence filter cube.	63
Figure 3.1 Cassi-Baxter, Wenzel, and hybrid wetting states	66
Figure 3.2. Example of AFM grain threshold processing.....	69
Figure 3.3. AFM images of SiC paper and rough PDMS.....	70
Figure 3.4. FWHM of PDMS features.....	71
Figure 3.5. 6 μ L water drop on rough PDMS.....	72

Figure 3.6. AFM image of flat PDMS.	73
Figure 3.7. Water drops on inverted PDMS surface.	74
Figure 3.8. f_{afm} vs height threshold of a rough PDMS surface	76
Figure 3.9. AFM images of other roughened PDMS surfaces.	81
Figure 3.10. Adhesive properties of PDMS at 60°	82
Figure 4.1. AUTMS deposition on PDMS.	87
Figure 4.2. AFM images of AUTMS coated PDMS	93
Figure 4.3. Morphology analysis	94
Figure 4.4. Vinculin staining of fibroblasts	95
Figure 4.5. Fibroblast on tiptless cantilever.	96
Figure 4.6. Frequency plot of AFM cellular adhesion measurements	97
Figure 4.7. FN, f-actin, and nuclear staining of fibroblasts of cells and cell extracted surfaces ...	98
Figure 4.8. Control figures of fluorescent staining	100
Figure 5.1. Cartoon of BSA and FN deposition on rough PDMS.	109
Figure 5.2. AFM images of PDMS with FN coating	116
Figure 5.3. Patterned photoresist and FN images	117
Figure 5.4. Cell growth on patterned rough and flat surfaces.	120
Figure 5.5. Cell morphology comparison.	121
Figure 5.6. Analysis of cell area	123
Figure 5.7. Gene expression of ECM and adhesion molecules	131
Figure 6.1. Example of PIPAAm chains attached to a surface in water.	135
Figure 6.2. Fabrication process of micro-roughened PS.	138
Figure 6.3. Schematic illustration of PIPAAm chemical attachment to a surface.	139
Figure 6.4. AFM images of PIPAAm-PS	142
Figure 6.5. FWHM of PS features.	144
Figure 6.6. AFM images of unmodified PS and PIPAAm-PS.	145
Figure 6.7. ATR FT-IR of PS, PIPAAm-PS, and NIPAAm.	146
Figure 6.8. Flat and micro-roughened PS discs	147
Figure 6.9. Cell sheet detachment from PIPAAm-PS.	148
Figure 6.10. Detached cell sheets from flat and rough PIPAAm-PS.	148
Figure 6.11. Confocal images of cell sheet f-actin	150
Figure 6.12. Cell sheet f-actin and FN.	152
Figure 7.1. Fibroblast bundles cultured on PIPAAm grafted PDMS	159
Figure 7.2. Examples of cytoskeletal actin	161

Figure 7.3. Examples of fibroblast in a 3-D collagen matrix.....	162
Figure 7.4. Examples of focal adhesions	163
Figure 7.5. Examples of FN fibrils	165
Figure 7.6. Average gene expression fold change	167
Figure 8.1. Research projects completed using micro-rough polymer surfaces	172

List of Tables

Table 1.1. Table of Young's Modulus Values	41
Table 3.1. Static contact angles and roughness values for flat and rough PDMS	72
Table 3.2. f_{afm} values calculated for different threshold heights.....	75
Table 3.3. Surface free energy for flat and rough PDMS substrates	78
Table 3.4. Advancing, receding, and CAH values and volume capacity at 60°	79
Table 3.5. Static contact angles and CAH values for other rough PDMS surfaces	80
Table 4.1. Roughness values and static contact angle for flat and rough PDMS	92
Table 5.1. Roughness average for f_{NFlat} , f_{NRough} , $f_{NPetri Dish}$, and $u_{NPetri Dish}$	112
Table 5.2. Primer sequences to validate expression levels from PCR array.....	114
Table 5.3. Relative changes in ECM/adhesion molecule transcript expression	126

List of Equations

Equation 1.1. Roughness average (R_a).....	24
Equation 1.2. Root mean squared roughness (R_{rms}).....	24
Equation 1.3. Young's modulus (E)	40
Equation 2.1. Snell's law for critical angle (θ_c)	53
Equation 2.2. Young's Equation.....	55
Equation 3.1. Cassie-Baxter Equation	75
Equation 3.2. Surface free energy (γ_{total}).....	77
Equation 4.1. Force of cell adhesion (F_{adh}).....	89

9.0 References

1. Feynman, R. P., There's plenty of room at the bottom. In *Handbook of Nanoscience, Engineering, and Technology*, 2 ed.; Goddard, W. A.; Brenner, D. W.; Lyshevski, S. E.; Iafate, G. J., Eds. CRC Press 2007.
2. Drexler, E. K., *Engines of creation*. 1st ed. ed.; Anchor Press: Garden City, NY, 1986.
3. Love, J. C.; Estroff, L. A.; Kriebel, J. K.; Nuzzo, R. G.; Whitesides, G. M., Self-assembled monolayers of thiolates on metals as a form of nanotechnology. *Chem. Rev.* **2005**, *105*, 1103 - 1169.
4. Mrksich, M.; Whitesides, G. M., Patterning self-assembled monolayers using microcontact printing: a new technology for biosensors. *Trends Biotechnol.* **1995**, *13*, 228 - 235.
5. Alves, N. M.; Pashkuleva, I.; Reis, R. L.; Mano, J. F., Controlling cell behavior through the design of polymer surfaces. *Small* **2010**, *6*, 2208 - 2220.
6. Schwann, T. H., *Microscopical researches into the accordance in the structure and growth of animals and plants*. 1847.
7. Tyson, J., *The cell doctrine: its history and present state.*; Lindsay & Blakiston: Philadelphia, 1870.
8. Buchanan, R. E., History and development of the american type culture collection. *The Quarterly Review of Biology* **1966**, *41*, 101 - 104.
9. Smalley, K. S. M.; Lioni, M.; Herlyn, M., Life isn't flat: taking cancer biology to the next dimension. *In Vitro Cell. Dev. Biol.: Anim.* **2006**, *42*, 242 - 247.
10. Abbott, A., Cell culture: biology's new dimension. *Nature* **2003**, *424*, 870 - 872.
11. Elsdale, T.; Bard, J. B., Collagen substrata for studies on cell behavior. *J. Cell Biol.* **1972**, *54*, 626 - 637.
12. Netzer, L.; Sagiv, J., A new approach to construction of artificial monolayer assemblies. *J. Am. Chem. Soc.* **1983**, *105*, 674 - 676.
13. Petronis, S.; Gretzer, C.; Kasemo, B.; Gold, J., Model porous surfaces for systematic studies of material-cell interactions. *J. Biomed. Mater. Res., Part A* **2003**, *66A*, 707 - 721.
14. Vitte, J.; Benoliel, A. M.; Pierres, A.; Bongrand, P., Is there a predictable relationship between surface physical-chemical properties and cell behavior at the interface? *Eur. Cells Mater.* **2004**, *7*, 52 - 63.
15. Abbasi, F.; Mirzadeh, H.; Katbab, A.-A., Modification of polysiloxane polymers for biomedical applications: a review. *Polym. Int.* **2001**, *50*, 1279 - 1287.
16. von der Mark, K.; Park, J.; Bauer, S.; Schmuki, P., Nanoscale engineering of biomimetic surfaces: cues from the extracellular matrix. *Cell Tissue Res.* **2010**, *339*, 131 - 153.
17. Flemming, R. G.; Murphy, C. J.; Abrams, G. A.; Goodman, S. L.; Nealey, P. F., Effects of synthetic micro- and nano-structured surfaces on cell behavior. *Biomaterials* **1999**, *20*, 573 - 588.
18. Mrksich, M.; Dike, L. E.; Tien, J.; Ingber, D. E.; Whitesides, G. M., Using microcontact printing to pattern the attachment of mammalian cells to self-assembled monolayers of alkanethiolates on transparent films of gold and silver. *Exp. Cell Res.* **1997**, *235*, 305 - 313.
19. Pankov, R.; Yamada, K. M., Fibronectin at a glance. *J. Cell Sci.* **2002**, *115*, 3861 - 3863.
20. Hasegawa, M.; Yamato, M.; Kikuchi, A.; Okano, T.; Ishikawa, I., Human periodontal ligament cell sheets can regenerate periodontal ligament tissue in an athymic rat model. *Tissue Eng.* **2005**, *11*, 469 - 478.
21. Mrksich, M.; Chen, C. S.; Xia, Y.; Dike, L. E.; Ingber, D. E.; Whitesides, G. M., Controlling cell attachment on contoured surfaces with self-assembled monolayers of alkanethiolates on gold. *Proc. Natl. Acad. Sci. U. S. A.* **1996**, *93*, 10775 - 10778.
22. Daley, W. P.; Peters, S. B.; Larsen, M., Extracellular matrix dynamics in development and regenerative medicine. *J. Cell Sci.* **2008**, *121*, 255 - 264.
23. Schoenwaelder, S. M.; Burridge, K., Bidirectional signaling between the cytoskeleton and integrins. *Curr. Opin. Cell Biol.* **1999**, *11*, 274 - 286.

24. Humphries, J. D.; Byron, A.; Humphries, M. J., Integrin ligands at a glance. *J. Cell Sci.* **2006**, *119*, 3901 - 3903.
25. Giancotti, F. G.; Ruoslahti, E., Signal transduction: integrin signaling. *Science* **1999**, *285*, 1028 - 1032.
26. Clark, E. A.; Brugge, J. S., Integrins and signal transduction pathways: the road taken. *Science* **1995**, *268*, 233 - 239.
27. Beningo, K. A.; Dembo, M.; Kaverina, I.; Small, J. V.; Wang, Y.-L., Nascent focal adhesions are responsible for the generation of strong propulsive forces in migrating fibroblasts. *J. Cell Biol.* **2001**, *153*, 881 - 888.
28. Hynes, R. O., Integrins: bidirectional, allosteric signaling machines. *Cell (Cambridge, MA, U. S.)* **2002**, *110*, 673 - 687.
29. Bacakova, L.; Filova, E.; Parizek, M.; Ruml, T.; Svorcik, V., Modulation of cell adhesion, proliferation and differentiation on materials designed for body implants. *Biotechnol. Adv.* **2011**, *29*, 739 - 767.
30. Luethen, F.; Lange, R.; Becker, P.; Rychly, J.; Beck, U.; Nebe, J. G. B., The influence of surface roughness of titanium on β 1- and β 3-integrin adhesion and the organization of fibronectin in human osteoblastic cells. *Biomaterials* **2005**, *26*, 2423 - 2440.
31. Boyan, B. D.; Hummert, T. W.; Dean, D. D.; Schwartz, Z., Role of material surfaces in regulating bone and cartilage cell response. *Biomaterials* **1996**, *17*, 137 - 146.
32. Okano, T.; Yamada, N.; Okuhara, M.; Sakai, H.; Sakurai, Y., Mechanism of cell detachment from temperature-modulated, hydrophilic-hydrophobic polymer surfaces. *Biomaterials* **1995**, *16*, 297 - 303.
33. Wegerer, J., Cell surface interactions. In *Wiley Encyclopedia of Biomedical Engineering*, John Wiley & Sons, Inc.2006.
34. Whitesides, G. M.; Ostuni, E.; Takayama, S.; Jiang, X.; Ingber, D. E., Soft lithography in biology and biochemistry. *Annu. Rev. Biomed. Eng.* **2001**, *3*, 335 - 373.
35. Mitragotri, S.; Lahann, J., Physical approaches to biomaterial design. *Nat. Mater.* **2009**, *8*, 15 - 23.
36. Totonelli, G.; Maghsoudlou, P.; Garriboli, M.; Riegler, J.; Orlando, G.; Burns, A. J.; Sebire, N. J.; Smith, V. V.; Fishman, J. M.; Ghionzoli, M.; Turmaine, M.; Birchall, M. A.; Atala, A.; Soker, S.; Lythgoe, M. F.; Seifalian, A.; Pierro, A.; Eaton, S.; De, C. P., A rat decellularized small bowel scaffold that preserves villus-crypt architecture for intestinal regeneration. *Biomaterials* **2012**, *33*, 3401 - 3410.
37. Quere, D., Wetting and roughness. *Annu. Rev. Mater. Res.* **2008**, *38*, 71 - 99.
38. Lincks, J.; Boyan, B. D.; Blanchard, C. R.; Lohmann, C. H.; Liu, Y.; Cochran, D. L.; Dean, D. D.; Schwartz, Z., Response of MG63 osteoblast-like cells to titanium and titanium alloy is dependent on surface roughness and composition. *Biomaterials* **1998**, *19*, 2219 - 2232.
39. Bennett, J. M., Characterization of Surface Roughness. In *Light Scattering and Nanoscale Surface Roughness*, Maradudin, A. A., Ed. Springer2007; pp 1 - 33.
40. Gadelmawla, E. S.; Koura, M. M.; Maksoud, T. M. A.; Elewa, I. M.; Soliman, H. H., Roughness parameters. *J. Mater. Process. Technol.* **2002**, *123*, 133 - 145.
41. Feng, B.; Weng, J.; Yang, B. C.; Qu, S. X.; Zhang, X. D., Characterization of surface oxide films on titanium and adhesion of osteoblast. *Biomaterials* **2003**, *24*, 4663 - 4670.
42. Jayaraman, M.; Meyer, U.; Buhner, M.; Joos, U.; Wiesmann, H.-P., Influence of titanium surfaces on attachment of osteoblast-like cells in vitro. *Biomaterials* **2004**, *25*, 625 - 631.
43. Intranuovo, F.; Favia, P.; Sardella, E.; Ingrosso, C.; Nardulli, M.; d'Agostino, R.; Gristina, R., Osteoblast-like cell behavior on plasma deposited micro/nanopatterned coatings. *Biomacromolecules* **2011**, *12*, 380 - 387.
44. Stanton, M. M.; Ducker, R. E.; MacDonald, J. C.; Lambert, C. R.; McGimpsey, W. G., Superhydrophobic, highly adhesive, polydimethylsiloxane (PDMS) surfaces. *J. Colloid Interface Sci.* **2012**, *367*, 502 - 508.
45. Thapa, A.; Miller, D. C.; Webster, T. J.; Haberstroh, K. M., Nano-structured polymers enhance bladder smooth muscle cell function. *Biomaterials* **2003**, *24*, 2915 - 2926.

46. Curtis, A. S.; Varde, M., Control of cell behavior: Topological factors. *J Natl Cancer Inst* **1964**, *33*, 15 - 26.
47. Wilkinson, C. D. W.; Riehle, M.; Wood, M.; Gallagher, J.; Curtis, A. S. G., The use of materials patterned on a nano- and micro-metric scale in cellular engineering. *Mater. Sci. Eng., C* **2002**, *C19*, 263 - 269.
48. Zhou, X.; Shi, J.; Zhang, F.; Hu, J.; Li, X.; Wang, L.; Ma, X.; Chen, Y., Reversed cell imprinting, AFM imaging and adhesion analyses of cells on patterned surfaces. *Lab Chip* **2010**, *10*, 1182 - 1188.
49. Loesberg, W. A.; te Riet, J.; van Delft, F. C. M. J. M.; Schoen, P.; Figdor, C. G.; Speller, S.; van Loon, J. J. W. A.; Walboomers, X. F.; Jansen, J. A., The threshold at which substrate nanogroove dimensions may influence fibroblast alignment and adhesion. *Biomaterials* **2007**, *28*, 3944 - 3951.
50. Milner, K. R.; Siedlecki, C. A., Submicron poly(L-lactic acid) pillars affect fibroblast adhesion and proliferation. *J. Biomed. Mater. Res., Part A* **2007**, *82A*, 80 - 91.
51. Unadkat, H. V.; Hulsman, M.; Cornelissen, K.; Papenburg, B. J.; Truckenmueller, R. K.; Post, G. F.; Uetz, M.; Reinders, M. J. T.; Stamatialis, D.; van Blitterswijk, C. A.; de Boer, J., An algorithm-based topographical biomaterials library to instruct cell fate. *Proc. Natl. Acad. Sci. U. S. A.* **2011**, *108*, 16565 - 16570, S16565/1 - S16565/5.
52. Xia, Y.; Yang, P.; Sun, Y.; Wu, Y.; Mayers, B.; Gates, B.; Yin, Y.; Kim, F.; Yan, H., One-dimensional nanostructures: synthesis, characterization, and applications. *Advanced Materials* **2003**, *15*, 353 - 389.
53. Prime, K. L.; Whitesides, G. M., Self-assembled organic monolayers: model systems for studying adsorption of proteins at surfaces. *Science (Washington, D. C., 1883-)* **1991**, *252*, 1164-7.
54. Singhvi, R.; Kumar, A.; Lopez, G. P.; Stephanopoulos, G. N.; Wang, D. I. C.; Whitesides, G. M.; Ingber, D. E., Engineering cell shape and function. *Science* **1994**, *264*, 696 - 698.
55. Nakanishi, J.; Kikuchi, Y.; Takarada, T.; Nakayama, H.; Yamaguchi, K.; Maeda, M., Photoactivation of a substrate for cell adhesion under standard fluorescence microscopes. *J. Am. Chem. Soc.* **2004**, *126*, 16314 - 16315.
56. Chen, Z.; Chen, W.; Yuan, B.; Xiao, L.; Liu, D.; Jin, Y.; Quan, B.; Wang, J.-O.; Ibrahim, K.; Wang, Z.; Zhang, W.; Jiang, X., In vitro model on glass surfaces for complex interactions between different types of cells. *Langmuir* **2010**, *26*, 17790 - 17794.
57. They, M.; Pepin, A.; Dressaire, E.; Chen, Y.; Bornens, M., Cell distribution of stress fibres in response to the geometry of the adhesive environment. *Cell Motil. Cytoskeleton* **2006**, *63*, 341 - 355.
58. Welle, A.; Horn, S.; Schimmelpfeng, J.; Kalka, D., Photo-chemically patterned polymer surfaces for controlled PC-12 adhesion and neurite guidance. *J. Neurosci. Methods* **2005**, *142*, 243 - 250.
59. Ulman, A., Formation and structure of self-assembled monolayers. *Chem. Rev. (Washington, D. C.)* **1996**, *96*, 1533 - 1554.
60. Gooding, J. J.; Mearns, F.; Yang, W.; Liu, J., Self-assembled monolayers into the 21st century: Recent advances and applications. *Electroanalysis* **2003**, *15*, 81 - 96.
61. Laibinis, P. E.; Whitesides, G. M.; Allara, D. L.; Tao, Y. T.; Parikh, A. N.; Nuzzo, R. G., Comparison of the structures and wetting properties of self-assembled monolayers of n-alkanethiols on the coinage metal surfaces, copper, silver, and gold. *J. Am. Chem. Soc.* **1991**, *113*, 7152 - 7167.
62. Adamson, A. W.; Gast, A. P., *Physical chemistry of surfaces*. 6th ed. ed.; John Wiley & Sons, Inc1997.
63. Langmuir, I., The mechanism of the surface phenomena of flotation. *Trans. Faraday Soc.* **1920**, *15*, 62 - 74.
64. Blodgett, K. B., Films built by depositing successive unimolecular layers on a solid surface. *J. Am. Chem. Soc.* **1935**, *57*, 1007 -1022.
65. Bigelow, W. C.; Pickett, D. L.; Zisman, W. A., Oleophobic monolayers. I. Films adsorbed from solution in nonpolar liquids. *J. Colloid Sci.* **1946**, *1*, 513 - 538.
66. Netzer, L.; Iscovici, R.; Sagiv, J., Adsorbed monolayers versus Langmuir-Blodgett monolayers - why and how? II. Characterization of built-up films constructed by stepwise adsorption of individual monolayers. *Thin Solid Films* **1983**, *100*, 67 - 76.

67. Netzer, L.; Iscovici, R.; Sagiv, J., Adsorbed monolayers versus Langmuir-Blodgett monolayers - why and how? I. From monolayer to multilayer, by adsorption. *Thin Solid Films* **1983**, *99*, 235 - 241.
68. Nuzzo, R. G.; Allara, D. L., Adsorption of bifunctional organic disulfides on gold surfaces. *J. Am. Chem. Soc.* **1983**, *105*, 4481 - 4483.
69. Senaratne, W.; Andruzzi, L.; Ober, C. K., Self-assembled monolayers and polymer brushes in biotechnology: current applications and future perspectives. *Biomacromolecules* **2005**, *6*, 2427 - 2448.
70. Vericat, C.; Vela, M. E.; Benitez, G.; Carro, P.; Salvarezza, R. C., Self-assembled monolayers of thiols and dithiols on gold: new challenges for a well-known system. *Chem. Soc. Rev.* **2010**, *39*, 1805 - 1834.
71. Sullivan, T. P.; Huck, W. T. S., Reactions on monolayers: organic synthesis in two dimensions. *Eur. J. Org. Chem.* **2003**, 17 - 29.
72. Tripp, C. P.; Hair, M. L., An infrared study of the reaction of octadecyltrichlorosilane with silica. *Langmuir* **1992**, *8*, 1120 - 1126.
73. Bierbaum, K.; Kinzler, M.; Woell, C.; Grunze, M.; Haehner, G.; Heid, S.; Effenberger, F., A near edge X-ray absorption fine structure spectroscopy and X-ray photoelectron spectroscopy study of the film properties of self-assembled monolayers of organosilanes on oxidized Si(100). *Langmuir* **1995**, *11*, 512 - 518.
74. Wasserman, S. R.; Tao, Y. T.; Whitesides, G. M., Structure and reactivity of alkylsiloxane monolayers formed by reaction of alkyltrichlorosilanes on silicon substrates. *Langmuir* **1989**, *5*, 1074 - 1087.
75. Brandriss, S.; Margel, S., Synthesis and characterization of self-assembled hydrophobic monolayer coatings on silica colloids. *Langmuir* **1993**, *9*, 1232 - 1240.
76. Dulcey, C. S.; Georger, J. H., Jr.; Krauthamer, V.; Stenger, D. A.; Fare, T. L.; Calvert, J. M., Deep UV photochemistry of chemisorbed monolayers: patterned coplanar molecular assemblies. *Science* **1991**, *252*, 551 - 554.
77. Nakanishi, J.; Kikuchi, Y.; Takarada, T.; Nakayama, H.; Yamaguchi, K.; Maeda, M., Spatiotemporal control of cell adhesion on a self-assembled monolayer having a photocleavable protecting group. *Anal. Chim. Acta* **2006**, *578*, 100 - 104.
78. Van Alsten, J. G., Self-assembled monolayers on engineering metals: structure, derivatization, and utility. *Langmuir* **1999**, *15*, 7605 - 7614.
79. Gao, W.; Dickinson, L.; Grozinger, C.; Morin, F. G.; Reven, L., Self-assembled monolayers of alkylphosphonic acids on metal oxides. *Langmuir* **1996**, *12*, 6429 - 6435.
80. Queffelec, C.; Petit, M.; Janvier, P.; Knight, D. A.; Bujoli, B., Surface modification using phosphonic acids and esters. *Chem. Rev.* **2012**, *112*, 3777 - 3807.
81. Guerrero, G.; Mutin, P. H.; Vioux, A., Anchoring of phosphonate and phosphinate coupling molecules on titania particles. *Chem. Mat.* **2001**, *13*, 4367 - 4373.
82. Gouzman, I.; Dubey, M.; Carolus, M. D.; Schwartz, J.; Bernasek, S. L., Monolayer vs. multilayer self-assembled alkylphosphonate films: X-ray photoelectron spectroscopy studies. *Surf. Sci.* **2006**, *600*, 773 - 781.
83. Gawalt, E. S.; Avaltroni, M. J.; Danahy, M. P.; Silverman, B. M.; Hanson, E. L.; Midwood, K. S.; Schwarzbauer, J. E.; Schwartz, J., Bonding organics to Ti alloys: facilitating human osteoblast attachment and spreading on surgical implant materials. *Langmuir* **2002**, *19*, 200 - 204.
84. Pulsipher, A.; Yousaf, M. N., Tandem surface microfluidic lithography and activation to generate patch pattern biospecific ligand and cell arrays. *Langmuir* **2010**, *26*, 4130 - 4135.
85. Chrisey, L. A.; Lee, G. U.; O'Ferrall, C. E., Covalent attachment of synthetic DNA to self-assembled monolayer films. *Nucleic Acids Res.* **1996**, *24*, 3031 - 3039.
86. Driscoll, P. F.; Milkani, E.; Lambert, C. R.; McGimpsey, W. G., A multilayered approach to complex surface patterning. *Langmuir* **2010**, *26*, 3731 - 3738.
87. Patel, N.; Davies, M. C.; Hartshorne, M.; Heaton, R. J.; Roberts, C. J.; Tendler, S. J. B.; Williams, P. M., Immobilization of protein molecules onto homogeneous and mixed carboxylate-terminated self-assembled monolayers. *Langmuir* **1997**, *13*, 6485 - 6490.

88. Yang, Z.; Belu, A. M.; Liebmann-Vinson, A.; Sugg, H.; Chilkoti, A., Molecular imaging of a micropatterned biological ligand on an activated polymer surface. *Langmuir* **2000**, *16*, 7482 - 7492.
89. Hudalla, G. A.; Murphy, W. L., Using “click” chemistry to prepare SAM substrates to study stem cell adhesion. *Langmuir* **2009**, *25*, 5737 - 5746.
90. Horton, R. C., Jr.; Herne, T. M.; Myles, D. C., Aldehyde-terminated self-assembled monolayers on gold: immobilization of amines onto gold surfaces. *J. Am. Chem. Soc.* **1997**, *119*, 12980 - 12981.
91. Hermanson, G. T., *Bioconjugate techniques.*; Academic Press: USA, 1996.
92. Falconnet, D.; Koenig, A.; Assi, F.; Textor, M., A combined photolithographic and molecular-assembly approach to produce functional micropatterns for applications in the biosciences. *Adv. Funct. Mater.* **2004**, *14*, 749 - 756.
93. Keselowsky, B. G.; Collard, D. M.; Garcia, A. J., Surface chemistry modulates fibronectin conformation and directs integrin binding and specificity to control cell adhesion. *J. Biomed. Mater. Res., Part A* **2003**, *66A*, 247 - 259.
94. Malmsten, M., Formation of adsorbed protein layers. *J. Colloid Interface Sci.* **1998**, *207*, 186 - 199.
95. Rabe, M.; Verdes, D.; Seeger, S., Understanding protein adsorption phenomena at solid surfaces. *Adv. Colloid Interface Sci.* **2011**, *162*, 87 - 106.
96. Daly, S. M.; Przybycien, T. M.; Tilton, R. D., Coverage-dependent orientation of lysozyme adsorbed on silica. *Langmuir* **2003**, *19*, 3848 - 3857.
97. Stanton, M. M.; Rankenberg, J. M.; Park, B.-W.; McGimpsey, W. G.; Malcuit, C.; Lambert, C. R., Cell behavior on surface modified polydimethylsiloxane (PDMS). *Macromol. Biosci.* **2014**, Ahead of Print.
98. Kumar, A.; Whitesides, G. M., Features of gold having micrometer to centimeter dimensions can be formed through a combination of stamping with an elastomeric stamp and an alkanethiol “ink” followed by chemical etching. *Appl. Phys. Lett.* **1993**, *63*, 2002 - 2004.
99. Xia, Y.; Whitesides, G. M., Soft lithography. *Angew. Chem., Int. Ed.* **1998**, *37*, 550 - 575.
100. Liu, K.; Yao, X.; Jiang, L., Recent developments in bio-inspired special wettability. *Chem. Soc. Rev.* **2010**, *39*, 3240 - 3255.
101. Ma, M.; Hill, R. M., Superhydrophobic surfaces. *Curr. Opin. Colloid Interface Sci.* **2006**, *11*, 193 - 202.
102. Ishizaki, T.; Saito, N.; Takai, O., Correlation of cell adhesive behaviors on superhydrophobic, superhydrophilic, and micropatterned superhydrophobic/superhydrophilic surfaces to their surface chemistry. *Langmuir* **2010**, *26*, 8147 - 8154.
103. Arima, Y.; Iwata, H., Effect of wettability and surface functional groups on protein adsorption and cell adhesion using well-defined mixed self-assembled monolayers. *Biomaterials* **2007**, *28*, 3074 - 3082.
104. Lee, J. H.; Khang, G.; Lee, J. W.; Lee, H. B., Interaction of different types of cells on polymer surfaces with wettability gradient. *J. Colloid Interface Sci.* **1998**, *205*, 323 - 330.
105. Lampin, M.; Warocquier-Clerout, R.; Legris, C.; Degrange, M.; Sigot-Luizard, M. F., Correlation between substratum roughness and wettability, cell adhesion, and cell migration. *J. Biomed. Mater. Res.* **1997**, *36*, 99 - 108.
106. DiMilla, P. A.; Folkers, J. P.; Biebuyck, H. A.; Haerter, R.; Lopez, G. P.; Whitesides, G. M., Wetting and protein adsorption on self-assembled monolayers of alkanethiolates supported on transparent films of gold. *J. Am. Chem. Soc.* **1994**, *116*, 2225 - 2226.
107. Tan, J. L.; Liu, W.; Nelson, C. M.; Raghavan, S.; Chen, C. S., Simple approach to micropattern cells on common culture substrates by tuning substrate wettability. *Tissue Eng.* **2004**, *10*, 865 - 872.
108. Chattopadhyay, R., *Surface wear: analysis, treatment, and prevention.*; ASM International: Materials Park, OH, 2001; p 318.
109. Good, R. J., Contact angles and the surface free energy of solids. In *Surface and colloid science.*, Good, R. J.; Stromberg, R. R., Eds. Springer US: New York, 1979; pp 1 - 29.
110. Fung, Y. C., *Biomechanics: mechanical properties of living tissue.*; Springer Science+Business Media New York: New York, 1981.
111. Roach, P.; Eglin, D.; Rohde, K.; Perry, C. C., Modern biomaterials: a review-bulk properties and implications of surface modifications. *J. Mater. Sci.: Mater. Med.* **2007**, *18*, 1263 - 1277.

112. Aritan, S., Bulk modulus. In *Wiley Encyclopedia of Biomedical Engineering*, Akay, M., Ed. 2006.
113. Pelham, R. J., Jr.; Wang, Y.-L., Cell locomotion and focal adhesions are regulated by substrate flexibility. *Proc. Natl. Acad. Sci. U. S. A.* **1997**, *94*, 13661 - 13665.
114. Kong, H. J.; Polte, T. R.; Alsberg, E.; Mooney, D. J., FRET measurements of cell-traction forces and nano-scale clustering of adhesion ligands varied by substrate stiffness. *Proc. Natl. Acad. Sci. U. S. A.* **2005**, *102*, 4300 - 4305.
115. Engler, A. J.; Griffin, M. A.; Sen, S.; Boenemann, C. G.; Sweeney, H. L.; Discher, D. E., Myotubes differentiate optimally on substrates with tissue-like stiffness: Pathological implications for soft or stiff microenvironments. *J. Cell Biol.* **2004**, *166*, 877 - 887.
116. Wong, J. Y.; Velasco, A.; Rajagopalan, P.; Pham, Q., Directed movement of vascular smooth muscle cells on gradient-compliant hydrogels. *Langmuir* **2003**, *19*, 1908 - 1913.
117. du Roure, O.; Saez, A.; Buguin, A.; Austin, R. H.; Chavrier, P.; Siberzan, P.; Ladoux, B., Force mapping in epithelial cell migration. *Proc. Natl. Acad. Sci. U. S. A.* **2005**, *102*, 2390 - 2395.
118. Evans, N. D.; Gentleman, E., The role of material structure and mechanical properties in cell-matrix interactions. *J. Mater. Chem. B* **2014**, *2*, 2345 - 2356.
119. Tilley, R. J. D., Understanding solids: The science of materials., 2nd ed. John Wiley & Sons, Ltd.: United Kingdom, 2013.
120. Lee, J. H.; Yu, H.-S.; Lee, G.-S.; Ji, A.; Hyun, J. K.; Kim, H.-W., Collagen gel three-dimensional matrices combined with adhesive proteins stimulate neuronal differentiation of mesenchymal stem cells. *J. R. Soc. Interface* **2011**, *8*, 998 - 1010.
121. Lee, J. N.; Jiang, X.; Ryan, D.; Whitesides, G. M., Compatibility of mammalian cells on surfaces of poly(dimethylsiloxane). *Langmuir* **2004**, *20*, 11684 - 11691.
122. Belanger, M.-C.; Marois, Y., Hemocompatibility, biocompatibility, inflammatory and in vivo studies of primary reference materials low-density polyethylene and polydimethylsiloxane: a review. *J. Biomed. Mater. Res.* **2001**, *58*, 467 - 477.
123. Lahiri, J.; Ostuni, E.; Whitesides, G. M., Patterning ligands on reactive SAMs by microcontact printing. *Langmuir* **1999**, *15*, 2055 - 2060.
124. Toepke, M. W.; Beebe, D. J., PDMS absorption of small molecules and consequences in microfluidic applications. *Lab Chip* **2006**, *6*, 1484 - 1486.
125. Mukhopadhyay, R., When PDMS isn't the best. *Anal. Chem.* **2007**, *79*, 3248 - 3253.
126. Lee, J. N.; Park, C.; Whitesides, G. M., Solvent compatibility of poly(dimethylsiloxane)-based microfluidic devices. *Anal. Chem.* **2003**, *75*, 6544 - 6554.
127. Silver, J. H.; Lin, J.-C.; Lim, F.; Tegoulia, V. A.; Chaudhury, M. K.; Cooper, S. L., Surface properties and hemocompatibility of alkyl-siloxane monolayers supported on silicone rubber: effect of alkyl chain length and ionic functionality. *Biomaterials* **1999**, *20*, 1533 - 1543.
128. Freshney, I. R., Culture vessels and substrates. In *Culture of Animal Cells : A Manual of Basic Technique and Specialized Applications*, 6 ed.; Wiley-Blackwell 2010; p 89.
129. Cras, J. J.; Rowe-Taitt, C. A.; Nivens, D. A.; Ligler, F. S., Comparison of chemical cleaning methods of glass in preparation for silanization. *Biosens. Bioelectron.* **1999**, *14*, 683 - 688.
130. Siow, K. S.; Britcher, L.; Kumar, S.; Griesser, H. J., Plasma methods for the generation of chemically reactive surfaces for biomolecule immobilization and cell colonization - a review. *Plasma Processes Polym.* **2006**, *3*, 392 - 418.
131. Chu, P. K.; Chen, J. Y.; Wang, L. P.; Huang, N., Plasma-surface modification of biomaterials. *Mater. Sci. Eng., R* **2002**, *R36*, 143 - 206.
132. Chan, C. M.; Ko, T. M.; Hiraoka, H., Polymer surface modification by plasmas and photons. *Surf. Sci. Rep.* **1996**, *24*, 1 - 54.
133. Owen, M. J.; Smith, P. J., Plasma treatment of polydimethylsiloxane. *J. Adhesion Sci. Technol.* **1994**, *8*, 1063 - 1075.
134. France, R. M.; Short, R. D., Effects of energy transfer from an argon plasma on the surface chemistry of poly(styrene), low density poly(ethylene), poly(propylene) and poly(ethylene terephthalate). *J. Chem. Soc., Faraday Trans.* **1997**, *93*, 3173 - 3178.

135. Kim, E. J.; Boehm, C. A.; Mata, A.; Fleischman, A. J.; Muschler, G. F.; Roy, S., Post microtextures accelerate cell proliferation and osteogenesis. *Acta Biomater.* **2010**, *6*, 160 - 169.
136. Stuart, B. H., *Infrared spectroscopy: fundamentals and applications.*; Wiley: Hoboken, NJ, 2004.
137. Pelletier, M. J.; Pelletier, C. C., Spectroscopic theory for chemical imaging. In *Raman, infrared, and near-infrared chemical imaging.*, Sasic, S.; Ozaki, Y., Eds. Wiley: Hoboken, NH, 2010.
138. Sheppard, N.; Erkelens, J., Vibrational spectra of species adsorbed on surfaces: forms of vibrations and selection rules for regular arrays of adsorbed species. *Appl. Spectrosc.* **1984**, *38*, 471 - 485.
139. Lee, B. S.; Chi, Y. S.; Lee, J. K.; Choi, I. S.; Song, C. E.; Namgoong, S. K.; Lee, S.-G., Imidazolium ion-terminated self-assembled monolayers on Au: effects of counter anions on surface wettability. *J. Am. Chem. Soc.* **2004**, *126*, 480 - 481.
140. Bain, C. D.; Whitesides, G. M., Correlations between wettability and structure in monolayers of alkanethiols adsorbed on gold. *J. Am. Chem. Soc.* **1988**, *110*, 3665-3666.
141. Crick, C. R.; Parkin, I. P., Preparation and characterisation of super-hydrophobic surfaces. *Chem. - Eur. J.* **2010**, *16*, 3568 - 3588.
142. De Gennes, P. G., Wetting: statics and dynamics. *Rev. Mod. Phys.* **1985**, *57*, 827 - 863.
143. Bonn, D.; Ross, D., Wetting transitions. *Rep. Prog. Phys.* **2001**, *64*, 1085 - 1163.
144. Yuan, Y.; Lee, T. R., Contact angle and wetting properties. In *Surface science techniques*, Bracco, G.; Holst, B., Eds. Springer: London, 2013; pp 3-34.
145. McHale, G.; Shirtcliffe, N. J.; Newton, M. I., Contact-angle hysteresis on super-hydrophobic surfaces. *Langmuir* **2004**, *20*, 10146 - 10149.
146. Extrand, C. W.; Kumagai, Y., Liquid drops on an inclined plane: the relation between contact angles, drop shape, and retentive force. *J. Colloid Interface Sci.* **1995**, *170*, 515 - 521.
147. Schmidt, D. L.; Brady, R. F., Jr.; Lam, K.; Schmidt, D. C.; Chaudhury, M. K., Contact angle hysteresis, adhesion, and marine biofouling. *Langmuir* **2004**, *20*, 2830 - 2836.
148. Wenzel, R. N., Resistance of solid surfaces to wetting by water. *J. Ind. Eng. Chem.* **1936**, *28*, 988 - 994.
149. Cassie, A. B. D.; Baxter, S., Wettability of porous surfaces. *Trans. Faraday Soc.* **1944**, *40*, 546 - 551.
150. Binnig, G.; Quate, C. F.; Gerber, C., Atomic force microscope. *Physical Review Letters* **1986**, *56*, 930 - 933.
151. Howland, R.; Benatar, L., A practical guide to scanning probe microscopy.; Symanski, C., Ed. ThermoMicroscopes2000.
152. Kuznetsova, T. G.; Starodubtseva, M. N.; Yegorenkov, N. I.; Chizhik, S. A.; Zhdanov, R. I., Atomic force microscopy probing of cell elasticity. *Micron* **2007**, *38*, 824 - 833.
153. Carpick, R. W.; Salmeron, M., Scratching the surface: fundamental investigations of tribology with atomic force microscopy. *Chem. Rev. (Washington, D. C.)* **1997**, *97*, 1163 - 1194.
154. Leite, F. L.; Herrmann, P. S. P., Application of atomic force spectroscopy (AFS) to studies of adhesion phenomena: a review. In *Atomic force microscopy in adhesion studies.*, Drelich, J.; Mittal, K. L., Eds. VSP2005; pp 3 - 43.
155. Kufer, S. K.; Puchner, E. M.; Gump, H.; Liedl, T.; Gaub, H. E., Single-molecule cut-and-paste surface assembly. *Science* **2008**, *319*, 594 - 596.
156. Butt, H.-J.; Cappella, B.; Kappl, M., Force measurements with the atomic force microscope: Technique, interpretation and applications. *Surf. Sci. Rep.* **2005**, *59*, 1-152.
157. Lakowicz, J. R., *Principles of fluorescence spectroscopy.* 2 ed.; Kluwer Academic/Plenum Publishers: New York, 1999.
158. Waters, J. C., Live-cell fluorescence imaging. In *Digital Microscopy*, 3rd ed.; Sluder, G.; Wolf, D. E., Eds. Academic Press: San Diego, 2007; Vol. 81, pp 63 -91.
159. Driscoll, P. F.; Milkani, E.; Lambert, C. r. R.; McGimpsey, W. G., A multilayered approach to complex surface patterning. *Langmuir* **2010**, *26*, 3731 - 3738.
160. Crick, C. R.; Parkin, I. P., Preparation and characterisation of super-hydrophobic surfaces. *Chem. Eur. J.* **2010**, *16*, 3568-3588.

161. Sun, M.; Luo, C.; Xu, L.; Ji, H.; Ouyang, Q.; Yu, D.; Chen, Y., Artificial lotus leaf by nanocasting. *Langmuir* **2005**, *21*, 8978 - 8981.
162. Roach, P.; Shirtcliffe, N. J.; Newton, M. I., Progress in superhydrophobic surface development. *Soft Matter* **2008**, *4*, 224 - 240.
163. Hong, X.; Gao, X.; Jiang, L., Application of superhydrophobic surface with high adhesive force in no lost transport of superparamagnetic microdroplet. *J. Am. Chem. Soc.* **2007**, *129*, 1478 - 1479.
164. Park, S.; Moon, J.; Lee, S. A.; Shim, J.; Yang, S., Bioinspired holographically featured superhydrophobic and supersticky nanostructured materials. *Langmuir* **2009**, *26*, 1468-1472.
165. Jin, M.; Feng, X.; Feng, L.; Sun, T.; Zhai, J.; Li, T.; Jiang, L., Superhydrophobic aligned polystyrene nanotube films with high adhesive force. *Adv. Mater.* **2005**, *17*, 1977 - 1981.
166. Zhao, W.; Wang, L.; Xue, Q., Fabrication of low and high adhesion hydrophobic Au surfaces with micro/nano-biomimetic structures. *J. Phys. Chem. C* **2010**, *114*, 11509 - 11514.
167. Feng, L.; Zhang, Y.; Xi, J.; Zhu, Y.; Wang, N.; Xia, F.; Jiang, L., Petal effect: a superhydrophobic state with high adhesive force. *Langmuir* **2008**, *24*, 4114 - 4119.
168. Cho, W. K.; Choi, I. S., Fabrication of hairy polymeric films inspired by geckos: wetting and high adhesion properties. *Adv. Funct. Mater.* **2008**, *18*, 1089 - 1096.
169. Cho, S. K.; Moon, H.; Kim, C. J., Creating, transporting, cutting, and merging liquid droplets by electrowetting-based actuation for digital microfluidic circuits. *J. Microelectromech. Syst.* **2003**, *12*, 70-80.
170. Fouillet, Y.; Jary, D.; Chabrol, C.; Claustre, P.; Peponnet, C., Digital microfluidic design and optimization of classic and new fluidic functions for lab on a chip systems. *Microfluid Nanofluid* **2008**, *4*, 159 - 165.
171. Wang, M.; Chen, C. S.; Ma, J.; Xu, J., Preparation of superhydrophobic cauliflower-like silica nanospheres with tunable water adhesion. *J. Mater. Chem.* **2011**, *21*, 6962 - 6967.
172. Bormashenko, E.; Stein, T.; Pogreb, R.; Aurbach, D., "Petal Effect" on surfaces based on lycopodium: high-stick surfaces demonstrating high apparent contact angles. *J. Phys. Chem. C* **2009**, *113*, 5568 - 5572.
173. Sitti, M.; Fearing, R. S., Synthetic gecko foot-hair micro/nano-structures as dry adhesives. *J. Adhes. Sci. Tech.* **2003**, *17*, 1055 - 1073.
174. Dawood, M. K.; Zheng, H.; Liew, T. H.; Leong, K. C.; Foo, Y. L.; Rajagopalan, R.; Khan, S. A.; Choi, W. K., Mimicking both petal and lotus effects on a single silicon substrate by tuning the wettability of nanostructured surfaces. *Langmuir* **2011**, *27*, 4126 - 4133.
175. Quere, D.; Reyssat, M., Non-adhesive lotus and other hydrophobic materials. *Philos. Trans. R. Soc., A* **2008**, *366*, 1539 - 1556.
176. Chibowski, E.; Holysz, L.; Terpilowski, K.; Jurak, M., Investigation of super-hydrophobic effect of PMMA layers with different fillers deposited on glass support. *Colloids Surf., A* **2006**, *291*, 181-190.
177. Chibowski, E.; Terpilowski, K., Comparison of apparent surface free energy of some solids determined by different approaches. *Contact Angle, Wettability Adhes.* **2009**, *6*, 283-299.
178. *CRC handbook of chemistry and physics*. 60 ed.; CRC Press: Boca Raton, 1981.
179. Magill, P. L., Formamide. *Ind. Eng. Chem.* **1934**, *26*, 611 - 614.
180. Clever, H. L.; Snead, C. C., Thermodynamics of liquid surfaces: the surface tension of dimethyl sulfoxide and some dimethyl sulfoxide-acetone mixtures. *J. Phys. Chem.* **1963**, *67*, 918 - 920.
181. Lee, S. A.; Oh, S. H.; Lee, W., The effect of direct fluorination of polydimethylsiloxane films on their surface properties. *J. Colloid Interface Sci.* **2009**, *332*, 461 - 466.
182. Rao, A. P.; Rao, A. V., Modifying the surface energy and hydrophobicity of the low-density silica aerogels through the use of combinations of surface-modification agents. *J. Mater. Sci.* **2010**, *45*, 51 - 63.
183. Bodas, D.; Khan-Malek, C., Hydrophilization and hydrophobic recovery of PDMS by oxygen plasma and chemical treatment-An SEM investigation. *Sens. Actuators, B* **2007**, *123*, 368 - 373.
184. Bhushan, B.; Jung, Y. C.; Koch, K., Self-cleaning efficiency of artificial superhydrophobic surfaces. *Langmuir* **2009**, *25*, 3240 - 3248.
185. Chang, F.-M.; Hong, S.-J.; Sheng, Y.-J.; Tsao, H.-K., High contact angle hysteresis of superhydrophobic surfaces: hydrophobic defects. *Appl. Phys. Lett.* **2009**, *95*, 064102/1 - 064102/3.

186. Xie, Y.-Y.; Zhou, Y.-L.; Yu, X.-C.; Xia, H.-P., Replication of superhydrophobic surfaces of polymer from abrasive papers. *Gaodeng Xuexiao Huaxue Xuebao* **2007**, *28*, 1577 - 1580.
187. Curtis, A. S.; Wilkinson, C., Topographical control of cells. *Biomaterials* **1998**, *18*, 1573 - 1583.
188. Stevens, M. M.; George, J. H., Exploring and engineering the cell surface interface. *Science (Washington, DC, U. S.)* **2005**, *310*, 1135 - 1138.
189. Ross, A. M.; Jiang, Z.; Bastmeyer, M.; Lahann, J., Physical aspects of cell culture substrates: topography, roughness, and elasticity. *Small* **2012**, *8*, 336 - 355.
190. Weaver, V. M.; Petersen, O. W.; Wang, F.; Larabell, C. A.; Briand, P.; Damsky, C.; Bissell, M. J., Reversion of the malignant phenotype of human breast cells in three-dimensional culture and in vivo by integrin blocking antibodies. *J. Cell Biol.* **1997**, *137*, 231 - 245.
191. Harunaga, J. S.; Yamada, K. M., Cell-matrix adhesions in 3D. *Matrix Biol.* **2011**, *30*, 363 - 368.
192. Girard, P. P.; Cavalcanti-Adam, E. A.; Kemkemer, R.; Spatz, J. P., Cellular chemomechanics at interfaces: sensing, integration and response. *Soft Matter* **2007**, *3*, 307 - 326.
193. Legant, W. R.; Chen, C. S.; Vogel, V., Force-induced fibronectin assembly and matrix remodeling in a 3D microtissue model of tissue morphogenesis. *Integr. Biol.* **2012**, *4*, 1164 - 1174.
194. Wang, F.; Weaver, V. M.; Petersen, O. W.; Larabell, C. A.; Dedhar, S.; Briand, P.; Lupu, R.; Bissell, M. J., Reciprocal interactions between β 1-integrin and epidermal growth factor receptor in three-dimensional basement membrane breast cultures: a different perspective in epithelial biology. *Proc. Natl. Acad. Sci. U. S. A.* **1998**, *95*, 14821 - 14826.
195. Abbott, A., Cell culture: Biology's new dimension. *Nature (London, U. K.)* **2003**, *424*, 870 - 872.
196. Alves, N. M.; Pashkuleva, I.; Reis, R. L.; Mano, J. F., Controlling cell behavior through the design of polymer surfaces. *Small* **2010**, *6*, 2208 - 2220.
197. Small, J. V.; Rottner, K.; Kaverina, I.; Anderson, K. I., Assembling an actin cytoskeleton for cell attachment and movement. *Biochim. Biophys. Acta, Mol. Cell Res.* **1998**, *1404*, 271 - 281.
198. Rottner, K.; Hall, A.; Small, J. V., Interplay between Rac and Rho in the control of substrate contact dynamics. *Curr. Biol.* **1999**, *9*, 640 - 648.
199. Chatterjee, K.; Lin-Gibson, S.; Wallace, W. E.; Parekh, S. H.; Lee, Y.; Cicerone, M. T.; Young, M. F.; Simon, C. G., The effect of 3D hydrogel scaffold modulus on osteoblast differentiation and mineralization revealed by combinatorial screening. *Biomaterials* **2010**, *31*, 5051 - 5062.
200. Indolfi, L.; Baker, A. B.; Edelman, E. R., The role of scaffold microarchitecture in engineering endothelial cell immunomodulation. *Biomaterials* **2012**, *33*, 7019 - 7027.
201. Xu, C.; Yang, F.; Wang, S.; Ramakrishna, S., In vitro study of human vascular endothelial cell function on materials with various surface roughness. *J. Biomed. Mater. Res., Part A* **2004**, *71A*, 154 - 161.
202. Milner, K. R.; Siedlecki, C. A., Submicron poly(L-lactic acid) pillars affect fibroblast adhesion and proliferation. *J. Biomed. Mater. Res., Part A* **2007**, *82A*, 80 - 91.
203. Tibbitt, M. W.; Anseth, K. S., Hydrogels as extracellular matrix mimics for 3D cell culture. *Biotechnol. Bioeng.* **2009**, *103*, 655 - 663.
204. Schmeichel, K. L.; Bissell, M. J., Modeling tissue-specific signaling and organ function in three dimensions. *J. Cell Sci.* **2003**, *116*, 2377 - 2388.
205. Smalley, K. S. M.; Lioni, M.; Herlyn, M., Life isn't flat: taking cancer biology to the next dimension. *In Vitro Cell. Dev. Biol.: Anim.* **2006**, *42*, 242 - 247.
206. Chou, L.; Firth, J. D.; Uitto, V.-J.; Brunette, D. M., Effects of titanium substratum and grooved surface topography on metalloproteinase-2 expression in human fibroblasts. *J. Biomed. Mater. Res.* **1998**, *39*, 437 - 445.
207. Totonelli, G.; Maghsoudlou, P.; Garriboli, M.; Riegler, J.; Orlando, G.; Burns, A. J.; Sebire, N. J.; Smith, V. V.; Fishman, J. M.; Ghionzoli, M.; Turmaine, M.; Birchall, M. A.; Atala, A.; Soker, S.; Lythgoe, M. F.; Seifalian, A.; Pierro, A.; Eaton, S.; De, C. P., A rat decellularized small bowel scaffold that preserves villus-crypt architecture for intestinal regeneration. *Biomaterials* **2012**, *33*, 3401 - 3410.
208. Tay, C.; Irvine, S. A.; Boey, F. Y. C.; Tan, L.; Venkatraman, S., Micro-/nano-engineered cellular responses for soft tissue engineering and biomedical applications. *Small* **2011**, *7*, 1361 - 1378.

209. Fischbach, C.; Chen, R.; Matsumoto, T.; Schmelzle, T.; Brugge, J. S.; Polverini, P. J.; Mooney, D. J., Engineering tumors with 3D scaffolds. *Nat. Methods* **2007**, *4*, 855 - 860.
210. Liu, E.; Treiser, M. D.; Johnson, P. A.; Patel, P.; Rege, A.; Kohn, J.; Moghe, P. V., Quantitative biorelevant profiling of material microstructure within 3D porous scaffolds via multiphoton fluorescence microscopy. *J. Biomed. Mater. Res., Part B* **2007**, *82B*, 284 - 297.
211. Cheng, K.; Lai, Y.; Kisaalita, W. S., Three-dimensional polymer scaffolds for high throughput cell-based assay systems. *Biomaterials* **2008**, *29*, 2802 - 2812.
212. Lutolf, M. P.; Hubbell, J. A., Synthetic biomaterials as instructive extracellular microenvironments for morphogenesis in tissue engineering. *Nat. Biotechnol.* **2005**, *23*, 47 - 55.
213. Stanton, M. M.; Ducker, R. E.; MacDonald, J. C.; Lambert, C. R.; McGimpsey, W. G., Superhydrophobic, highly adhesive, polydimethylsiloxane (PDMS) surfaces. *J. Colloid Interface Sci.* **2012**, *367*, 502 - 508.
214. Li, F.; Redick, S. D.; Erickson, H. P.; Moy, V. T., Force measurements of the alpha5beta1 integrin-fibronectin interaction. *Biophys. J.* **2003**, *84*, 1252 - 1262.
215. Helenius, J.; Heisenberg, C.-P.; Gaub, H. E.; Muller, D. J., Single-cell force spectroscopy. *J. Cell Sci.* **2008**, *121*, 1785 - 1791.
216. Maaloum, M.; Levy, R., Manipulation of single macromolecules and properties of interfacial systems using atomic force microscopy. *Recent Res. Dev. Macromol.* **2002**, *6*, 323 - 338.
217. Tooley, W. W.; Fegghi, S.; Han, S. J.; Wang, J.; Sniadecki, N. J., Thermal fracture of oxidized polydimethylsiloxane during soft lithography of nanopost arrays. *J. Micromech. Microeng.* **2011**, *21*, 054013/1 - 054013/9.
218. Berry, C. C.; Campbell, G.; Spadicino, A.; Robertson, M.; Curtis, A. S. G., The influence of microscale topography on fibroblast attachment and motility. *Biomaterials* **2004**, *25*, 5781 - 5788.
219. Novotny, G. E.; Gnoth, C., Variability of fibroblast morphology in vivo: a silver impregnation study on human digital dermis and subcutis. *J Anat* **1991**, *177*, 195 - 207.
220. Cukierman, E.; Pankov, R.; Stevens, D. R.; Yamada, K. M., Taking cell-matrix adhesions to the third dimension. *Science (Washington, DC, U. S.)* **2001**, *294*, 1708 - 1712.
221. Bard, J. B.; Hay, E. D., The behavior of fibroblasts from the developing avian cornea. Morphology and movement in situ and in vitro. *J Cell Biol* **1975**, *67*, 400 - 418.
222. Wieland, M.; Chehroudi, B.; Textor, M.; Brunette, D. M., Use of Ti-coated replicas to investigate the effects on fibroblast shape of surfaces with varying roughness and constant chemical composition. *J. Biomed. Mater. Res.* **2002**, *60*, 434 - 444.
223. Chou, L.; Firth, J. D.; Uitto, V.; Brunette, D. M., Substratum surface topography alters cell shape and regulates fibronectin mRNA level, mRNA stability, secretion and assembly in human fibroblasts. *J. Cell Sci.* **1995**, *108*, 1563 - 1573.
224. Gentile, F.; Tirinato, L.; Battista, E.; Causa, F.; Liberale, C.; di, F. E. M.; Decuzzi, P., Cells preferentially grow on rough substrates. *Biomaterials* **2010**, *31*, 7205 - 7212.
225. Decuzzi, P.; Ferrari, M., Modulating cellular adhesion through nanotopography. *Biomaterials* **2010**, *31*, 173 - 179.
226. Pierres, A.; Benoliel, A.-M.; Touchard, D.; Bongrand, P., How cells tiptoe on adhesive surfaces before sticking. *Biophys. J.* **2008**, *94*, 4114 - 4122.
227. Discher, D. E.; Janmey, P.; Wang, Y.-l., Tissue cells feel and respond to the stiffness of their substrate. *Science (Washington, DC, U. S.)* **2005**, *310*, 1139 - 1143.
228. Hakkinen, K. M.; Harunaga, J. S.; Doyle, A. D.; Yamada, K. M., Direct comparisons of the morphology, migration, cell adhesions, and actin cytoskeleton of fibroblasts in four different three-dimensional extracellular matrices. *Tissue Eng., Part A* **2011**, *17*, 713 - 724.
229. Singh, P.; Carraher, C.; Schwarzbauer, J. E., Assembly of fibronectin extracellular matrix. *Annu. Rev. Cell Dev. Biol.* **2010**, *26*, 397 - 419.
230. Vogel, V., Mechanotransduction involving multimodular proteins: Converting force into biochemical signals. *Annu. Rev. Biophys. Biomol. Struct.* **2006**, *35*, 459 - 488.

231. Birgersdotter, A.; Sandberg, R.; Ernberg, I., Gene expression perturbation in vitro--a growing case for three-dimensional (3D) culture systems. *Semin Cancer Biol* **2005**, *15*, 405 - 412.
232. Wilkinson, C. D. W.; Riehle, M.; Wood, M.; Gallagher, J.; Curtis, A. S. G., The use of materials patterned on a nano- and micro-metric scale in cellular engineering. *Mater. Sci. Eng., C* **2002**, *C19*, 263 - 269.
233. Canas, N.; Kamperman, M.; Voelker, B.; Kroner, E.; McMeeking, R. M.; Arzt, E., Effect of nano- and micro-roughness on adhesion of bioinspired micropatterned surfaces. *Acta Biomater.* **2012**, *8*, 282 - 288.
234. Owen, G. R.; Jackson, J.; Chehroudi, B.; Burt, H.; Brunette, D. M., A PLGA membrane controlling cell behaviour for promoting tissue regeneration. *Biomaterials* **2005**, *26*, 7447 - 7456.
235. Linez-Bataillon, P.; Monchau, F.; Bigerelle, M.; Hildebrand, H. F., In vitro MC3T3 osteoblast adhesion with respect to surface roughness of Ti6Al4V substrates. *Biomol. Eng.* **2002**, *19*, 133 - 141.
236. Liu, H.; Lin, J.; Roy, K., Effect of 3D scaffold and dynamic culture condition on the global gene expression profile of mouse embryonic stem cells. *Biomaterials* **2006**, *27*, 5978 - 5989.
237. Klapperich, C. M.; Bertozzi, C. R., Global gene expression of cells attached to a tissue engineering scaffold. *Biomaterials* **2004**, *25*, 5631 - 5641.
238. Lord, M. S.; Foss, M.; Besenbacher, F., Influence of nanoscale surface topography on protein adsorption and cellular response. *Nano Today* **2010**, *5*, 66 - 78.
239. Solanki, A.; Shah, S.; Memoli, K. A.; Park, S. Y.; Hong, S.; Lee, K., Controlling differentiation of neural stem cells using extracellular matrix protein patterns. *Small* **2010**, *6*, 2509 - 2513.
240. Nakanishi, J.; Kikuchi, Y.; Takarada, T.; Nakayama, H.; Yamaguchi, K.; Maeda, M., Spatiotemporal control of cell adhesion on a self-assembled monolayer having a photocleavable protecting group. *Anal. Chim. Acta* **2006**, *578*, 100 - 104.
241. Mrksich, M.; Dike, L. E.; Tien, J.; Ingber, D. E.; Whitesides, G. M., Using microcontact printing to pattern the attachment of mammalian cells to self-assembled monolayers of alkanethiolates on transparent films of gold and silver. *Exp. Cell Res.* **1997**, *235*, 305 - 313.
242. Phong, H.; Wang, S.; Wang, M., Cell behaviors on micro-patterned porous thin films. *Mater. Sci. Eng., B* **2010**, *169*, 94 - 100.
243. Papenburg, B. J.; Rodrigues, E. D.; Wessling, M.; Stamatialis, D., Insights into the role of material surface topography and wettability on cell-material interactions. *Soft Matter* **2010**, *6*, 4377 - 4388.
244. Kunzler, T. P.; Drobek, T.; Schuler, M.; Spencer, N. D., Systematic study of osteoblast and fibroblast response to roughness by means of surface-morphology gradients. *Biomaterials* **2007**, *28*, 2175 - 2182.
245. Koepsel, J. T.; Murphy, W. L., Patterning discrete stem cell culture environments via localized self-assembled monolayer replacement. *Langmuir* **2009**, *25*, 12825 - 12834.
246. Friedrich, J.; Eder, W.; Castaneda, J.; Doss, M.; Huber, E.; Ebner, R.; Kunz-Schughart, L. A., A reliable tool to determine cell viability in complex 3-D culture: the acid phosphatase assay. *J. Biomol. Screening* **2007**, *12*, 925 - 937.
247. Wikswow, J. P.; Block, F. E., 3rd; Cliffel, D. E.; Goodwin, C. R.; Marasco, C. C.; Markov, D. A.; McLean, D. L.; McLean, J. A.; McKenzie, J. R.; Reiserer, R. S.; Samson, P. C.; Schaffer, D. K.; Seale, K. T.; Sherrod, S. D., Engineering challenges for instrumenting and controlling integrated organ-on-chip systems. *IEEE transactions on bio-medical engineering* **2013**, *60*, 682-90.
248. Isenberg, B. C.; Tsuda, Y.; Williams, C.; Shimizu, T.; Yamato, M.; Okano, T.; Wong, J. Y., A thermoresponsive, microtextured substrate for cell sheet engineering with defined structural organization. *Biomaterials* **2008**, *29*, 2565 - 2572.
249. Seidlits, S. K.; Schmidt, C. E.; Shear, J. B., High-Resolution patterning of hydrogels in three dimensions using direct-write photofabrication for cell guidance. *Adv. Funct. Mater.* **2009**, *19*, 3543 - 3551.
250. Kunz-Schughart, L. A.; Freyer, J. P.; Hofstaedter, F.; Ebner, R., The use of 3-D cultures for high-throughput screening: the multicellular spheroid model. *J. Biomol. Screening* **2004**, *9*, 273 - 285.

251. Stevens, M. M.; Mayer, M.; Anderson, D. G.; Weibel, D. B.; Whitesides, G. M.; Langer, R., Direct patterning of mammalian cells onto porous tissue engineering substrates using agarose stamps. *Biomaterials* **2005**, *26*, 7636 - 7641.
252. Chen, W.; Lam, R. H. W.; Fu, J., Photolithographic surface micromachining of polydimethylsiloxane (PDMS). *Lab Chip* **2012**, *12*, 391 - 395.
253. Kim, E. J.; Boehm, C. A.; Mata, A.; Fleischman, A. J.; Muschler, G. F.; Roy, S., Post microtextures accelerate cell proliferation and osteogenesis. *Acta Biomater.* **2010**, *6*, 160 - 169.
254. Zeiger, A. S.; Hinton, B.; J., V. V. K., Why the dish makes a difference: Quantitative comparison of polystyrene culture surfaces. *Acta Biomater.* **2013**, *9*, 7354 - 7361.
255. Lee, J. N.; Jiang, X.; Ryan, D.; Whitesides, G. M., Compatibility of mammalian cells on surfaces of poly(dimethylsiloxane). *Langmuir* **2004**, *20*, 11684 - 11691.
256. Oral, I.; Guzel, H.; Ahmetli, G., Measuring the Young's modulus of polystyrene-based composites by tensile test and pulse-echo method. *Polym. Bull.* **2011**, *67*, 1893 - 1906.
257. Truskey, G. A.; Proulx, T. L., Quantitation of cell area on glass and fibronectin-coated surfaces by digital image analysis. *Biotechnol Prog* **1990**, *6*, 513 - 519.
258. Janmey, P. A.; Winer, J. P.; Murray, M. E.; Wen, Q., The hard life of soft cells. *Cell Motil Cytoskeleton* **2009**, *66*, 597 - 605.
259. Zamani, F.; Amani-Tehran, M.; Latifi, M.; Shokrgozar, M. A., The influence of surface nanoroughness of electrospun PLGA nanofibrous scaffold on nerve cell adhesion and proliferation. *J Mater Sci Mater Med* **2013**.
260. Palchesko, R. N.; Zhang, L.; Sun, Y.; Feinberg, A. W., Development of polydimethylsiloxane substrates with tunable elastic modulus to study cell mechanobiology in muscle and nerve. *PLoS One* **2012**, *7*, e51499.
261. Totonelli, G.; Maghsoudlou, P.; Garriboli, M.; Riegler, J.; Orlando, G.; Sebire, N. J.; Smith, V. V.; Fishman, J. M.; Ghionzoli, M.; Turmaine, M.; Birchall, M. A.; Atala, A.; Soker, S.; Lythgoe, M. F.; Seifalian, A.; Pierro, A.; Eaton, S.; De, C. P., A rat decellularized small bowel scaffold that preserves villus-crypt architecture for intestinal regeneration. *Biomaterials* **2012**, *33*, 3401 - 3410.
262. Wang, X.; Ni, Q., Determination of cortical bone porosity and pore size distribution using a low field pulsed NMR approach. *J Orthop Res* **2003**, *21*, 312 - 319.
263. Curtis, A. S. G.; Forrester, J. V., The competitive effects of serum proteins on cell adhesion. *J. Cell Sci.* **1984**, *71*, 17 - 35.
264. Novotny, G. E.; Gnoth, C., Variability of fibroblast morphology in vivo: a silver impregnation study on human digital dermis and subcutis. *J. Anat.* **1991**, *177*, 195 - 207.
265. Itoh, Y.; Seiki, M., MT1-MMP: A potent modifier of pericellular microenvironment. *J. Cell. Physiol.* **2006**, *206*, 1 - 8.
266. Okada, A.; Tomasetto, C.; Lutz, Y.; Bellocq, J.-P.; Rio, M.-C.; Basset, P., Expression of matrix metalloproteinases during rat skin wound healing: evidence that membrane type-1 matrix metalloproteinase is a stromal activator of pro-gelatinase A. *J. Cell Biol.* **1997**, *137*, 67 - 77.
267. Isackson, D.; McGill, L. D.; Bachus, K. N., Percutaneous implants with porous titanium dermal barriers: an in vivo evaluation of infection risk. *Med Eng Phys* **2011**, *33*, 418 - 426.
268. Akiyama, Y.; Kikuchi, A.; Yamato, M.; Okano, T., Ultrathin poly(N-isopropylacrylamide) grafted layer on polystyrene surfaces for cell adhesion/detachment control. *Langmuir* **2004**, *20*, 5506 - 5511.
269. Komori, K.; Udagawa, M.; Shinohara, M.; Montagne, K.; Tsuru, T.; Sakai, Y., Formation and harvesting of thick pancreatic β -cell sheets on a highly O₂-permeable plate modified with poly(N-isopropylacrylamide). *Biomater. Sci.* **2013**, *1*, 510 - 518.
270. Fukumori, K.; Akiyama, Y.; Kumashiro, Y.; Kobayashi, J.; Yamato, M.; Sakai, K.; Okano, T., Characterization of ultra-thin temperature-responsive polymer layer and its polymer thickness dependency on cell attachment/detachment properties. *Macromol. Biosci.* **2010**, *10*, 1117 - 1129.
271. Lim, H. L.; Hwang, Y.; Kar, M.; Varghese, S., Smart hydrogels as functional biomimetic systems. *Biomaterials Science* **2014**.

272. Schild, H. G., Poly(N-isopropylacrylamide): experiment, theory and application. *Prog. Polym. Sci.* **1992**, *17*, 163 - 249.
273. Cooperstein, M. A.; Canavan, H. E., Biological cell detachment from poly(N-isopropyl acrylamide) and its applications. *Langmuir* **2010**, *26*, 7695 - 7707.
274. Nash, M. E.; Healy, D.; Carroll, W. M.; Elvira, C.; Rochev, Y. A., Cell and cell sheet recovery from pNIPAm coatings; motivation and history to present day approaches. *J. Mater. Chem.* **2012**, *22*, 19376 - 19389.
275. Reiners, J. J.; Mathieu, P.; Okafor, C.; Putt, D. A.; Lash, L. H., Depletion of cellular glutathione by conditions used for the passaging of adherent cultured cells. *Toxicol. Lett.* **2000**, *115*, 153 - 163.
276. Elloumi-Hannachi, I.; Yamato, M.; Okano, T., Cell sheet engineering: a unique nanotechnology for scaffold-free tissue reconstruction with clinical applications in regenerative medicine. *J. Intern. Med.* **2009**, *267*, 54 - 70.
277. Williams, C.; Tsuda, Y.; Isenberg, B. C.; Yamato, M.; Shimizu, T.; Okano, T.; Wong, J. Y., Aligned cell sheets grown on thermo-responsive substrates with microcontact printed protein patterns. *Adv. Mater. (Weinheim, Ger.)* **2009**, *21*, 2161 - 2164.
278. Isenberg, B. C.; Backman, D. E.; Kinahan, M. E.; Jesudason, R.; Suki, B.; Stone, P. J.; Davis, E. C.; Wong, J. Y., Micropatterned cell sheets with defined cell and extracellular matrix orientation exhibit anisotropic mechanical properties. *J Biomech* **2012**, *45*, 756 - 761.
279. Tsuda, Y.; Shimizu, T.; Yamato, M.; Kikuchi, A.; Sasagawa, T.; Sekiya, S.; Kobayashi, J.; Chen, G.; Okano, T., Cellular control of tissue architectures using a three-dimensional tissue fabrication technique. *Biomaterials* **2007**, *28*, 4939 - 4946.
280. Guillame-Gentil, O.; Semenov, O.; Roca, A. S.; Groth, T.; Zahn, R.; Voros, J.; Zenobi-Wong, M., Engineering the extracellular environment: strategies for building 2D and 3D cellular structures. *Adv. Mater.* **2010**, *22*, 5443 - 5462.
281. da Silva, R. M. P.; Mano, J. F.; Reis, R. L., Smart thermoresponsive coatings and surfaces for tissue engineering: switching cell-material boundaries. *Trends Biotechnol* **2007**, *25*, 577 - 583.
282. Hatakeyama, H.; Kikuchi, A.; Yamato, M.; Okano, T., Patterned biofunctional designs of thermoresponsive surfaces for spatiotemporally controlled cell adhesion, growth, and thermally induced detachment. *Biomaterials* **2007**, *28*, 3632 - 3643.
283. Takahashi, H.; Matsuzaka, N.; Nakayama, M.; Kikuchi, A.; Yamato, M.; Okano, T., Terminally functionalized thermoresponsive polymer brushes for simultaneously promoting cell adhesion and cell sheet harvest. *Biomacromolecules* **2012**, *13*, 253 - 260.
284. Duarte, A. R. C.; Mano, J. F.; Reis, R. L., Thermosensitive polymeric matrices for three-dimensional cell culture strategies. *Acta Biomater.* **2011**, *7*, 526 - 529.
285. Matsuda, T., Poly(N-isopropylacrylamide)-grafted gelatin as a thermoresponsive cell-adhesive, mold-releasable material for shape-engineered tissues. *J. Biomater. Sci., Polym. Ed.* **2004**, *15*, 947 - 955.
286. Tibbitt, M. W.; Anseth, K. S., Hydrogels as extracellular matrix mimics for 3D cell culture. *Biotechnol. Bioeng.* **2009**, *103*, 655 - 663.
287. Tay, C. Y.; Irvine, S. A.; Boey, F. Y. C.; Tan, L. P.; Venkatraman, S., Micro-/nano-engineered cellular responses for soft tissue engineering and biomedical applications. *Small* **2011**, *7*, 1361 - 1378.
288. Danen, E. H. J.; Yamada, K. M., Fibronectin, integrins, and growth control. *J. Cell. Physiol.* **2001**, *189*, 1 - 13.
289. Hakkinen, K. M.; Harunaga, J. S.; Doyle, A. D.; Yamada, K. M., Direct comparisons of the morphology, migration, cell adhesions, and actin cytoskeleton of fibroblasts in four different three-dimensional extracellular matrices. *Tissue Eng., Part A* **2011**, *17*, 713 - 724.
290. Isenberg, B. C.; Tsuda, Y.; Williams, C.; Shimizu, T.; Yamato, M.; Okano, T.; Wong, J. Y., A thermoresponsive, microtextured substrate for cell sheet engineering with defined structural organization. *Biomaterials* **2008**, *29*, 2565 - 2572.
291. Ishida, N.; Biggs, S., Direct observation of the phase transition for a poly(N-isopropylacrylamide) layer grafted onto a solid surface by AFM and QCM-D. *Langmuir* **2007**, *23*, 11083 - 11088.

292. Sun, B.; Lin, Y.; Wu, P., Structure analysis of poly(N-isopropylacrylamide) using near-infrared spectroscopy and generalized two-dimensional correlation infrared spectroscopy. *Appl. Spectrosc.* **2007**, *61*, 765 - 771.
293. Dorman, G.; Prestwich, G. D., Benzophenone photophores in biochemistry. *Biochemistry* **1994**, *33*, 5661 - 5673.
294. Ma, D.; Chen, H.; Shi, D.; Li, Z.; Wang, J., Preparation and characterization of thermo-responsive PDMS surfaces grafted with poly(N-isopropylacrylamide) by benzophenone-initiated photopolymerization. *J. Colloid Interface Sci.* **2009**, *332*, 85 - 90.
295. Lin, J. B.; Isenberg, B. C.; Shen, Y.; Schorsch, K.; Sazonova, O. V.; Wong, J. Y., Thermo-responsive poly(N-isopropylacrylamide) grafted onto microtextured poly(dimethylsiloxane) for aligned cell sheet engineering. *Colloids Surf., B* **2012**, *99*, 108 - 115.
296. Uchida, E.; Uyama, Y.; Ikada, Y., A novel method for graft polymerization onto poly(ethylene terephthalate) film surface by UV irradiation without degassing. *J. Appl. Polym. Sci.* **1990**, *41*, 677 - 687.
297. Richey, T.; Iwata, H.; Oowaki, H.; Uchida, E.; Matsuda, S.; Ikada, Y., Surface modification of polyethylene balloon catheters for local drug delivery. *Biomaterials* **2000**, *21*, 1057 - 1065.
298. Hu, S.; Ren, X.; Bachman, M.; Sims, C. E.; Li, G. P.; Allbritton, N., Surface modification of poly(dimethylsiloxane) microfluidic devices by ultraviolet polymer grafting. *Anal. Chem.* **2002**, *74*, 4117 - 4123.
299. Zhang, X.-Z.; Yang, Y.-Y.; Chung, T.-S.; Ma, K.-X., Preparation and characterization of fast response macroporous poly(N-isopropylacrylamide) hydrogels. *Langmuir* **2001**, *17*, 6094 - 6099.
300. Wu, C.; Keivens, V. M.; O'Toole, T. E.; McDonald, J. A.; Ginsberg, M. H., Integrin activation and cytoskeletal interaction are essential for the assembly of a fibronectin matrix. *Cell* **1995**, *83*, 715 - 724.
301. Sottile, J.; Hocking, D. C., Fibronectin polymerization regulates the composition and stability of extracellular matrix fibrils and cell-matrix adhesions. *Mol. Biol. Cell* **2002**, *13*, 3546 - 3559.
302. Beningo, K. A.; Dembo, M.; Wang, Y.-l., Responses of fibroblasts to anchorage of dorsal extracellular matrix receptors. *Proc. Natl. Acad. Sci. U. S. A.* **2004**, *101*, 18024 - 18029.
303. Mao, Y.; Schwarzbauer, J. E., Fibronectin fibrillogenesis, a cell-mediated matrix assembly process. *Matrix Biol.* **2005**, *24*, 389 - 399.
304. Mao, Y.; Schwarzbauer, J. E., Stimulatory effects of a three-dimensional microenvironment on cell-mediated fibronectin fibrillogenesis. *J. Cell Sci.* **2005**, *118*, 4427 - 4436.
305. Nakagawa, Y.; Suzuki, T.; Tayama, S., Metabolism and toxicity of benzophenone in isolated rat hepatocytes and estrogenic activity of its metabolites in MCF-7 cells. *Toxicology* **2000**, *156*, 27 - 36.
306. Bacakova, L.; Filova, E.; Rypacek, F.; Svorcik, V.; Stary, V., Cell adhesion on artificial materials for tissue engineering. *Physiol Res* **2004**, *53 Suppl 1*, S35 - 45.
307. Parsons, J. T.; Martin, K. H.; Slack, J. K.; Taylor, J. M.; Weed, S. A., Focal adhesion kinase: a regulator of focal adhesion dynamics and cell movement. *Oncogene* **2000**, *19*, 5606 - 5613.
308. Chou, L.; Firth, J. D.; Uitto, V.-J.; Brunette, D. M., Substratum surface topography alters cell shape and regulates fibronectin mRNA level, mRNA stability, secretion and assembly in human fibroblasts. *J. Cell Sci.* **1995**, *108*, 1563 - 1573.
309. Sternlicht, M. D.; Werb, Z., How matrix metalloproteinases regulate cell behavior. *Annu. Rev. Cell Dev. Biol.* **2001**, *17*, 463 - 516.
310. Alexander, C. M.; Howard, E. W.; Bissell, M. J.; Werb, Z., Rescue of mammary epithelial cell apoptosis and entactin degradation by a tissue inhibitor of metalloproteinases-1 transgene. *J. Cell Biol.* **1996**, *135*, 1669 - 1677.
311. Sato, T.; Del Carmen Ovejero, M.; Hou, P.; Heegaard, A.-M.; Kumegawa, M.; Foged, N. T.; Delaisse, J.-M., Identification of the membrane-type matrix metalloproteinase MT1-MMP in osteoclasts. *J. Cell Sci.* **1997**, *110*, 589 - 596.
312. Murphy, D. A.; Courtneidge, S. A., The 'ins' and 'outs' of podosomes and invadopodia: characteristics, formation and function. *Nat. Rev. Mol. Cell Biol.* **2011**, *12*, 413 - 426.

313. Hotary, K. B.; Allen, E. D.; Brooks, P. C.; Datta, N. S.; Long, M. W.; Weiss, S. J., Membrane type I matrix metalloproteinase usurps tumor growth control imposed by the three-dimensional extracellular matrix. *Cell* **2003**, *114*, 33 - 45.